ENVIRO-MECHANICAL DURABILITY OF GRAPHITE/EPOXY COMPOSITE MATERIALS

Sneha Patel Davison

Dissertation Submitted to the
Faculty of the Virginia Polytechnic Institute and State University
in Partial Fulfillment of the Requirements of the Degree of

Doctor of Philosophy
in
Engineering Mechanics

S. W. Case, Chairman
K. L. Reifsnider
R. M. Davis
S. L. Hendricks
A.C. Loos

November 5, 2003
Blacksburg, Virginia

Keywords: Polymer Composite, Moisture, Temperature, Fatigue, Strength, Durability

ENVIRO-MECHANICAL DURABILITY OF GRAPHITE/EPOXY COMPOSITE MATERIALS

Sneha Patel Davison

(ABSTRACT)

Carbon/epoxy laminates are receiving greater attention by the infrastructure, marine, and offshore oil industries due to the need for superior performance capabilities. Such applications generally involve subjecting materials to harsh temperature and moisture conditions. The objective of this study was to provide a greater understanding of how temperature and moisture affect the strength and fatigue behavior of carbon/epoxy composites and the issues involved in modeling these effects. Results from thermal analysis and quasi-static testing on neat resin and unidirectional laminates as a function of temperature and moisture are presented which provide insight into how material properties vary with temperature and moisture and form the inputs necessary to evaluate composite strength and damage models. Fatigue life and damage accumulation testing results provide further insight into the effects of temperature and moisture and also provide a means for model validation. Generally, composite strength was found to be compromised by temperature but enhanced with moisture, while fatigue life was reduced by both temperature and moisture. Crack density with fatigue cycles was found to decrease with temperature but increase for immersed fatigue. Testing also revealed discrepancies between the edge replication and radiography methods for determining crack density.

The analytical phase of the work considered a composite strength model and a damage evolution model to predict crack density. The composite strength model was found to provide an accurate dry, room temperature prediction which could be extended to an accurate prediction of wet specimen strength, but the results at elevated temperature fell conservative. The validation of the

damage model proved inconclusive as it was found that the results are very sensitive to quantities such as thermal residual stresses and first ply failure. Currently, no reliable methods are available in the literature to determine these values accurately. However, the model was able to predict the decrease in crack density at elevated temperatures. The increase in crack density for immersed fatigue was not predicted. Overall, the study revealed that a more basic understanding of "in-situ" ply properties are needed before one can consider the use of predictive models in practical applications, especially in varying environments.

DEDICATION

This work is dedicated to Mya Sneha Davison (12-14-03). The joy over her anticipated arrival kept me going on many a long night and her presence during my defense truly made it an extra special event.

ACKNOWLEDGEMENTS

First, I am so thankful for the support I've had from my family and friends throughout this experience. My parents, **Ramesh and Hemlatta Patel**, have been patient, supportive, and encouraging in everything I have ventured to do. My husband **James** has been my rock to whom I could always turn for comfort, understanding, and motivation. I could not have made it this far without them.

I would also like to extend my gratitude and appreciation to the following individuals/groups:

Dr. Scott Case, who has been my advisor throughout my graduate career. His patience, understanding, and encouragement has made my graduate experience an enjoyable one. He has provided me with much opportunity to travel, network, and present my own work in all settings, showing his dedication to my academic and professional growth. His interest in me did not end at the professional level, but also extended to the personal level. He has not only been a wonderful advisor, but also a great friend.

Dr. Ken Reifsnider, who not only served on both my M.S. and Ph.D committees, but also initially hired me into the Materials Response Group and initiated my contact with Scott. He is one of the most motivating individuals I have ever come across.

Dr. Richey Davis, Dr. Scott Hendricks, and Dr. Al Loos, who graciously made time to serve on my graduate committee. Their suggestions on my proposal and dissertation have been very helpful and appreciated.

Schlumberger-Doll Research, Inc., and particularly Dr. Olivier Sindt, for not only funding this research, but giving me free reign to choose a project of interest to me and affording me the opportunity to work with them directly and use their facilities.

Dr. Howard Halverson, who has always been extremely generous with his time, whether I needed technical advice or someone to "goof off" with. He has been a great friend and I wish him all the luck in the world for his future.

Past and present student members of the MRG, particularly Tozer Bandorawalla and Blair Russell, who made coming into the lab fun and interesting and were always ready to lend a helping hand.

Mac McCord, who always has an answer for experimental challenges. His dedication to the work of the students of the MRG goes above and beyond the call of duty and his expertise has proven priceless.

Shelia Collins and Beverly Williams, who keep things running in the MRG, whether this calls for making sure a paper or proposal gets submitted on time or remembering somebody on a special day. The work they do is invaluable, and without them, students and faculty alike would be lost.

David Simmons and the ESM Machine Shop, who always managed to turn around work orders in an extremely timely manner. The work has always been exactly to order. Dave in particular was very helpful at times when I came to him with "urgent" projects and never complained or failed to deliver. He always has a smile on his face and a kind word.

Danny Reed, for helping me make what seemed like an endless number of composite panels.

Loretta Tickle, Joyce Smith, and Pat Baker, who always had an answer to my graduate school or administrative needs as far as the Engineering Science and Mechanics Department was concerned.

The PEO Sisterhood, and especially the Blacksburg chapter, who awarded me a generous stipend and took a special interest in me and my work and helping me obtain my degree.

Davenport Fellowship and Virginia Space Grant Consortium, for also awarding me with generous stipends.

TABLE OF CONTENTS

LIST OF FIGURES

LIST OF TABLES

1 INTRODUCTION

While the aerospace industry has traditionally been the major driver for the advancement of composite materials, current trends find these materials used in a wider variety of applications. Among those industries leading research efforts related to the expanded utilization of composites are the infrastructure industry, marine industry, and the offshore oil industry- all of which require composite materials to endure harsh moisture and temperature environments. Traditionally, glass fiber composites have received great consideration for such applications; however, the need for better performance has lead back to the use of carbon fiber composites. While the effects of moisture and temperature on composite properties and behavior have been studied extensively, the studies involving carbon fiber composite fatigue behavior have been limited in number and in scope. A review of the literature pertaining to such topics is given in Chapter 2.

The goal of this work was to study and relate the durability and damage evolution of carbon/epoxy composites subjected to elevated temperature and moisture conditions, both combined and individually. The experimental phase of the effort included acquiring detailed information of how matrix and composite ply properties evolve in the presence of moisture and elevated temperature conditions, and the role this evolution plays in the strength and fatigue behavior of the composite material. While obvious indication of composite property degradation may be provided by strength, stiffness, and fatigue life data, damage growth (e.g. crack density and delamination) with loading also provides insight into the source and mechanism behind the property degradation. Thus, minimally invasive methods were used to characterize damage accumulation. Experimental methods and results can be found in Chapter 3.

In the analytical phase of the study, the combined information provided by matrix and composite strength and stiffness data was used to form the inputs necessary to assess the ability of composite damage and strength models to incorporate both mechanical and environmental loading conditions into the analysis. Many models claim to be robust in their ability to adapt to varying temperatures and environments, but the claims are rarely validated with experimental

evidence. Where validation is offered, the model is generally of an empirical nature such that no physical significance may be clearly drawn from adjusting parameters to suit varying environments. Thus, in Chapter 4, consideration was given to a composite strength model and a damage evolution model for which the inputs have obvious physical correspondence.

As mentioned above, very little work of this type is available in the current literature, particularly for carbon/epoxy materials. Relevant experimental data is difficult to find, and validated models robust enough to include combined environmental and mechanical effects are virtually non-existent. This study provides a well-rounded set of experimental data on a single material system that is not generally found in the literature. The assessment of composite strength and damage modeling efforts provides unique insight into the unresolved issues that must be considered before modeling efforts can move forward reliably. Thus, the work presented in this study, both the experimental and analytical phases, provides original contributions to the literature.

2 LITERATURE REVIEW

Since carbon fibers are inert to moisture and temperature, the matrix and fiber/matrix interface components of the carbon fiber composite are of the greatest concern when considering the effects of moisture and temperature on these materials. The potential effects of each condition are very similar in nature: interfacial degradation, matrix property degradation, build up of residual intralaminar stresses due to expansion and swelling, and changes in fracture toughness and ductility. The presence of moisture may also result in a decrease in glass transition temperature. Under load, viscoelastic effects (e.g. creep, relaxation) may also become important. The extent to which any of these effects are realized may vary significantly between composite material systems, even those of the same general type (e.g. carbon/epoxy). However, the literature available provides some insight as to what one may expect to find and the various ways in which the effects of temperature and moisture manifest themselves. Such literature is investigated in more detail below. Note that the discussion will be limited to carbon fiber composites. References for similar studies on glass fiber composites include [1, 2, and 3] among others.

2.1 The Influence of Moisture

An extensive body of literature is available concerning the effects of moisture on material properties and the moisture absorption behavior of composite materials. Conversely, very little literature is available concerning the fatigue behavior of carbon fiber composite materials in fluid environments. Both bodies of literature are discussed in the Sections 2.1.1- 2.1.2 and Section 2.1.3, respectively.

2.1.1 Moisture Absorption

Moisture absorption characteristics comprise an important aspect of moisture/durability studies. Such information can generally be used to obtain some insight into how and why the material is influenced by moisture. For instance, in Figure 2.1, Curve C is indicative of significant interfacial degradation, Curve D is indicative of material leaching, Curves A and B represents

typical, reversible, moisture absorption behavior, and curve LF is classical Fickian moisture absorption [4].

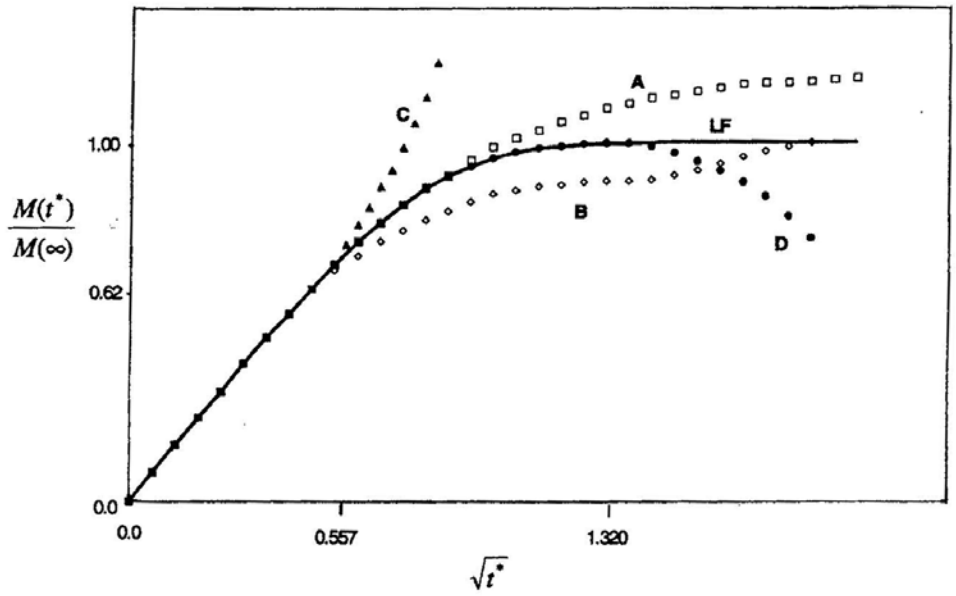

Figure 2.1: Schematic of potential moisture absorption curves [1]

Such characteristic features of moisture absorption are dependent on the composite system, fluid, and exposure condition and time. Fluid absorption that follows along curve A or curve B is typically thought to occur as a result of the competing rate processes of water diffusion and polymer relaxation [5]. Such absorption behavior may also be a result of the combination of two distinct absorption mechanisms which result in two physical residence states – bound water and free water [5,6]. The diffusion of bound water is reversible, but the diffusion of free water is not.

External factors can also influence composite moisture absorption. For instance, applied stress has been shown to increase saturation moisture concentration [4,7,8]. Of course, damage due to applied stress and/or moisture diffusion and temperature also plays a major role in composite absorption behavior. Some studies have reported increased diffusion but unchanged saturation concentration [9 , 10], while others report unchanged diffusion but increased saturation concentration [11]. Roy et al. [12] developed a damage mechanics based model to predict moisture absorption behavior as a function of transverse and longitudinal cracking. Other factors

that influence diffusion and/or saturation concentration are temperature, fluid acidity, and exposure duration [4]. These factors all become important in considering the composite durability issues in immersed conditions.

2.1.2 Influence of Moisture on Static Strength/Stiffness

The mechanical response of carbon/polymer laminates is largely determined by the matrix and the interfacial properties since carbon fibers are insensitive to moisture (as opposed to glass fibers which are known to degrade in the presence of moisture [4]). Of the known possible effects of moisture are the formation of residual hygral stresses (generally compressive) [7,13], polymer and interfacial degradation, and polymer plasticization. Combined, these effects can act to enhance or degrade the fracture toughness of the material. Moreover, the plasticization can result in decreased glass transition temperature [14] which may affect how the composite behaves in elevated temperature environments.

The tensile properties of carbon/polymer composite laminates, particularly those with orientations other than $[90]_n$, are generally considered to be insensitive to moisture. However, at moisture contents above 1%, 0° and 45° degree laminates have shown up to a 20% decrease in tensile strength [15]. In addition, laminates of orientation $[90]_n$ have been reported to undergo significant tensile strength and modulus reductions [15,16]. Moreover, some interlaminar shear strength degradation has also been reported for carbon/epoxy systems [17]. Bradley and Grant [16] found that for a graphite/epoxy system, the reduction in transverse strength due to water saturation is similar to the observed change in interfacial shear strength. The interfacial strength was measured using a microindentation technique. The authors consequently hypothesized that for their graphite/epoxy material system, the degradation of the composite system was primarily interfacial in nature rather than in the matrix.

Zhuang and Wightman [18] studied the effect of moisture on interfacial shear strength using single fiber fragmentation testing. Samples were stored in a 100% relative humidity environment at either 23°C or 75°C prior to testing. The results indicate that exposure to humidity does cause interfacial shear strength reduction. The reduction is insensitive to aging temperature. To distinguish between the effect of temperature and humidity, a parallel study was

conducted on specimens aged at the same temperatures in dry conditions. No reduction in interfacial strength was found. The reduction in interfacial strength with humidity exposure was attributed to moisture induced matrix plasticization and subsequent decrease in matrix T_g.

2.1.3 Influence of Moisture on Fatigue and Durability

The fatigue durability of composite materials is largely affected by the static strength and stiffness issues discussed above. Fracture toughness changes due to plasticization of the matrix are also of concern as they could affect the damage propagation rate during fatigue. A study by Mear et al. [19] on unidirectional graphite/epoxy compact tension specimens showed that, in fact, the fracture toughness and compliance of the material were not affected by water saturation or moisture immersion. However, the crack growth rates of saturated specimens fatigued in air were lower than that of "as-received" specimens fatigued in air. Similarly, while the crack growth rates of "as-received" specimens and saturated specimens tested submerged in distilled water were an order of magnitude higher than those of "as-received" specimens fatigued in air, the crack growth rates for saturated specimens tested submerged were lower than those of "as-received" specimens tested submerged. These results are in contrast to results by Sloan [20] who found lower crack growth rates in submerged fatigue of graphite/epoxy laminates tested in compact tension. The lower crack growth rates in that case were attributed to fiber-bridging arising from moisture induced interfacial degradation.

In the Mear et al. [19] study, the authors attributed the decrease in crack growth rates for saturated specimens to their increased strain to failure (though failure stress remained unchanged). For such a case, the energy required to propagate a crack would also increase. A second possibility offered was the moisture induced relief of residual cure stresses. Other interesting findings in the study were that saturated specimens were observed to "sweat" moisture from the crack tips during fatigue, as were "as-received" specimens initially fatigued in water and subsequently fatigued in air. The observation suggests that moisture is transported to the crack tip during fatigue and is trapped there during the unloading portion of the fatigue cycle.

More general fatigue and fatigue damage results are given in separate studies conducted by Weitsman et al. [21,22] The results of tension-tension fatigue testing of dry and sea-water

saturated cross-ply graphite/epoxy specimens tested in air and immersed are shown in Figure 2.2. No immersed fatigue tests were conducted on dry specimens.

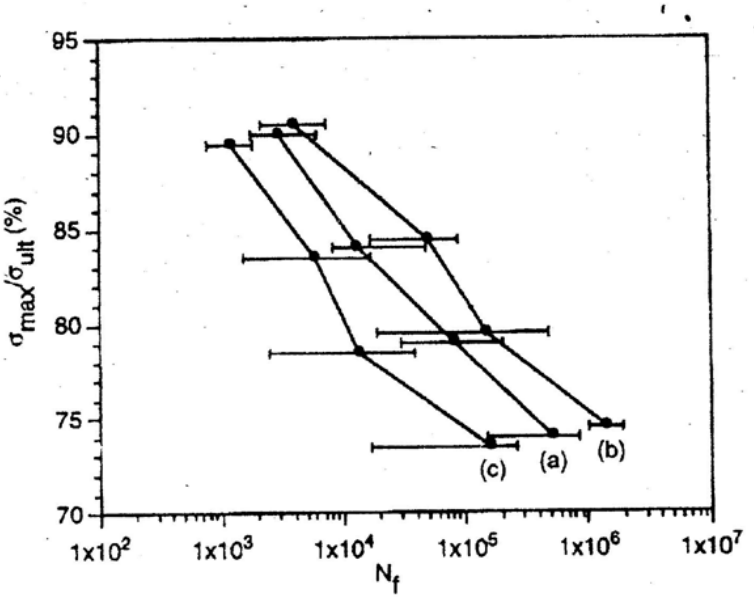

Figure 2.2: Fatigue S-N data from [22]. Curve "a" represents dry specimens fatigued in air, curve "b" represents sea-water saturated specimens fatigued in air, and curve "c" represents sea-water saturated specimens fatigued immersed in sea-water.

The results of the testing show that pre-saturated specimens fatigued in air have increased fatigue resistance over each of the other two cases. However, the extent to which this is true is somewhat ambiguous given the magnitude of the error. On the other hand, the saturated specimens fatigued in the immersed condition clearly exhibit decreased fatigue resistance. Moreover, saturated specimens fatigued immersed exhibited greater delaminations along the fiber/matrix interface and fewer transverse cracks in the transverse plies. The increase in fatigue lives in the case of the saturated specimens fatigued in air and the reduced number of transverse cracks for the saturated-immersed fatigue specimens was attributed to the moisture induced relief of residual cure stresses.

The decrease in fatigue lives for saturated specimens fatigued immersed was attributed to "a synergistic effect between water drawn by capillary action and cyclic mechanical loading." That is, the authors hypothesized that in the case of immersed fatigue, water is drawn into the

transverse cracks by capillary action through a random walk process. Tests conducted as part of the study indicate that the time scale involved for this capillary movement is much larger than that of the loading cycle (5 Hz), so the water remains essentially trapped in the crack. During the unloading phase of the loading cycle, the entrapped water exerts pressure against the crack faces. A shear lag analysis described by Smith and Weitsman [22] accounting for this effect shows that the immersed condition gives rise to cyclic tension-compression internal stresses despite the applied tensile loading. In addition, a finite element analysis shows that the total fracture energy is lowest for saturated specimens fatigued in air while the maximum total fracture energies for the dry specimens fatigued in air and saturated specimens fatigued immersed were comparable. However, the analysis shows that the fracture energy for the saturated specimens fatigued immersed is nearly entirely of Mode I, thus accounting for the extensive delaminations and decrease in fatigue lives observed for immersed fatigue.

A similar type of study was conducted by Komai et al. [23] on ± 45° carbon/epoxy laminates. In this case, swelling in the material caused interlaminar delamination prior to loading. In tensile testing, it was noted that the yield stress and strain to failure of saturated specimens was lower than that of dry specimens. That result was attributed to interfacial degradation that was evident from SEM micrography. Such micrography also revealed more plastic deformation in wet specimens than in the dry. Fatigue testing revealed the fatigue lives of immersed specimens were reduced from that of specimens fatigued in air. Accordingly, the internal damage of specimens fatigued immersed was greater than that of specimens fatigued in air. The latter result was attributed to interfacial degradation.

Nakanishi and Shindo [24] conducted fatigue tests on unidirectional carbon fiber reinforced epoxy in salt water and also found decreased fatigue strength in the immersed condition over fatigue in air. It was not made clear whether the specimens tested immersed were pre-saturated. Based on other results of the study, the salinity of the water was not considered to be a source of degradation in fatigue behavior.

2.2 The Influence of Temperature

The potential effects of temperature are very similar to the potential effects of moisture. Just as with moisture, for carbon fiber composites, changes in response with temperature are dependent on changes in the matrix and interfacial regions. Carbon fibers tend to be unaffected up to temperatures of 600°C [25]. Also similar to the moisture case, little work is reported in the literature regarding mechanical (as opposed to thermal) fatigue at elevated temperatures. Both general temperature effects (Section 2.2.1) and elevated temperature fatigue (Section 2.2.2) will be discussed in more detail below. Note that some work has been done at elevated temperatures far exceeding the glass transition temperature of the material, but this discussion will be limited to results for elevated temperatures below T_g.

2.2.1 The Influence of Elevated Temperature on Composite Strength and Stiffness

Though carbon fiber composite tensile strength and modulus are generally only minimally affected by temperature alone, distinct strength changes may occur even below the glass transition temperature. More often, one finds degradation in the matrix dominated properties and fiber/matrix interfacial properties. This type of degradation is ultimately responsible for changes one sees in carbon fiber composite strength and is especially important in fatigue.

Takeda and Ogihara [26] studied the microscopic failure processes of two graphite/epoxy cross-ply composite laminates at room temperature and at 80°C. One of the systems consisted of a toughened epoxy while the other consisted of a conventional epoxy. Among the issues considered was the identification of thermal residual strains, for which two methods of calculation were compared. The first method was based on classical lamination theory, while the second method involved measurements of the radius of curvature in unsymmetrical cross-ply laminates. It was found that the two different methods provided two very different sets of results. Establishing accurate thermal residual strains (and stresses) is important when considering material properties that may vary with temperature, such as composite strength. For instance, the stress-state in the cross-ply laminates was evaluated using a shear-lag analysis which accounted for the temperature effect by including thermal residual strains. The analysis was used to predict transverse matrix cracking, though unsuccessfully. In the case of where a

strength criterion was used, the thermal residual strains had a large impact on the outcome; however, in the case where an energy criterion was used, the impact of thermal residual strain was considerably smaller.

Experimentally, it was found that tensile strength increased with temperature for the thinnest laminate (6-ply), but decreased slightly for the thicker laminates. Moreover, in the toughened epoxy composite system the crack density decreased with temperature while the first crack strain increased with temperature. Delamination at the fiber/matrix interface was also observed in this system due to fiber/matrix interfacial debonding. However, the amount of delamination decreased with temperature while the delamination onset strain increased with temperature. The amount and rate of delamination also increased with thicker 90° layers. SEM images of failure surfaces indicated that little or no additional interfacial debonding took place at elevated temperature than at room temperature. For the conventional epoxy composite system, the crack density increased with temperature, but the first cracking strain remained the same as at room temperature. While a significant amount of delamination was observed for this system, SEM images indicated that interfacial degradation did take place with temperature. In both systems, the first cracking strain was about the same or larger than the 90° unidirectional ultimate strain and the resin fracture toughness was found to increase with temperature.

Detassis et al. [27] used fragmentation testing on single-fiber model composites to study the interfacial shear strength on carbon/epoxy composites as a function of temperature. The study considered both sized and de-sized fibers (Besfight HTA-7-3000), and the epoxy was a low T_g variety (T_g = 39°C). While interfacial shear strength values were found to decrease with temperature in single fiber composites, sized and de-sized, the values of the sized single-fiber composites were generally much higher than that of the de-sized single fiber. Moreover, the de-sized single fiber composite interfacial shear strength values were very similar to matrix shear strength values. The higher interfacial strength values for the sized single fiber composites were hypothesized to be a result of superior *interphase* (region where properties of fiber, interface, and matrix combine) properties as compared to the bulk matrix. In the case of the de-sized single fiber composites, the fact that the interfacial shear strengths were similar to the matrix shear

strengths was said to imply that the fiber/matrix adhesion in that case was highly dependent on bulk matrix properties.

Zhuang and Wightman [18] also studied the effect of temperature on interfacial shear strength in carbon epoxy composites using single fiber fragmentation testing. In considering the effect of temperatures below T_g (144°C in this case), the interfacial shear strengths of three different types of fibers in epoxy were found to decrease monotonically. It was suggested that the interphase region exhibits a lower T_g and modulus than the bulk matrix, and that the sharp decrease in interfacial shear strength seen around 80°C coincides with the degradation of this interphase region. Note that this hypothesis is somewhat in contrast to that put forth by Detassis et al. [27], as discussed above. Subsequently, the interfacial shear strength is matrix controlled, as can be evidenced by the fact that the data for all three fibers coincide. A similar study was conducted by Wimolkiatisak and Bell [28] with similar results.

While such results would seem to indicate that composite tensile strength would also decrease with temperature and the subsequent degradation in interfacial properties, data given in Reifsnider and Case [29] show that, in some cases, tensile strength may actually increase with temperature. Moreover, it is shown that the increase in strength may come as a result of degradation in interfacial properties. The interfacial properties affect the ineffective length at a fiber break, or the axial distance from the plane of the fiber break it takes for the fiber to regain full load bearing capacity. Very short ineffective lengths can lead to significant stress concentrations close to the break, causing fiber fractures to increase unstably. Very long ineffective lengths can cause fiber fracture regions to interact and connect to cause global failure. Thus, if a composite initially has very stiff interfacial properties and short ineffective lengths, matrix softening caused by temperature, or equivalently moisture, may act to increase the ineffective lengths and reduce stress concentrations, thereby increasing the composite strength. On the other hand, in the extreme case where stress concentrations are completely eliminated, the composite effect also disappears, so the composite would be expected to be weaker. These type of phenomena suggest that a non-monotonic composite strength versus temperature relationship is possible.

2.2.2 The Influence of Elevated Temperature on Composite Fatigue Durability

McLaughlin et al. [25] developed a static strength and fatigue model for unidirectional composites based on the cumulative weakening and chain-of-bundles mechanism. The model was modified to include a linear elastic fracture mechanics micromechanics model of the growth of fiber debonds and ineffective lengths with both increasing quasi-static load and tension-tension fatigue cycles. The model was also modified to include thermal stresses. In light of the fact that the model neglects several type of damage propagation mechanisms (e.g. transverse fiber breaks caused by adjacent fiber stress concentrations near single or multiple fiber breaks), the model is recognized to provide an upper bound to failure. To predict static strength and fatigue life at temperature, three material property issues are taken into account: 1) variation of properties with temperature as it increases to a given level, 2) degradation of properties as temperature is maintained at that level, and 3) permanent alteration of material properties even when the temperature is removed.

The results of the analysis revealed that, for the graphite/epoxy considered in the study, no significant thermal stress related fiber/matrix interface damage occurs with heating and that the primary loss in strength and fatigue life with temperature is due to matrix shear properties and fiber/matrix degradation. Moreover, in fatigue, room temperature S-N curves are reduced by aging for long times (60 minutes or greater) at temperatures as low as 80° below T_g as long as the maximum applied stress is above the heat-degraded static strength level. It stands to reason, then, that one might expect to see such changes in elevated temperature fatigue tests.

Case [30] studied the effects of elevated temperature on the residual strength and stiffness of IM7/K3B notched and un-notched composites. The change in matrix properties with temperature was evident from the decrease in transverse strength and stiffness properties from that at room temperature. During fatigue, a greater phase lag was observed between applied load and material response in elevated temperature specimens (177°C) than in room temperature specimens. This increase in phase lag corresponds with a greater rate of energy dissipation that was attributed to the viscoelasticity of the material. The rate of damage progression was also observed to increase in elevated temperature specimens, though the damage modes remained the same.

Obst et al. [10] evaluated the microcracking behavior of an AS4/PR500 (T_g = 200°C) five-harness satin weave. Testing conditions included static and fatigue testing at room temperature and 120°C, among others. Static test data revealed that specimens tested at 93°C exhibited higher initial crack strains and lower overall crack densities. This behavior was related to temperature induced residual stress relief. In fatigue, the crack density at 121°C developed faster than at room temperature though the actual crack density was lower. In addition, interlaminar shear strength, as measured by short-beam four-point bend tests, was 23% lower at 121°C than at room temperature. This result could explain the lower crack density as a lower interlaminar shear strength corresponds to longer ineffective lengths.

Loverich et al. [31] performed fatigue tests on unidirectional carbon fiber reinforced PPS composites (T_g = 130°C) at room temperature and at 90°C. The elevated temperature fatigue life data was found to lie between elevated temperature stress rupture data and room temperature fatigue data. While no specific fatigue damage mechanisms were studied in detail, a residual strength based life prediction methodology was employed which used room temperature fatigue data and elevated stress rupture data with good results. Thus, the study shows that the time at temperature dependence of the material properties are important when considering elevated temperature fatigue.

Sjogren and Asp [32] studied the interlaminar toughness of the 0°/5° interface for a Hexcel carbon/epoxy composite subjected to tension-tension mechanical fatigue at elevated temperature (100°C). The double cantilever beam (DCB) test was used to evaluate pure Mode I loading, the end notched flexure (ENF) test to evaluate pure Mode II loading, and a mixed-mode bending test (MMB) to evaluate a combination of Mode I and Mode II loading. In the study, the strain energy release rate at crack growth was taken to represent the interlaminar fracture toughness. The testing revealed that the strain energy release rate threshold values for delamination growth were significantly affected by fatigue loading (in comparison to static testing) and that, depending on the loading mode, the values at elevated temperature were 30-50% lower than those at room temperature. These results indicate that one might expect to find increased delamination during fatigue for those specimens tested at elevated temperature than for those tested at room

temperature. Despite the finding, fracture surfaces for specimens tested at room temperature and elevated temperature were similar for all loadings except for Mode II static loading. No explanation was investigated for the deviation in Mode II static loading.

2.3 Moisture/Temperature Interaction

Various studies examine the effect of the moisture/temperature combination on composite tensile strength and modulus. Almen et al. [33,34] presented results showing degradation of a variety of carbon fiber reinforced epoxy woven composite properties in hot/wet environments. Shen and Springer [15] found moisture related degradations in tensile strength and stiffness of 0° and 45° carbon/epoxy composites to be independent of temperature. On the other hand, tensile properties of 90° laminates were significantly affected by moisture and temperature. Significant degradation in transverse strength of a carbon/epoxy composite with moisture and temperature was also found by Browning et al. [35]

The work done to date in examining the effect of the combination of moisture and temperature on the durability and damage of carbon fiber polymer matrix composites has been quite limited. Karasek et al. [36,37] performed a study on the influence of moisture and temperature on the impact resistance of graphite/epoxy composites. They found that damage initiation energy decreased with temperature due to reduced matrix properties with temperature. Also, while moisture individually was found to have no effect on damage initiation energy or subsequent energy absorption at ambient temperatures, the influence of moisture at elevated temperatures was significant and dependent on the matrix behavior and wet glass transition temperature of the matrix. The damage initiation energy of a composite consisting of unmodified epoxy increased with moisture at elevated temperature, while that of toughened epoxy decreased with moisture at elevated temperature.

In examining the nature of the damage, the authors found that moisture exposure in general does result in a decrease in the number of delaminations and matrix cracks after impact, indicating that the energy absorption per unit area of damage is higher in the wet state than in the dry state. This result is consistent with the idea that the strain energy release rate increases with moisture.

On the other hand, it was also found that the number of delaminations and matrix cracks increased with temperature (dry), which is consistent with a reduction in strain energy release rate with temperature. In the case of including moisture at elevated temperature, the number of delaminations and matrix cracks decreased. These changes in behavior were generally attributed to plasticization and increased ductility in the matrix, as well as degradation of properties.

A number of studies have been performed to determine how hygrothermal environments affect the strain energy release rates of carbon/epoxy composites. A review of these is given by Asp [38]. The combined results of the studies point to an ambiguity as to the effects of moisture and temperature on strain energy release rates, implying that each carbon/epoxy system must be examined individually.

2.4 Literature Review Conclusions

A good deal of literature exists characterizing the effect of temperature and moisture on static mechanical properties of carbon/epoxy composites. However, these effects vary between material systems and thus must be determined on an individual material basis. In considering moist environments, much information can be learned just from examining moisture uptake curves, where the nature of the curve may reveal whether or not material degradation is taking place of an either reversible or irreversible nature. Aside from obvious problems such as material leeching, general issues to be cognizant of are strength and stiffness changes, particularly in $[90]_n$ laminates, as well as the build up of hygrothermal residual stresses and interfacial degradation. In regards to fatigue and durability, it is important to consider the effects of damage on moisture uptake and subsequently the effects of moisture absorption on material properties. Other factors include viscoelastic effects, particularly at elevated temperature, and the effects of material property degradation and other material changes with temperature and moisture on fatigue damage.

The results of the studies discussed above were used to guide the experimental efforts of the current study. In Chapter 3, the experimental plan, methods, and results are discussed. In addition, an investigation into the inclusion of environmental effects in analytical models, a topic which was not found to be well discussed in the literature to date, was conducted. The analytical

plan, methods, and results are given in Chapter 4. A summary and list of conclusions for the current study is given in Chapter 5, while suggestions for future work and a list of references are provided in Chapters 6 and 7, respectively.

3 EXPERIMENTAL TESTING AND RESULTS

In this chapter, the experimental phase of the study will be discussed in detail. Discussion will include an overview of the general experimental plan (Section 3.1), a description of the experimental methods used in carrying out the experimental plan (Section 3.3), and a presentation of the experimental results (Section 3.3.5.1). Finally, a summary of experimental results will be given in Section 3.4.

3.1 Experimental Plan

The goal of the experimental effort was to characterize the effect of temperature and moisture, individually and combined, on the resin, ply, and laminate level for a carbon/epoxy composite. More specifically, the following information was sought from the respective constituents:

1) resin – moisture absorption behavior, shear strength and shear modulus as functions of temperature and moisture, glass transition temperature as a function of moisture content
2) transverse (90°unidirectional) laminate – strength and stiffness as functions of temperature and moisture
3) cross-ply laminate – moisture absorption behavior, glass transition temperature as a function of moisture content, and strength, stiffness, and fatigue life and damage as functions of temperature and moisture

All mechanical testing was conducted on MTS servohydraulic load frames. Cross-ply tension-tension (R=0.1) fatigue tests were carried out at 10 Hz under the following conditions:

1) Dry, room temperature
2) Dry, elevated temperature: 125°C
3) Dry, pre-saturated (in 65°C water) specimens tested at room temperature
4) Dry specimens tested immersed in water at room temperature and 90°C

Note that the “pre-saturated” description refers to virgin specimens which, prior to testing, were immersed in water (unstressed) until moisture saturation was achieved. All composite laminates

tested were 4-ply laminates. Cross-ply laminates were layed up as $[0/90]_s$. The thin laminates allowed for relatively rapid moisture saturation times (resulting in uniform moisture distribution through the thickness) for pre-saturated specimen testing, and they also allowed for ease of damage assessment.

3.2 Material

The material used in this study consisted of T300 fiber reinforced with F593 toughened epoxy resin. The material was received from Hexcel in the form of prepreg tape and was layed up and consolidated at Virginia Tech at the fabrication lab in the Center for Composite Materials and Structures. Neat F593 resin was also obtained from Hexcel for testing.

It should be noted that, as disclosed by the manufactured, the prepreg received was actually "non-spec" in nature in that it was of lower viscosity than the commercially sold variety. This tended to make the prepreg excessively tacky and difficult to handle. While the expectation was for the material behavior to be minimally affected, if at all, in actuality the material was quite difficult to process. The excessively tacky nature of the prepreg made cleanliness and proper alignment of the individual plies during layup difficult to maintain. While these issues most likely did affect the composite properties overall, properties of each panel were found to be consistent. However, inconsistency across different panels was found to be problematic, particularly since the adverse behavior of the prepreg was exacerbated over time despite the fact that it was stored in the recommended refrigerated conditions. .

3.3 Experimental Methods

3.3.1 Composite Specimen Fabrication

Composite panels were layed up from the prepreg tape and cured in a hot press with a cure schedule as follows:

1) Apply vacuum and touch pressure of 15 psi
2) Ramp temperature up to 355°F at a rate of 5° F/min.
3) Apply pressure of 85 psi at 270°F.
4) After hold, release pressure and allow laminate to air cool to room temp.

This cure schedule was slightly modified for panels cured towards the end of the study. As mentioned previously, the prepreg appeared to age with time. Because it was thought that this condition would decrease the gel point, the temperature at which the higher pressure was applied was decreased to 260°F.

Upon curing, specimens were cut and ground in the ESM machine shop with a wet diamond saw. Unidirectional specimens were cut to a length of 6 inches and a width of 0.5 inches, while cross-ply specimens were cut to a length of 8 inches and a width of 1 inch. Specimens were then post-cured for 24 hrs at 250°F.

3.3.2 Thermal Analysis

The main material thermal parameters of concern are generally glass transition temperature, the coefficients of thermal expansion (CTE), and stress-free temperature. Glass transition temperature tends to dictate upper limits on use temperature and CTE's and stress-free temperature are necessary to assess laminate strain and strain at temperature. The methods used in this study for determining these values, as well as the results, are described below.

3.3.2.1 Glass Transition Temperature

Glass transition temperature was determined by DMA. Temperature scans (2°C/min) were performed in flexure mode on a TA Instruments 983 DMA system, with the glass transition temperature indicated by the peak in the phase angle,δ.

3.3.2.2 Coefficients of Thermal Expansion

The coefficients of thermal expansion (CTE) of the unidirectional composite material as well as the resin were determined with expansion data acquired by a linear dilatometer (Netzsch Dilatometer 402C). A $[0]_4$ laminate specimen was used to determine the composite axial CTE, α_1, and a $[90]_4$ laminate specimen was used to determine the composite transverse CTE, α_2. Results are shown in Figure 3.1, Figure 3.2, and Figure 3.3.

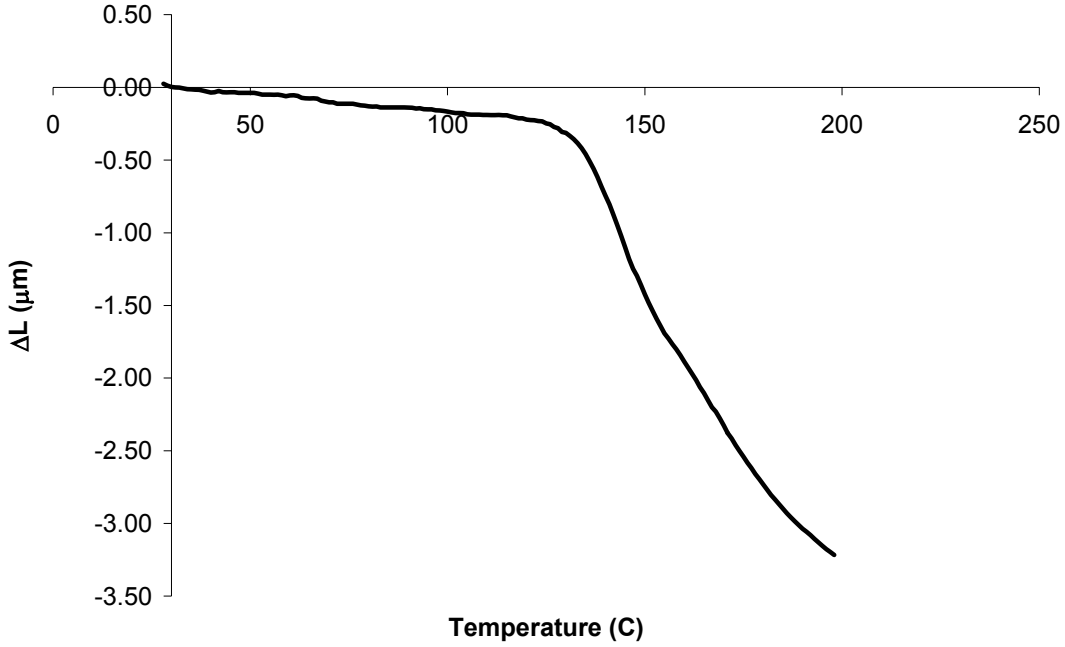

Figure 3.1: 0° Specimen dilatometer results

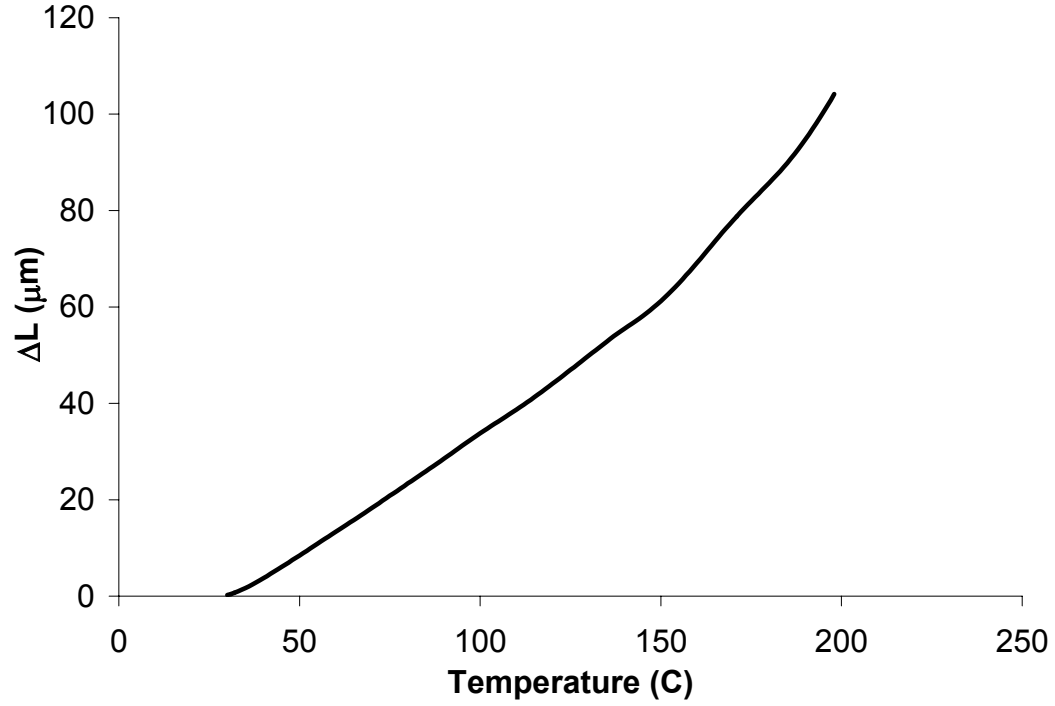

Figure 3.2: 90° Specimen dilatometer results

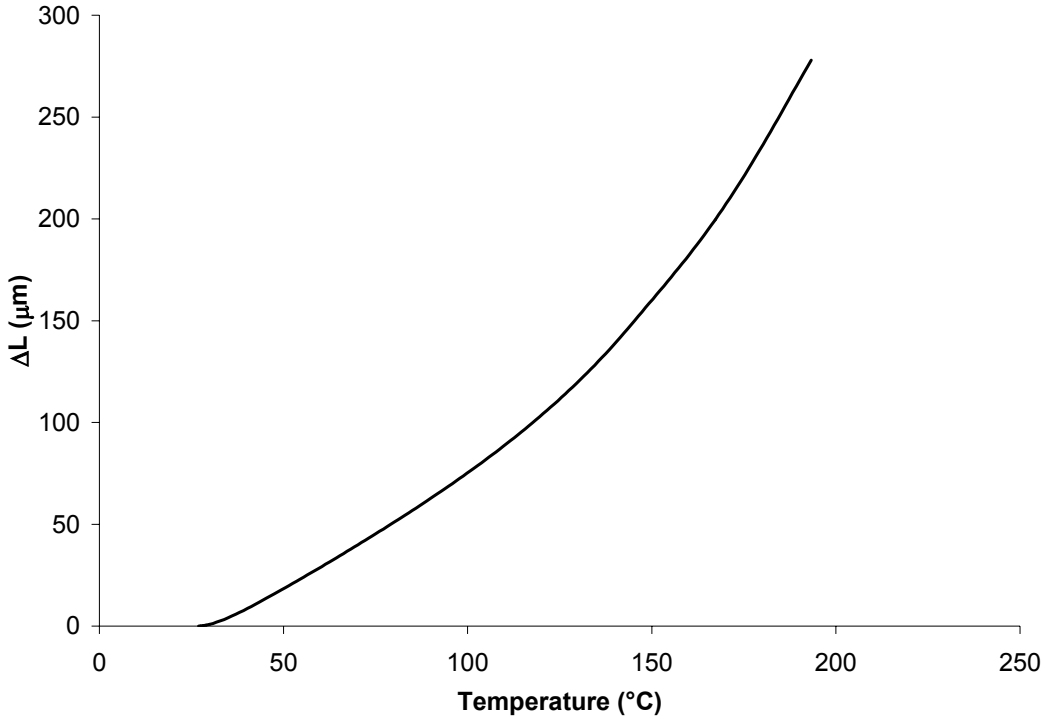

Figure 3.3: Neat resin dilatometer results

As can be seen from the data, both the axial and transverse expansion curves are bilinear, so the coefficients of expansion were determined by calculating moduli at temps below and above the knee ($\alpha = \frac{\Delta L}{L \Delta T}$). However, in the case of the resin, the expansion curve is quite nonlinear, so a curve was fit to the data and the derivative taken to establish the CTE as a function of temperature. The numerical results are given in Table 3.1.

Table 3.1: CTE results

Composite α_1 (/°C)	-2.30×10^{-7} < 130°C, -1.54×10^{-6} >130°C
Composite α_2 (/°C)	4.08×10^{-5} < 155°C, 6.32×10^{-5} > 155°C
Neat Resin Thermal Expansion (with T in °C)	2.66E-08 $T^2 - 3.12 \times 10^{-7}$ T + 7.94×10^{-5}

3.3.2.3 Stress-Free Temperature

Because of the mismatch in coefficients of thermal expansion (CTE's) between plies, a $[0_m/90_n]$ laminate (in this case a $[0_2/90_2]$ laminate was used), will have a significant curvature upon cool down from the stress-free temperature during the curing process. When the laminate is heated back up the process is reversed - the thermal stresses decrease and thus, the specimen is expected to flatten out at as the temperature reaches the stress-free temperature. Thus, in order to obtain the value of the stress-free temperature for the material in this study, antisymmetric cross-ply laminates ($[0_2/90_2]$) were layed up, cured, and cut into 8 inch long by 1 inch wide specimens. While the panel was curved in both directions, the aspect ratio of the cut specimens made the curvature along the specimen length much more prominent.

Theoretically, the stress-free temperature could be obtained by calculating the expected strain at the peak of the curved specimen prior to heating as well as monitoring strain during the heating process. The temperature for which the negative of the calculated strain is reached is the stress-free temperature. However, an attempt to use this method proved unsuccessful. According to the strain measurements made, the stress-free temperature was determined to be under 100°C. Since the specimen was still visibly curved at temperatures above and beyond 100°C, it was clear that the stress-free temperature measured in this way was inaccurate. Thus, the value of the stress-free temperature was obtained by simply observing the specimen during the heating process and noting when the specimen appeared to reach a flat state. This temperature was determined to be approximately 155°C.

3.3.3 Moisture Absorption

The merit of obtaining moisture absorption data was discussed in Section 2.1.1. Specimens that were to be tested in the "pre-saturated" condition were allowed to soak in a water (tap water) bath at 65°C. Prior to immersion, specimens were dried in an oven for 24 hours at 120°C. Weight gain was monitored by periodically removing representative specimens from the water bath and recording their weights. Three representative samples were chosen randomly from each set of specimens immersed. Percent moisture absorption was calculated as:

$$\%M = \frac{Weight_{wet} - Weight_{dry}}{Weight_{dry}} \text{ x } 100 \quad (1)$$

3.3.3.1 Moisture Absorption Results

The moisture absorption curves of unidirectional ($[0_6]$) and cross-ply laminates, as well as neat resin, are given in Figure 3.4. The corresponding diffusion coefficients and maximum moisture contents are given in Table 3.2. The diffusion coefficients were calculated by assuming 1-D Fickian absorption and solving the following equation (from Shen and Springer [39]) for *D*:

$$M = \frac{4M_m}{h}\left(\sqrt{\frac{t}{\pi}}\sqrt{D}\right) \quad (2)$$

where M is the moisture content of a specimen of initial thickness h at any given time t, M_m is the saturation moisture content of the material, and D is the diffusion coefficient. Specifically, the diffusion coefficient was solved for by calculating the initial slope of the curve obtained by plotting $\left(\frac{M}{M_m}\right)^2$ versus $\frac{t}{h^2}$ and multiplying the slope by the factor $\frac{\pi}{16}$. The specimen thickness *h* in this case was nominally 0.032 inches. As mentioned in Section 3.3.1, unidirectional specimens were 0.5 inches wide and the cross-ply specimens were 1 inch wide.

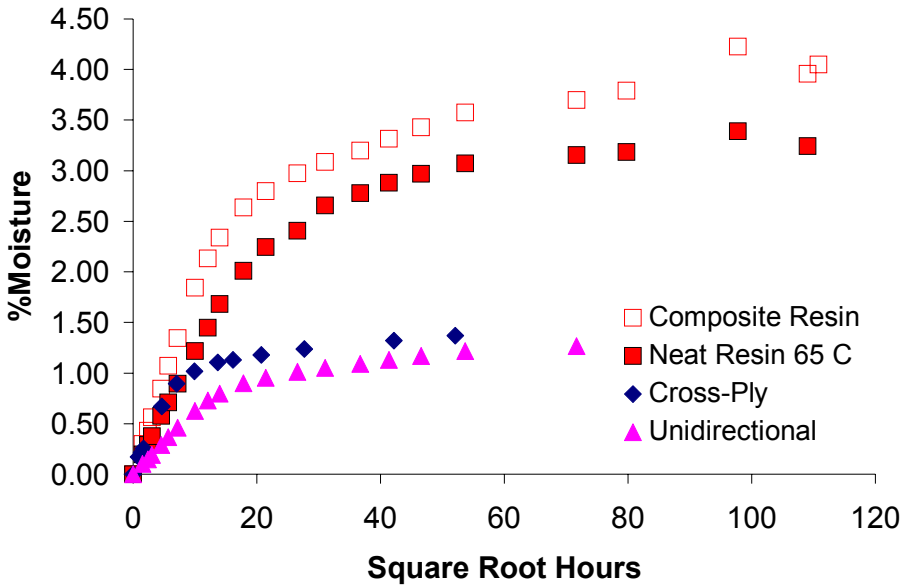

Figure 3.4: Moisture absorption data

Table 3.2: Moisture absorption parameters at 65°C

Specimen type	Diffusion Coefficient (D) (cm^2/s)	Maximum Moisture Content (%)
Neat Resin	8.48×10^{-9}	3.24 ± 0.02
Unidirectional laminate	1.73×10^{-9}	1.39 ± 0.02
Cross-ply laminate	3.15×10^{-9}	1.37 ± 0.03
Composite Resin	1.76×10^{-9}	4.05 ± 0.02

The data points labeled "composite resin" represent the moisture uptake of the resin within the composite and were calculated using the unidirectional composite fiber volume fraction (53%) and assuming all the moisture in the composite was absorbed by the matrix. One item of note is that the cross-ply laminate data exhibit a higher diffusion coefficient than that of the unidirectional laminate. Another item of note is that the "composite resin" appears to have a higher diffusion coefficient and moisture content than the actual neat resin. While these results have not been extensively investigated, it may be postulated that wicking along the fiber or processing induced differences may play a role in both results.

The fact that the curves are strictly monotonic suggests that materials degradation is not a factor; however, the extent to which moisture absorption slows down also indicates minimal, if any, interfacial degradation. Finally, the lack of a plateau indicates non-Fickian behavior. Such results are typical for carbon/epoxy composites [40,41].

One of the most obvious ramifications of moisture absorption for all the materials is the decrease in glass transition temperature, T_g. The T_g versus moisture concentration results from this study are given in Figure 3.5. One interesting result is the linear nature of the T_g decrease with moisture content. The behavior of the neat resin is modeled quite accurately by the Fox equation, a rule-of-mixtures type representation: $\frac{1}{T_g} = \frac{w_A}{T_{g_A}} + \frac{w_B}{T_{g_B}}$ where, in this case, w_A is the weight fraction of water, w_B is the weight fraction of the resin (1- w_A), T_{gA} is the glass transition temperature of water (-130°C), and T_{gB} is the glass transition temperature of the resin (172°C).

While it appears from the data labeled "Composite Data" that the composite samples suffer a greater decrease in T_g with moisture than the neat resin, it should be noted that the weight fraction of water in the composite is calculated by considering the total composite (fibers and resin). Since the resin dominates the T_g value, one must consider the weight fraction of water in the resin portion of the composite. If this is done (see "Composite Resin Data" in Figure 3.5), it can be seen that the composite actually fares better than the neat resin. Upon drying, the glass transition temperatures of the neat resin and composites rebound to the dry values.

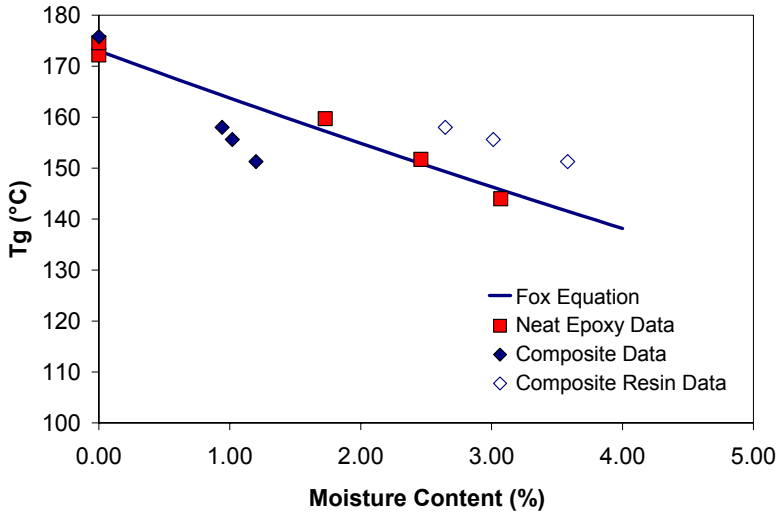

Figure 3.5: Glass transition temperature with moisture

3.3.4 Determination of Coefficients of Moisture Expansion

Determination of the coefficients of moisture expansion (CME), β_1 and β_2, is based on basically the same ideas as that involved in determining the stress-free temperature. Again, consider a $[0_m/90_n]$ laminate and recall that such a laminate will exhibit a curvature upon cool down from curing due CTE mismatch and the resulting build up of thermal stresses. Introducing moisture into such a laminate can similarly result in hygric stresses as the coefficients of moisture expansion are also mismatched between plies. However, the hygric stresses act in a way that counterbalance the thermal stresses, resulting in a flattening effect for the antisymmetric laminate. The methodology developed by Tsai et al. [42] makes use of this phenomenon. The combination of experimental measurements of curvature and curvature predictions given by classical lamination theory give rise to a set of equations which may be solved for the CME's in both the axial and transverse ply directions. Theoretically, the method could also be used to determine the stress-free temperature simultaneously with the CME's; however, the calculated value (133°C) did not agree with the observational experiment run to determine the stress-free temperature (Section 3.3.2.3) and was discarded in favor of the value found previously (155°C).

In addition to curvature versus time of immersion data (discussed in more detail below), the inputs required in this method are given in Table 3.3 for a $[0_m/90_n]$ laminate.

Table 3.3: Table of inputs for coefficients of moisture expansion calculation

Notation	Value	Description
E_1	17.3 msi	Unidirectional axial modulus
E_2	1.27 msi	Unidirectional transverse modulus
ν_{12}	0.31	Unidirectional Poisson's ratio
D	4.4×10^{-10} cm^2/sec	Laminate moisture diffusion coefficient
M_{max}	1.4 %	Saturation moisture content
α_1	-2.30×10^{-7}/°C	Unidirectional axial coefficient of thermal expansion
α_2	4.08×10^{-5}/°C	Transverse coefficient of thermal expansion
ρ	62.4 lb/ft^3	Immersion fluid (water) specific weight
h	.032 in	Ply thickness
T_{ref}	27°C and 65°C	Reference temperature

All material properties are calculated at room temperature while moisture absorption parameters correspond to the reference temperature.

As mentioned above, the method requires curvature data as a function of moisture immersion time. The radius of curvature was measured initially before immersion into the water tank and then periodically after immersion. To make the measurements, the shape of the specimen was simply traced onto a sheet of paper and the distances *d* and *2a*, as shown in Figure 3.6, measured directly with a ruler. The radius of curvature, *R*, could then be calculated using geometry (assuming that the curvature forms part of a circle):

$$R = \frac{a}{Sin\left(2\,ArcTan\left(\frac{a}{d}\right)\right)} \tag{3}$$

and the curvature obtained simply by inverting *R*. In Figure 3.7, radius of curvature data is plotted as a function of immersion time.

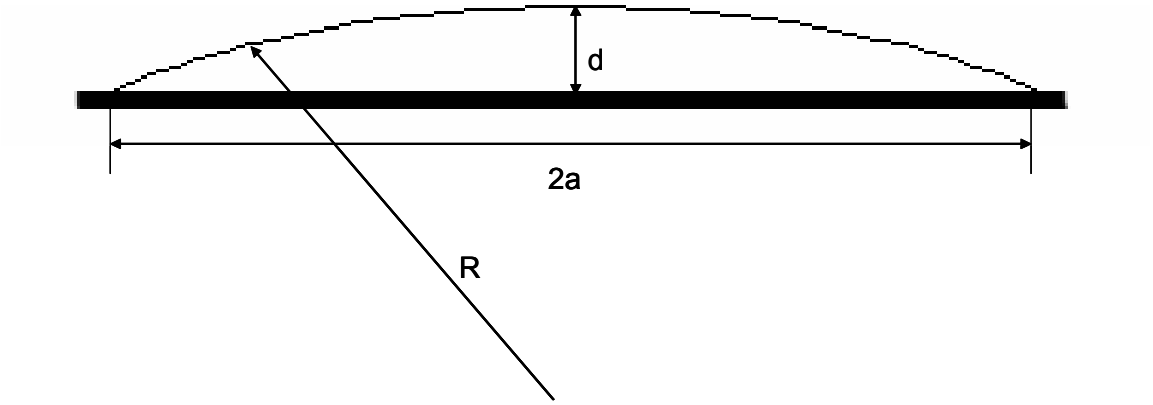

Figure 3.6: Curved specimen geometry

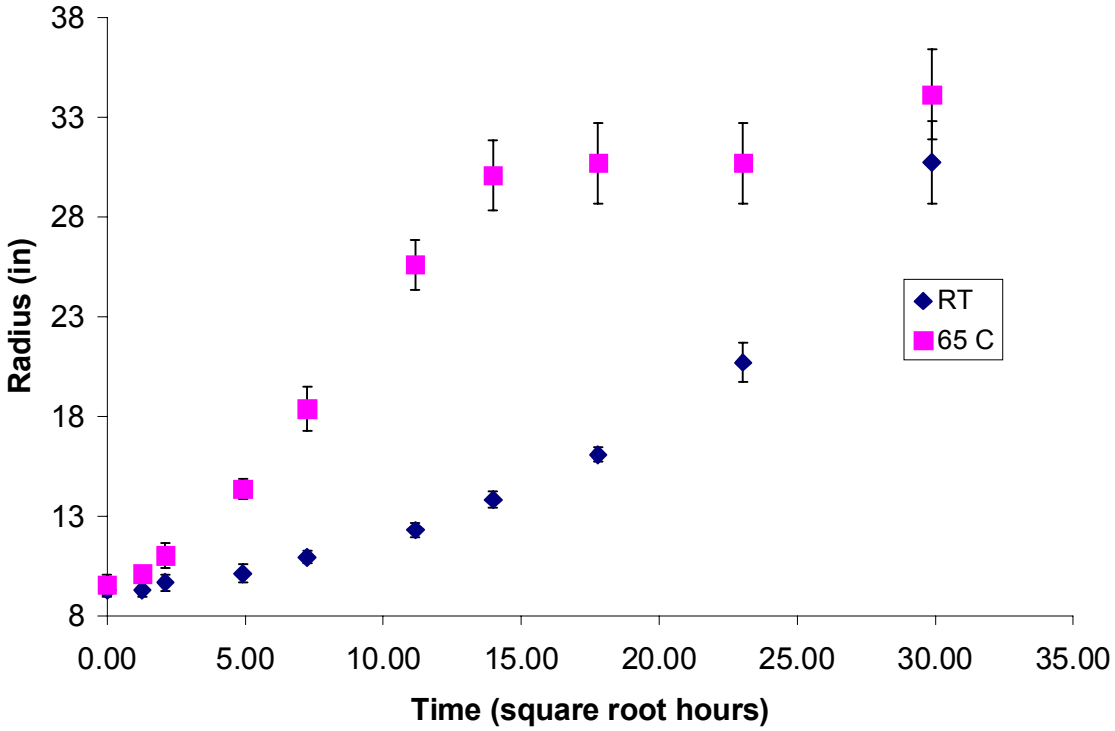

Figure 3.7: Radius versus immersion time

The CME's calculated from the analysis are:

β_1 = .00016 / %M

β_2 = .00186 / %M

3.3.5 Mechanical Testing

Quasi-static and fatigue testing was conducted in load control on MTS servohydraulic test frames. Quasi-static tests on 0° and cross-ply composite samples were loaded at 80 lbs/sec, while analogous tests on resin samples and transverse composite samples were loaded at 5 lbs/sec. Fatigue tests were carried out at 10 Hz with an R-ratio of 0.1. All data was acquired using a custom LabView based data acquisition software.

Elevated temperature tests were conducted within an environmental chamber (see Figure 3.8) which enclosed the entire specimen, thus eliminating temperature gradients along the test section. Samples were allowed 10 minutes to reach temperature prior to testing. Immersed fatigue was achieved by fitting the gage section of specimens with a plexiglass fluid cell (Figure 3.9) through which fluid is circulated with the use of a water pump with heating capabilities. In the case of elevated temperature immersed fatigue, the specimen was heated in the environmental chamber in addition to having heated water circulated through the fluid cell.

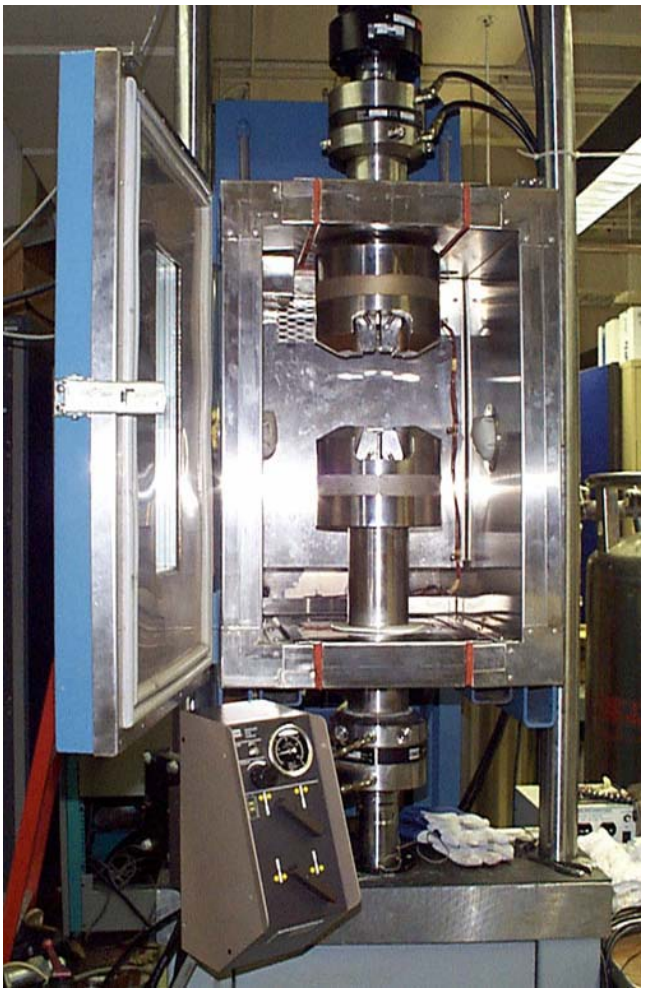

Figure 3.8: Environmental chamber

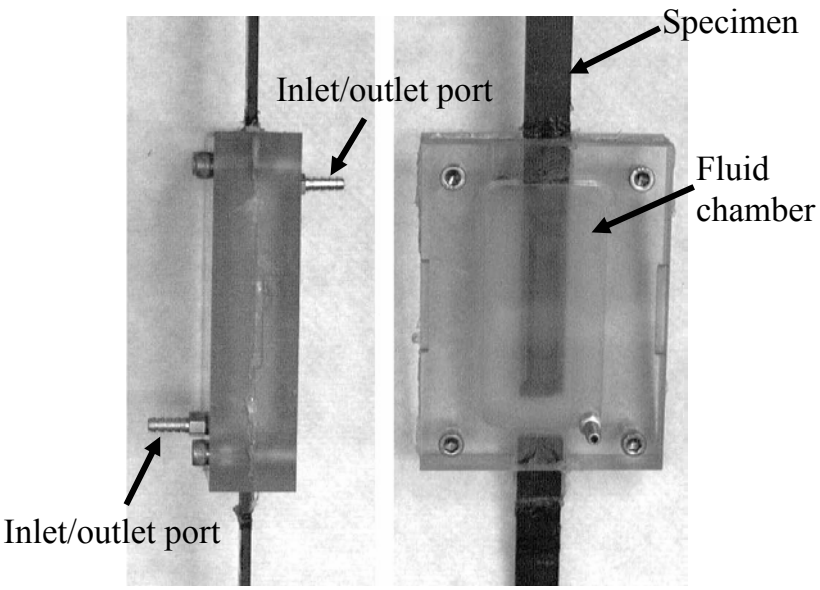

Figure 3.9: Fluid cell configuration

Stiffness measurements were taken by using either a 1 inch gage length MTS extensometer or a Vishay Micromeasurements CEA-06-125UW-350 type strain gage. In the case where an extensometer was used, the knife edges of the extensometer were mounted on the specimen by way of V-notched aluminum tabs that were centered and bonded to the specimen using GE silicone adhesive. The extensometer was mounted to the aluminum tabs with rubber bands. Strain gages for room temperature testing were bonded to the specimens using M-bond 200, while those for elevated temperature testing were bonded using M-bond 600. In addition, for elevated temperature testing, "dummy" specimens were used for temperature compensation. The dummy specimen consisted of a strain gage bonded to an unstressed sample of material that was placed in the test chamber with the test specimen. All strain gaged specimens were connected to a Wheatstone bridge circuit, and for the elevated temperature, the dummy gage was also inserted into the Wheatstone bridge (as shown in Figure 3.10). Note that for room temperature testing, the dummy gage in the circuit is replaced with a 350-ohm resistor. Both the wheatstone bridge and extensometer signals were connected to an amplifier and acquired using Labview software.

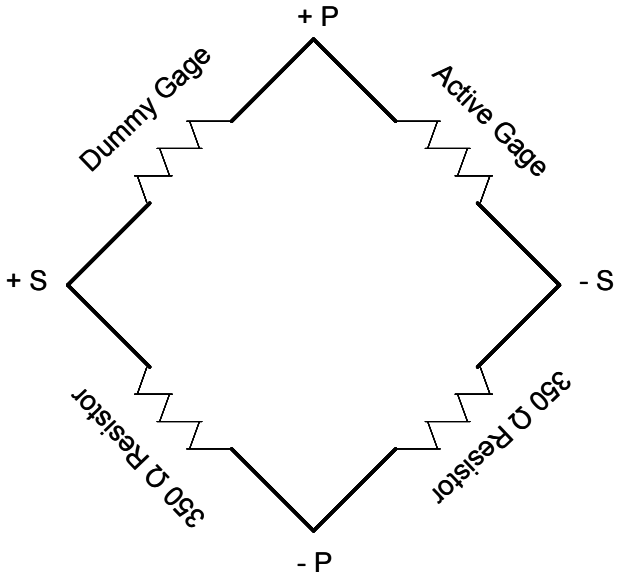

Figure 3.10: Wheatstone bridge used for elevated temperature testing

Specimens were endtabbed for gripping in the test frame such that a 3 inch gage length was left. The tabs consisted of a steel woven wire cloth (100 x 100 linear inch mesh with 0.0045 inch wire diameter, obtained from McMaster Carr) overlaid with a soft aluminum.

3.3.5.1 Mechanical Testing Results

Experimental results were used to both guide the direction of the ensuing modeling work as well as validate the analytical models. Quasi-static testing results (Section 3.3.6) and fatigue results (Section 3.3.7) are described below.

3.3.6 Quasi-Static Test Results

The variation of matrix and transverse laminate modulus with temperature and moisture is given in Figure 3.11. The role of matrix shear modulus is determining overall composite strength is discussed in Section 4.1. The transverse composite modulus is also important in predicting laminate stiffness for other laminate structures as well as for computing residual thermal and hygral stresses. All modulus data presented in this section were obtained using the portion of the

tensile stress-strain curve extending from 0.1% to 0.3% strain as measured by strain gage. For the resin, both the axial and transverse strains were measured during loading to facilitate the calculation of shear modulus. Assuming isotropic properties, the resin shear modulus, G, could be calculated as $G = \frac{E}{2(1+\nu)}$, where E is the axial modulus, and ν is the Poisson's ratio. Results from this study and others [43] indicate that the Poisson's ratio does not change with temperature. In this case, the Poisson's ratio value is approximately 0.45. Thus, the change in resin shear modulus with environment is directly proportional to the change in axial modulus.

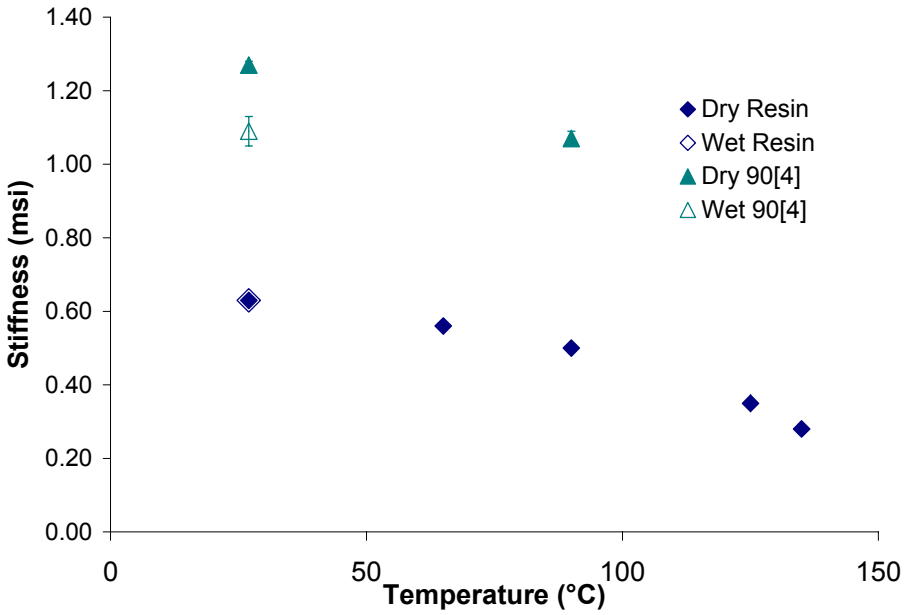

Figure 3.11: Matrix modulus variation with temperature

While each plotted point represents the average of at least two data points, in most cases the errors are very small and do not show up on the plot. The data show that the modulus of the resin and transverse laminate reduces significantly, even at temperatures well below the T_g. One interesting result is that the transverse laminate modulus appears to be noticeably reduced with moisture, while that of the resin is not. This result may be caused by processing induced differences.

The tensile strengths of the matrix and of the transverse laminates ($[90]_4$) as a function of temperature, wet and dry, are given in Figure 3.12. The roles of the matrix shear strength and transverse tensile strength in modeling efforts are discussed in detail further on in Sections 4.1.1 and 4.2.2.1 Because the matrix shear strengths are difficult to measure, they will be assumed to be directly proportional to the tensile strength. The results show that in case of the resin, the temperature initially causes an increase in strength, but ultimately the strength decreases. The addition of moisture appears to have little effect on the strength at room temperature, but causes a significant reduction at 90°C. On the other hand, in the case of the transverse laminate, the strength decreases monotonically with temperature and moisture causes a significant reduction in strength even at room temperature. No yielding behavior was observed in either the matrix or the transverse laminate.

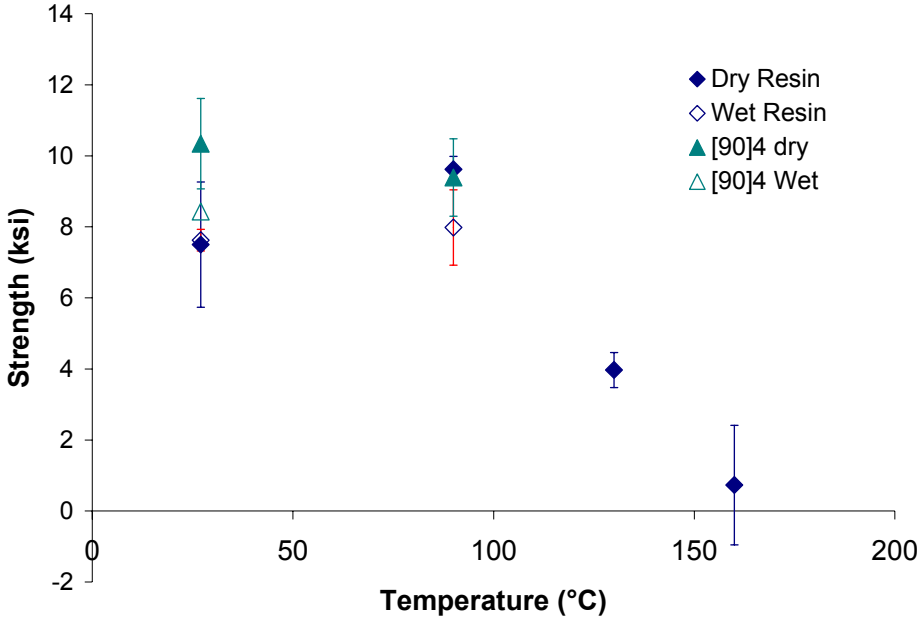

Figure 3.12: Matrix and transverse laminate strength variations with temperature and moisture

Finally, composite strength as a function of temperature and moisture is given in Figure 3.13. The unidirectional results are normalized by room temperature strength. The cross-ply results represent the value obtained when the load to failure is divided by the area of the 0° plies in the laminate. In this case, that area is half of the total area. Those results are normalized by the

room temperature value. The actual average strength value of the unidirectional laminate is 254 ± 28 ksi and that of the cross-ply laminate (using total area) is 129 ± 6.31 ksi.

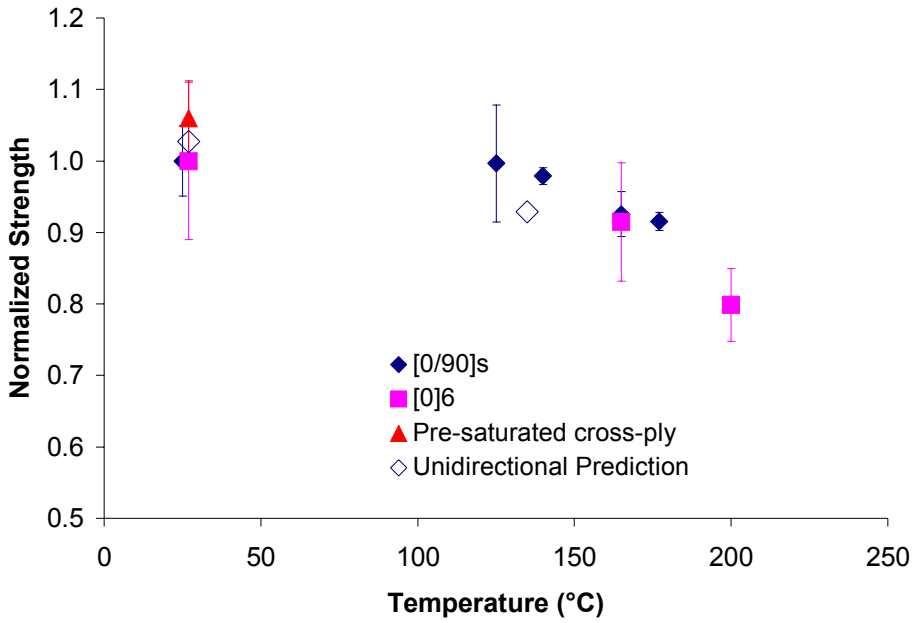

Figure 3.13: Composite strength with temperature and moisture

As expected, the cross-ply laminates and unidirectional laminates vary with temperature in much the same way, with noticeable reductions in strength taking place approximately 20° below T_g. The average strength of the pre-saturated cross-ply, 136 ± 6.8 ksi, is 6% higher than that of dry samples. Since, upon drying, the strength returns to the dry sample strength, it is likely that the increase in strength with moisture is due to the moisture induced relief of thermal residual cure stresses. Indeed, a classical lamination theory analysis supports such an assumption, as discussed in Section 4.1.3.

3.3.7 Fatigue Results

Fatigue results for the various environments, described in Section 3.1, are given in Figure 3.14-Figure 3.16. Because of scatter in the test data, a common result in composite fatigue, statistical analysis was used to determine whether differences exist between the various data sets. A spreadsheet provided with the unofficial MIL Handbook 17 [44] performs the Anderson-Darling

statistical analysis determines the probability that input data sets are the same or different with 95% confidence. The analysis indicates the following results:

1) Dry fatigue at 125°C results in lower fatigue lives for fatigue at both 80% and 85% of the ultimate tensile strength (UTS) than for fatigue at room temperature.
2) There appears to be no difference between dry fatigue of dry samples at room temperature and dry fatigue of pre-saturated samples at room temperature.
3) Results for immersed fatigue are ambiguous. Immersed fatigue at room temperature at 85% UTS exhibits results in lower fatigue lives than dry fatigue at room temperature at 85% UTS. However, no such difference exists at 80% UTS at room temperature.

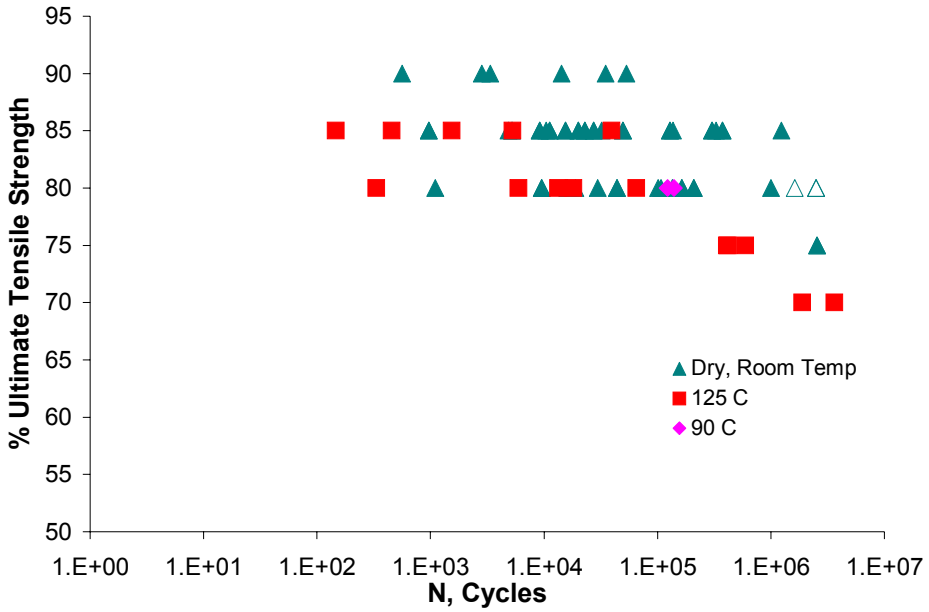

Figure 3.14: Fatigue life results – dry, elevated temperature results versus dry, room temperature results

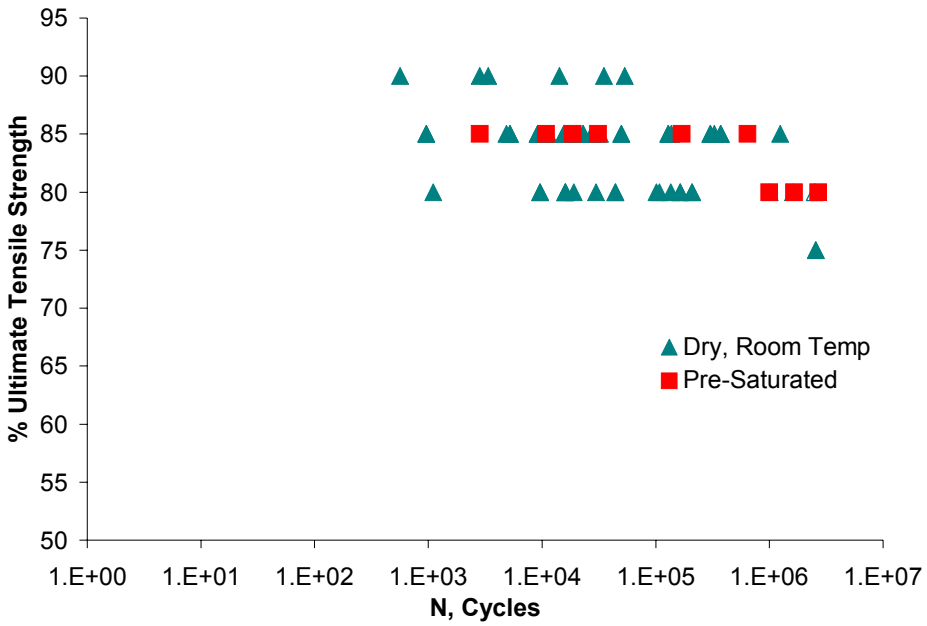

Figure 3.15: Fatigue life results – Pre-saturated, fatigued in air results versus dry, room temperature results

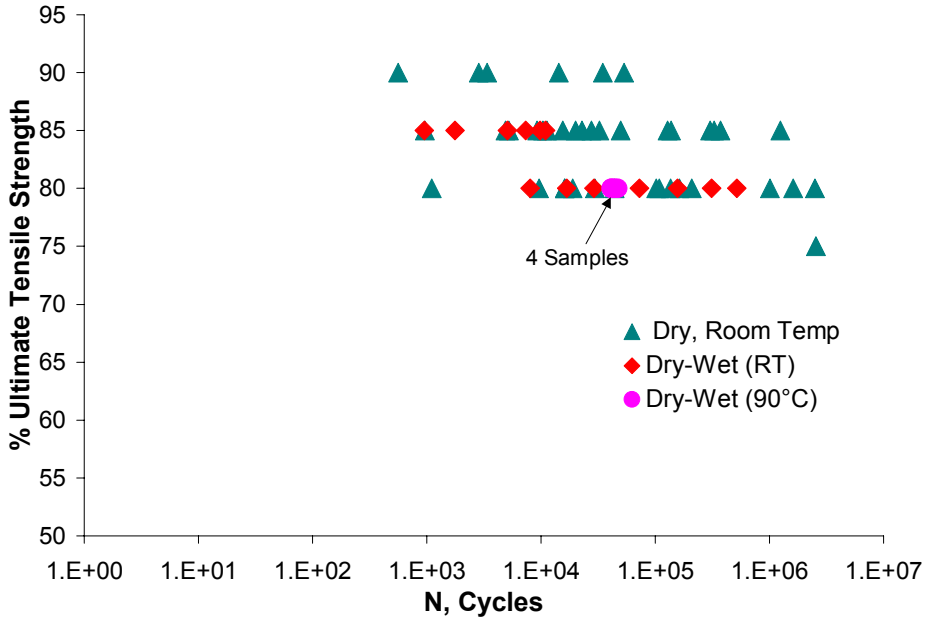

Figure 3.16: Fatigue life results - Dry, immersed fatigue at room temperature and at elevated temperature results versus dry, room temperature results

In general, no differences in fracture surfaces were observed among the specimens tested under the different environmental conditions. Specimens that exhibited similar lifetimes also exhibited similar fracture surface patterns, no matter the test condition. Such a results suggests that the amount and effect of fiber fracture did not vary significantly among the different test conditions.

As mentioned above, scatter in fatigue data is common in carbon fiber composites. However, in this case, some of the scatter in the data is also attributed to the material problems discussed in 3.2. In addition, many difficulties were encountered with the test frame used for the majority of the testing, especially when operated at elevated temperature. The wedge grips were prone to coming off track and pinching the specimens in such a way as to cause failure at the grip and the grip housings were prone to coming loose and out of alignment.

3.3.8 Damage Assessment

The three forms of damage assessment used were scanning electron microscope (SEM) microscopy, radiography, and edge replication. The radiographs were used to assess environmental and loading induced crack density and delaminations, while SEM was used to explore finer details such as interfacial degradation. Edge replication was also used to determine crack density and was conducted in the following manner:

1. Unpolished specimens were loaded to a constant load of 80% UTS.
2. Using a syringe, a small drop of acetone was placed on an approximately 2 inch strip of acetate tape (11340 replicating tape manufactured by Ernest F. Fullam, Inc.). Before the acetone could gel on the tape, the "wet" section of the tape was held against the edge of the specimen, usually along the gage section. Thumb pressure was applied for approximately one minute.
3. The tape was peeled from the specimen and sandwiched between two microscope slides. The ends of the slides were taped together to keep the replica flat. Once in slide form, the replicas were viewed under a Nikon epiphot optical microscope with digital photographic capabilities.

The results of such a method have been found to be consistent across different test specimens despite the fact that the locations along the specimens from which the replications were taken and the amount of pressure applied in obtaining the replications could not be exactly duplicated.

Radiography was conducted using a cabinet X-ray system (Hewlett Packard 43805N Faxitron Series X-ray System). Surfaces and edges of specimens intended for radiography were coated with a zinc iodide solution (60 grams of ZnI_2 mixed in 10 ml each of water, isopropyl alcohol, and Kodak Photo-Flo 200) and left to "soak" overnight. The specimens were then X-rayed at 35 kVP for one minute and the film developed. Film negatives were scanned into the computer and magnified for clear imaging of the cracks.

3.3.8.1 Damage Assessment Results

Post-failure analysis provided some insight into how the various environments affect the fatigue behavior of the composites. Crack density at failure was determined by counting cracks as visualized with the aid of X-radiography of failed specimens. Cracks were counted over several 1-inch sections of each specimen and the results averaged to obtain single specimen results. Standard deviations from this procedure were generally only 1-2 cracks for each specimen. Examples of X-rays of specimens subjected to dry and wet fatigue are shown in Figure 3.17 and Figure 3.18. Examination of representative fatigue samples revealed that fatigue at temperature, wet or dry, tended to result in cracks that did not grow across the full width of the specimen. Also, only a minimal amount of delamination was observed for any of the fatigue conditions.

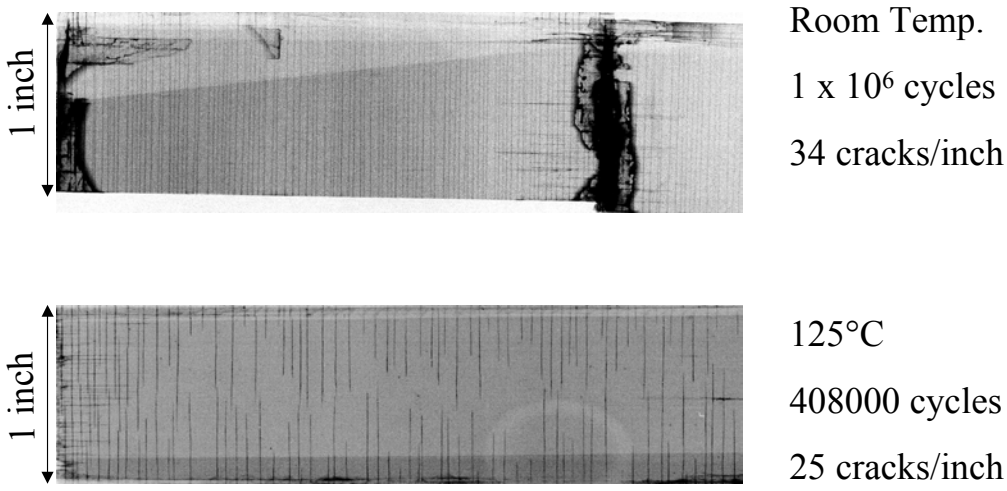

Figure 3.17: X-rays of failed dry fatigue specimens

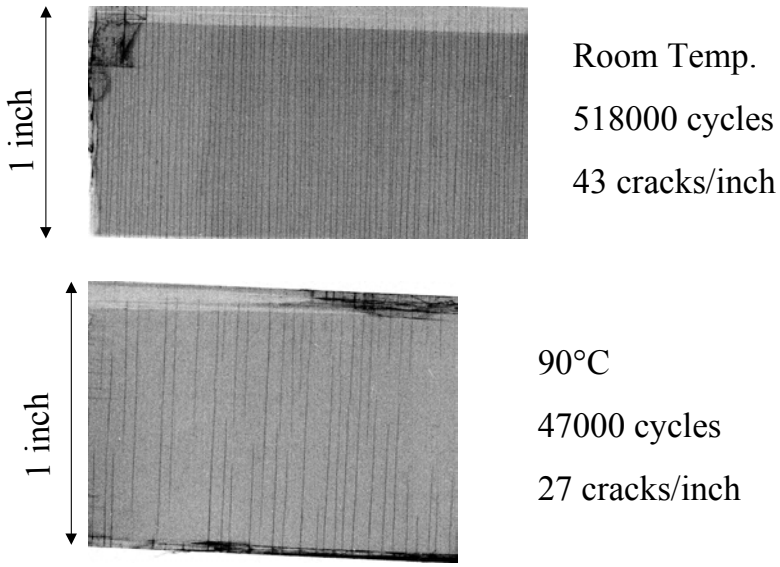

Figure 3.18: X-rays of immersed fatigue specimens

A quantification of the crack density results is given in Figure 3.19. Note that the percentage values in the legend refer to the maximum fatigue load in terms of percent of UTS. Results indicate that immersed fatigue at room temperature results in an increase in crack density while dry fatigue at 125°C results in a decrease in fatigue crack density.

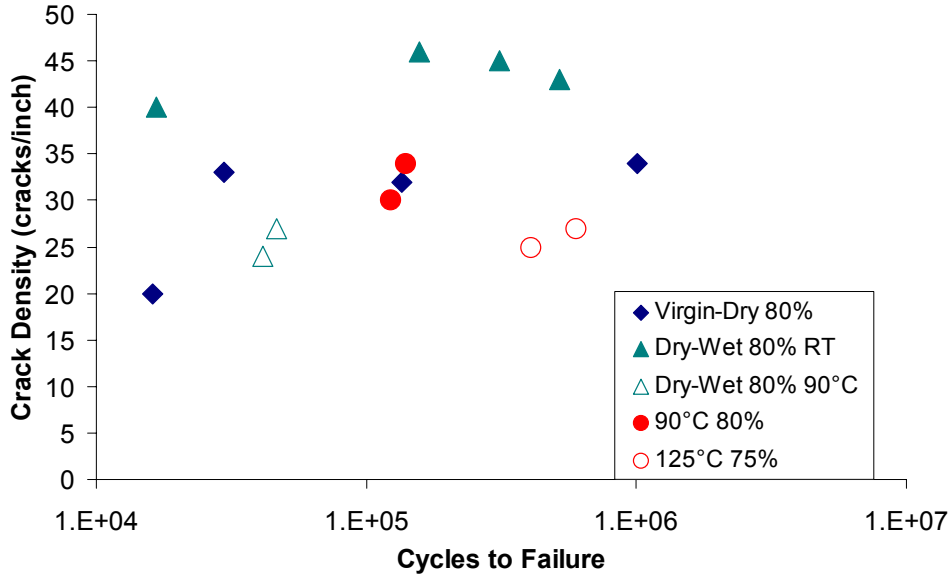

Figure 3.19: Fatigue crack density results

Other experimental results are presented in Chapter 4 for easy comparison with analytical results.

3.3.9 Edge Replication versus Radiography

The crack density results presented above are based on radiographic images. However, in later observing edge replication results, it became evident that the results did not agree with radiography results, but actually indicated higher crack densities. Moreover, the edge replica results exhibited no difference in the crack saturation densities among the different environmental conditions. Two possible explanations for this discrepancy in results between the two different methods are 1) the edge replica exhibits smaller edge cracks that either do not show up with radiography or are simply not counted due to size and 2) cracks show up better with edge replication due to the fact that the replicas are taken while the specimen is under tensile load and the cracks are opened.

The first theory seems somewhat unlikely since one would still expect to find a difference in the results among the different test conditions. To test the second theory, a specimen was fatigued and an edge replica performed. Subsequently, dye penetrant was applied and left to soak while the specimen remained under tensile load. The specimen was then radiographed. Results still indicated a smaller but still significant discrepancy between the two methods. A combination of the first and second theories may also be a possible explanation.

This problem is clearly in need of further investigation as both methods are commonly used to establish crack density quantities, but no comparison of the two methods appears in the literature. Thus, such a study would be useful and necessary, but is beyond the scope of the current study.

3.4 Experimental Summary

Complications with material and testing equipment made interpretation of experimental data difficult. Further confusion was created by the discovery that crack density results as determined by edge replication and radiography do not agree in quantity or trends. However, much of the necessary experimental data needed for input into the analytical models was obtained. The data

also provided some insight into how temperature and moisture affect composite strength and fatigue behavior:

1) Thermal analysis and resin and ply property data will be used in composite strength and damage modeling, as will be described in Chapter 4.
2) Axial and cross-ply composite data were both affected by temperature and/or moisture and will be used for validation of composite strength modeling.
3) Fatigue testing revealed that fatigue lives are at least somewhat degraded with temperature and with moisture (but only in the immersed case). The fact that delamination did not appear to be an issue in any case has implications in the damage modeling, while crack density data is necessary for model validation.
4) The fact that crack density decreased in the immersed fatigue condition from that of dry, room temperature conditions contradicts the theory put forth by Weitsman et al. [4] that the moisture in an immersed fatigue case puts pressure on the crack face and results in greater delamination and smaller crack density.

4 ANALYTICAL METHODS AND RESULTS

Experimental work can be used to quantify how composite strength and durability may be affected by environment, but the question of why these changes occur remains difficult to answer experimentally. Evaluating strength and damage evolution models can be of use in this case. In using such models, the underlying assumptions and included factors are known. Thus, if one can find a model that works for the baseline situation, in this case the dry, room temperature condition, then one can make inferences about what may be happening in other environments based on whether or not the models continues to provide accurate predictions. For instance, in the case of the immersed fatigue environment, do changes in the fatigue damage process occur solely due to the changes in material properties with moisture, or is a more mechanical effect taking place as proposed by Weitsman [22] (discussed in further detail in Section 2.1.3). The accuracy of a model that attempts to incorporate moisture only by changing material properties would help answer such a question, provided that it has been established that the model works otherwise (i.e. for the dry, room temperature case).

Thus, the goal of the analytical phase of this work was to assess the ability of strength and damage evolution models from the literature to include moisture and temperature effects accurately. The assessment considers the nature of the required inputs and the feasibility of obtaining them and also the accuracy of the models given only changes in material properties (i.e., without the inclusion of other possible mechanical or chemical mechanisms). The models chosen to be examined were determined based on the input data required and the apparent adaptability to variable temperature and moisture environments.

4.1 Composite Strength

The development of composite strength models has varied in complexity through the years. The simplest of these models is the bundle strength model in which the strength of the composite is approximated to be the strength of a bundle of dry fibers (not held together with resin) [45]. This type of model that ignores the resin would tend to provide a very conservative strength

estimate, as the role of the matrix in determining composite strength is an important one. Many more complicated models which include both the matrix and the statistical nature of fiber failure have been given by such researchers as Rosen [46], Smith [47], Zhou and Curtin [48], and Hedgepeth and Van Dyke [49], among others. A more thorough description of these models and others is given by Bandorawalla [50].

The main strength prediction model utilized in this work was the Gao and Reifsnider model [51]. This model provides the structure necessary to incorporate matrix property changes with temperature and moisture and has been shown to predict even non-monotonic composite strength changes [52]. Non-monotonic strength changes are often seen as a result of changes in ineffective lengths at fiber breaks and the corresponding stress concentrations in intact neighboring fibers. Ineffective length is generally defined as the length along a fiber from the site of a fiber break that it takes for the fiber to regain its ability to carry full load. This concept is illustrated in Figure 4.1, where σ_f in the figure is the fiber stress and δ is the ineffective length. Changes in ineffective lengths can be a function of temperature and moisture as matrix properties change. The approach of the model consists of using a modified shear lag model to calculate the ineffective lengths and stress concentrations around fiber breaks in unidirectional composites. The calculated values are then input into the Batdorf [53] probability based model to determine strength.

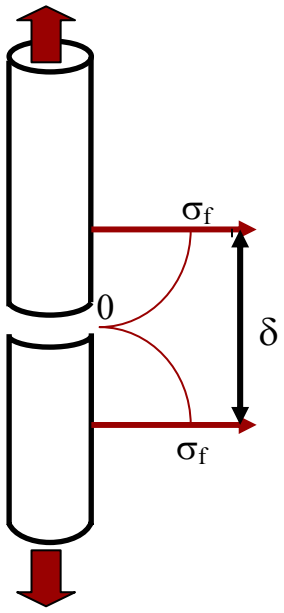

Figure 4.1: Ineffective length

According to Gao and Reifsnider [51], tensile properties of fiber-reinforced composites are dependent on three main factors:

1) fiber strength and modulus
2) strength and chemical stability of matrix
3) efficiency of fiber/matrix interfacial bond in transferring load

In the case of carbon fibers, the fiber strength and modulus can be assumed to remain unchanged with temperature and moisture. Conversely, epoxy matrix is subject to property changes, and those changes must be accounted for in the application of this model. Finally, the efficiency of the fiber/matrix interface is related to these changes in matrix properties and consequently can also be expected to change. However, because interfacial properties are difficult to measure, the interfacial bonding strength is assumed to be directly related to the yield stress of the matrix and interface, τ_0. Interfacial failure is said to occur when the shear stress of the interface reaches τ_0. This assumption is backed up in recent literature in which it was found that for high T_g resin systems, the interfacial shear strength in the composites are near the shear strength of the bulk matrix [54]. However, for low T_g resin systems reinforced with sized fibers, studies indicate that such an approximation may be conservative [27].

One aspect of the Gao and Reifsnider model that distinguishes it from other similar shear lag models is the inclusion of local damage in the form of interfacial debonding and plasticity. In this region, the shear stress of the matrix and interface is assumed constant at the value $\eta\tau_0$. Here, η is a shear parameter which defines the shear stress in the inelastic region. When η equals zero, no shear transfer takes place between broken fibers and their neighbors in that region. This would be the case in a completely debonded region or matrix cracked region. Conversely, when $\eta = 1$, the shear stress in the inelastic region is equal to τ_0, as in the case of an elastic-perfectly plastic material. In the application of this model in this study, η is taken to be 1.

4.1.1 Problem Formulation

A schematic of this problem is given in Figure 4.2. The model assumes there exists a central core of *i* broken fibers which are flanked by unbroken fibers which are subject to stress concentrations from the broken fibers. The unbroken fibers are, in turn, flanked by a homogenous "effective" material that is considered to be strained uniformly. It is further assumed that broken core can be approximated by a homogeneous material with circular cross-section whose Young's modulus may be obtained by the rule-of-mixtures:

$$E = \frac{iA_f E_f + [iA_m - \pi(r_0^2 - (r_0 - d)^2)]E_m}{\pi(r_0 - d)^2} \tag{4}$$

where A corresponds to area and E corresponds to modulus and the properties subscripted with *f* refer to fiber properties and the properties subscripted with *m* refer to matrix properties.

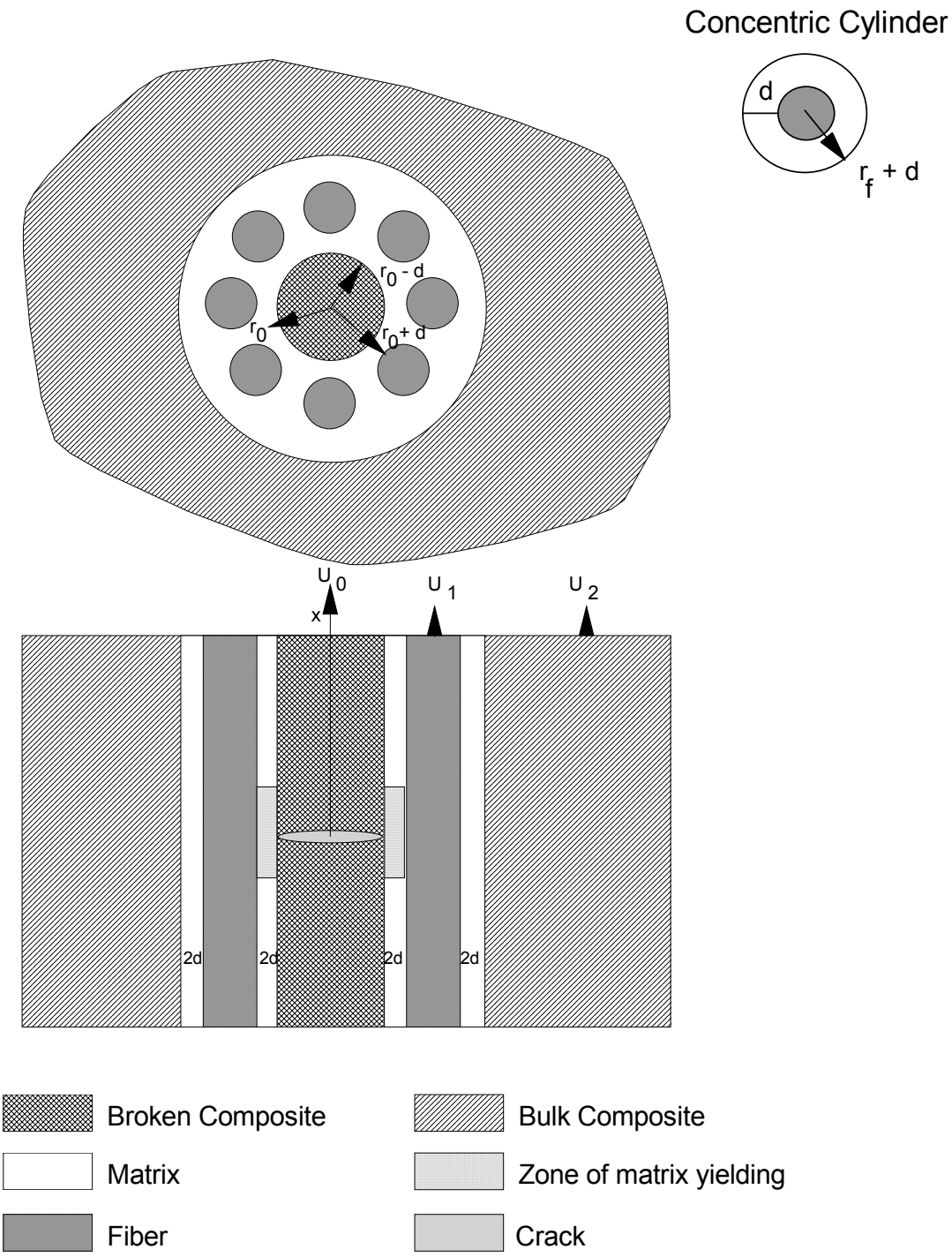

Figure 4.2: Schematic representation of problem modeled in Gao and Reifsnider [51]

As mentioned earlier, local damage is included in the model by introducing a region of debonding and local plasticity where shear stress of the matrix and interface is held constant at $\eta\tau_0$. The equilibrium equations in this region are written [55]:

$$
\begin{aligned}
& iA_f E_f \beta \frac{d^2 U_0}{dx^2} - 2\pi r_0 \eta \tau_0 = 0 \\
& n_i A_f E_f \frac{d^2 U_1}{dx^2} + 2\pi (r_0 + 2d + 2r_f) \frac{G_m}{2d} (U_2 - U_1) + 2\pi r_0 \eta \tau_0 = 0 \\
& 0 \le x \le a
\end{aligned} \tag{5}
$$

where β is given as a function of geometry and fiber and matrix moduli and *a* is the half length of the region of debonding and plasticity. Solving these equations with the boundary conditions:

1) At x = 0, the stress in the broken core, σ, equals 0 (alternatively, $\frac{dU_0}{dx} = 0$)

2) At x = 0, $U_1 = 0$ (symmetry)

and assuming fibers adjacent to the broken core are not affected by the broken core (i.e., $U_2 = \frac{\sigma_c}{E_c} x$, where the *c* subscript refers to the bulk composite), one can obtain solutions for U_0 and U_1. These solutions are given in Eq. (6) below:

$$
\begin{aligned}
& U_0(x) = \frac{\eta \tau_0}{r_0 E_1} x^2 + C_0 \\
& U_1(x) = C_1 (e^{\lambda x} - e^{-\lambda x}) + \frac{2 r_0 \eta \tau_0}{(R_2^{\,2} - r_0^{\,2}) E \lambda^2} (1 - e^{-\lambda x}) + \frac{\sigma_c}{E_c} x \\
& (0 \le x \le a \le)
\end{aligned} \tag{6}
$$

where C_0 and C_1 are constants of integration, E_1 is the modulus of the adjacent intact fibers, R_2 is the geometrical quantity $R_2 = r_0 + 2r_f + d$, and $\lambda = \frac{2R_2}{R_2^{\,2} - r_0^{\,2}} \frac{G_m}{E} \frac{1}{2d}$ is an eigenvalue that is obtained by solving the second of the equations in Eq. (2).

Similarly, for the region where no interfacial yielding occurs, the equilibrium equations are [55]:

$$
\begin{aligned}
& E\pi (r_0 - d)^2 \frac{d^2 U_0}{dx^2} + 2\pi r_0 \frac{G_m}{2d} (U_1 - U_0) = 0 \\
& n_i A_f E_f \frac{d^2 U_1}{dx^2} + 2\pi (r_0 + 2d + r_f) \frac{G_m}{2d} (U_2 - U_1) - 2\pi r_0 \frac{G_m}{2d} (U_1 - U_0) = 0 \\
& a \le x < \infty
\end{aligned} \tag{7}
$$

In this case, the form of the displacements is assumed:

$$U_0 = \overline{U}_0 e^{-\gamma x}$$
$$U_1 = \overline{U}_1 e^{-\gamma x} \tag{8}$$
$$U_2 = \frac{\sigma_c}{E_c} x$$

Substituting Eq. (8) into Eq. (7), one obtains:

$$U_0(x) = C_3 e^{-\sqrt{\gamma_1} x} + C_4 e^{-\sqrt{\gamma_2} x} + \frac{\sigma_c}{E_c} x$$
$$U_1(x) = C_3 (1 - \frac{\gamma_1}{\alpha}) e^{-\sqrt{\gamma_1} x} + C_4 (1 - \frac{\gamma_2}{\alpha}) e^{-\sqrt{\gamma_2} x} + \frac{\sigma_c}{E_c} x \tag{9}$$
$$(a \le x \le \infty)$$

where γ_1, γ_2, and α are algebraic quantities that fall out of the solution and are known. Applying appropriate boundary conditions, one can solve for the constants C_1-C_4 and thus the displacements $U_0(x)$ and $U_1(x)$. The length of the region of interfacial yielding *a* can also be found. In this case, continuity of stress and strain for the broken core (2 equations) and the adjacent intact fibers (2 equations) at x = *a* allows one to solve for C_1-C_4 in terms of *a*. The length of *a* can be found by imposing continuity of shear stress at x = *a*. Recognizing the shear stress to be the constant value τ_0 at $0 \le x \le a$ (region of plasticity) and the shear stress in the region outside the plastic region ($a \le x < \infty$) to be generally:

$$\tau(x) = (U_0(x) - U_1(x)) \frac{G_m}{2d_1} \tag{10}$$

continuity of shear stress is satisfied at x = *a* if:

$$\tau_0 = (U_0(a) - U_1(a)) \frac{G_m}{2d_1} \tag{11}$$

Once the value of *a* is known, one can then obtain $U_0(x)$ and $U_1(x)$ in terms of known quantities. It should be noted that solutions must be found for each of the number of possible adjacent breaks for each load step considered.

The stress concentrations, C_i, for *i* broken fibers, then are

$$C_i = \frac{\left.\frac{dU_1(x)}{dx}\right|_{x=0}}{\sigma / E}. \tag{12}$$

The ineffective lengths can be calculated by solving for the distances along x it takes for the stresses along the broken fibers to reach the applied stress value (or $C_i = 1$).

Once the stress concentrations and ineffective lengths at the fiber breaks are known, they can be directly input to the probability analysis developed by Batdorf [53] to predict composite strength. The Batdorf analysis uses the assumption that fiber failure follows a two-parameter Weibull fit so that the probability of fiber failure is given by

$$P_f(\sigma) = 1 - \exp\left[-\frac{l}{l_o}\left(\frac{\sigma}{\sigma_o} \right)^m \right] \tag{13}$$

where l is the fiber length, l_o is the reference length, and σ_o and m are the Weibull characteristic value and Weibull modulus, respectively. The probability that a composite containing N number or fibers each of length l will contain i adjacent breaks at a given load is calculated. When the load required for $i+1$ adjacent breaks is calculated to be the same or lower than that required to cause i adjacent breaks, the system is considered to be unstable and the composite is said to fail.

A Mathematica code was written to carry out both the Gao and Reifsnider and Batdorf analysis and is provided in Appendix A.

4.1.2 Strength Prediction Inputs

The following inputs are necessary for the strength predictions:

1) Fiber modulus, E_f
2) Fiber statistical parameters - Weibull modulus (m), reference length (l_o), and reference strength (σ_o)
3) Matrix tensile and shear moduli, E_m and G_m
4) Matrix shear yield stress, τ_o

5) Fiber volume fraction, v_f
6) Specimen geometry – gage length (L), width (w), thickness (t)
7) Fiber radius, r_f

Actual values used in the analysis are given in Table 4.1.

Table 4.1: Composite strength modeling inputs

Model Input	Value		Method of Determination
	27°C	**125°C**	
E_f (msi)	34	34	Literature [56]
v_f (%)	53	53	Measured
m	5.1	5.1	Literature [56]
σ_o (msi)	34	34	Literature [56]
l_o (in)	1	1	Literature [56]
E_m (msi)	0.64	0.4	Measured
G_m (msi)	0.23	0.1	Calculated from matrix Young's modulus (assuming isotropy)
τ_o (msi)	3.76	1.80	Approximated from matrix tensile ultimate strength ($\tau_o = \frac{\sigma_{ult}}{2}$)
L (in)	3	3	Measured
r_f (in)	0.00012	0.00012	Assumed
t (in)	0.048	0.048	Measured
w (in)	0.5	0.5	Measured

Experimental methods are described in Section 3.3 and results are presented in Section 3.3.5.1.

4.1.3 Composite Strength Prediction Results

A plot of prediction results along with experimental data is given in Figure 4.3. In the plot, experimental and predicted strength values are normalized by the average dry, room temperature

(27°C) experimental value. In the case of cross-ply specimens, the strength is further normalized by dividing the failure load by the area of only the 0° plies (in this case, half the total area) to give a more direct comparison to unidirectional results. In this way, we see that the unidirectional and cross-ply results correspond very well. Such a result implies that cross-ply strength predictions can be obtained directly from unidirectional strength predictions. Moreover, it appears that reasonable estimates of unidirectional strength can be obtained based on cross-ply results, which is significant since [0/90] laminates are much easier to test than [0] laminates.

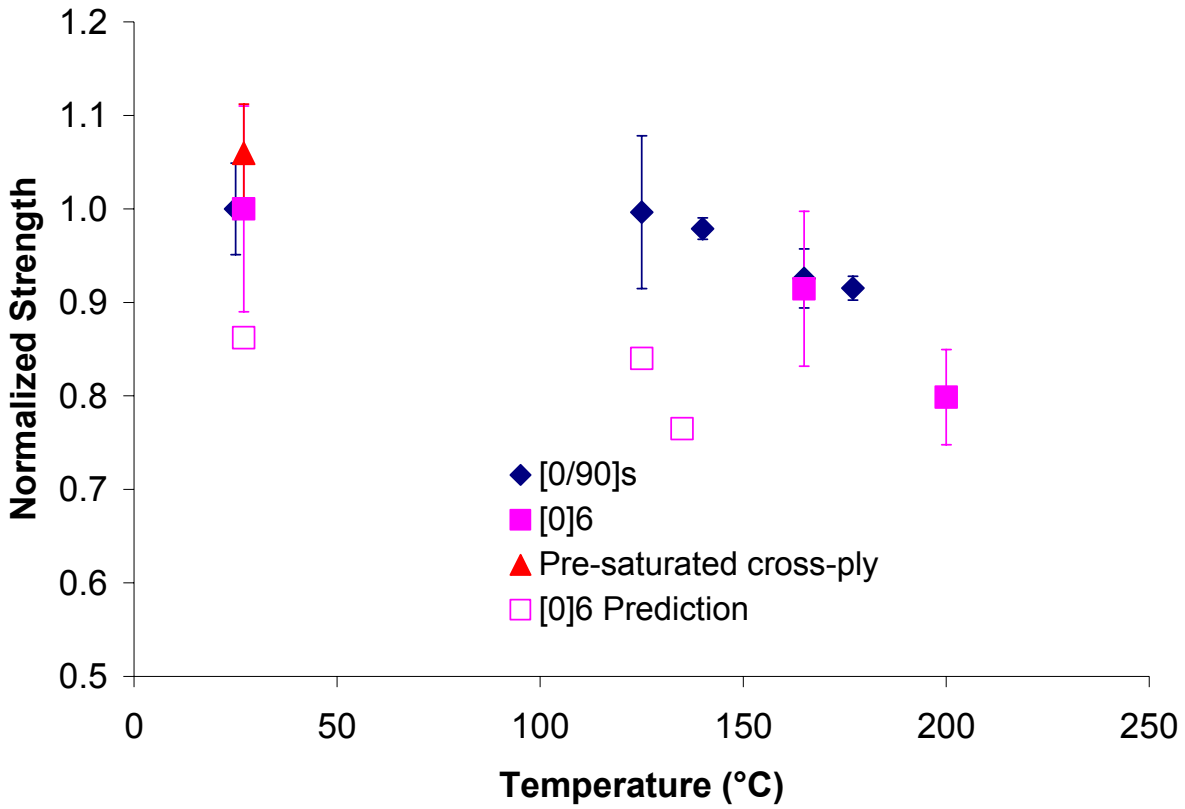

Figure 4.3: Composite strength prediction results

The increase in strength of the pre-saturated specimens over the dry specimens at room temperature appears to occur as a result of moisture induced relief of residual curing stresses. This conclusion is drawn from performing a classical lamination theory (CLT) analysis, along with the fact that no strength change with moisture content was observed for unidirectional specimens. When moisture and thermal coefficients of expansion and stress-free temperature

(see Sections 3.3.2.2 and 3.3.4 for procedures used to obtain values and results) are included in the analysis along with moisture content and temperature, the compressive residual stresses calculated nearly match that of the increase in strength found with pre-saturated specimens. That is, the CLT analysis indicated a 6.5 ksi compressive residual stress in a saturated laminate at room temperature, while the experimental increase in strength for a pre-saturated specimen at room temperature was, on average, 7.2 ksi. Thus, one can predict strength as a function of moisture content for cross-ply specimens by including CLT as part of the analysis.

Generally, the strength predictions are clearly conservative. At room temperature, it can be seen that the predicted strength value is within 15% of the average experimental value. Since fiber data were obtained from the literature, it is possible that the values used were conservative. However, at elevated temperatures, the strength prediction becomes increasingly conservative. To identify the explanation behind the increasingly conservative results, the three temperature dependent parameters in the analysis were examined in more detail. Figure 4.4 below illustrates the sensitivity of the strength prediction to the three variables in the analysis that vary with temperature: matrix shear modulus, matrix Young's modulus, and matrix shear yield strength. The figure shows that the prediction is sensitive to matrix shear strength but not to matrix shear stiffness or matrix Young's modulus. In addition, recalling that the matrix shear yield strength was estimated from the matrix tensile strength, the possibility that the estimation is inaccurate is a consideration. However, the sensitivity analysis also shows that the matrix shear yield strength would have to be twice the value input initially (see Table 4.1 above), or equal to the matrix tensile strength, for the predicted value to match the experimental value. Generally, such a situation would seem unlikely; however due to the constraining effect of the 0° plies and processing differences, it is reasonable to expect the tensile strength of the matrix within the laminate to be higher than the value measured from the neat resin samples. Consequently, it may be hypothesized that more accurate values for the matrix shear yield strength as a function of temperature would indeed close the gap between predicted and experimental results. The accuracy of the correlation between matrix tensile and shear properties, especially "in-situ" within the composite, however, is difficult to determine experimentally and no literature was found to be available on this topic.

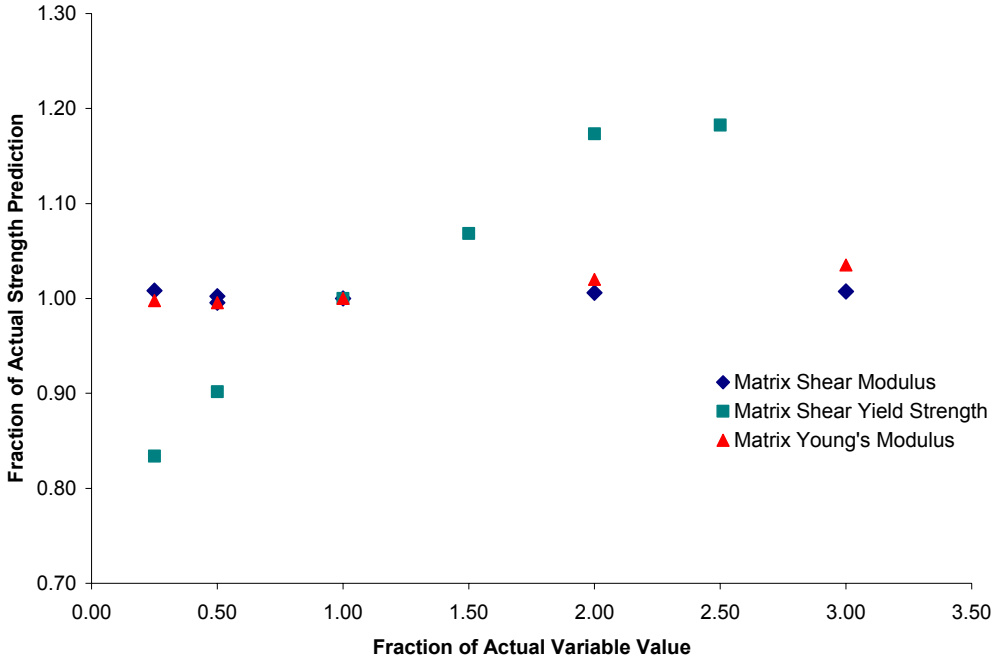

Figure 4.4: Strength prediction sensitivity

4.2 Damage Evolution

Many different types models exist to predict matrix crack formation and subsequent stiffness loss in cross-ply composites. References for various types of approaches (i.e. FEM, micromechanics, variational, etc.) can be found in Henaff-Gardin and Lafarie-Frenot [57]. Of the various approaches, the micromechanics approach appears to be best suited to the current study since the type of data required to implement such models (e.g. matrix and ply-level property and geometrical data) are easily determined (see Sections 3.3 and 3.3.5.1). Of the many micromechanics based models presented in the literature, only a relative few consider progressive cracking with fatigue.

The model focused on in this study is one developed by Henaff-Gardin et al. [57,58,59,60] These authors have performed an extensive study generating a great deal of experimental data and developing a two-dimensional shear lag analysis that predicts crack evolution in symmetric cross-ply laminates subjected to fatigue loading. The advantage of the model is that it does not

utilize any empirical parameters (with the possible exception of the number of cycles to cracking), and generation of inputs requires minimal experimental effort. The model also accounts for temperature variations.

One of the major drawbacks to this model is that it ignores delamination. However, the addition of delamination to a fatigue damage evolution model would be quite difficult since the growth of delamination with fatigue is difficult to quantify. In this study, only an empirical model (Akshantala and Talreja [61,62]) has been found that accounts for delamination. Power law constants must be determined from cracks density versus cycles data at a particular stress level to make predictions at other stress levels. Since the constants have no specific physical significance, such a model would not prove anymore useful in identifying precisely the effects of environment than the already available experimental data.

4.2.1 Problem Formulation

The Henaff-Gardin model is generalized to account for cracks in both the 0° and 90° plies, assuming a double periodicity along the loading axis and transverse axis. The representative unit cell used for modeling is given in Figure 4.5. Cracks are assumed to be uniformly spaced and plane and normal to the x-axis in the 90° ply and to the y-axis in the 90° ply. Crack spacing in the 90° ply is denoted as $\frac{1}{d_{90}}$ and crack spacing in the 0° ply is denoted as $\frac{1}{d_0}$.

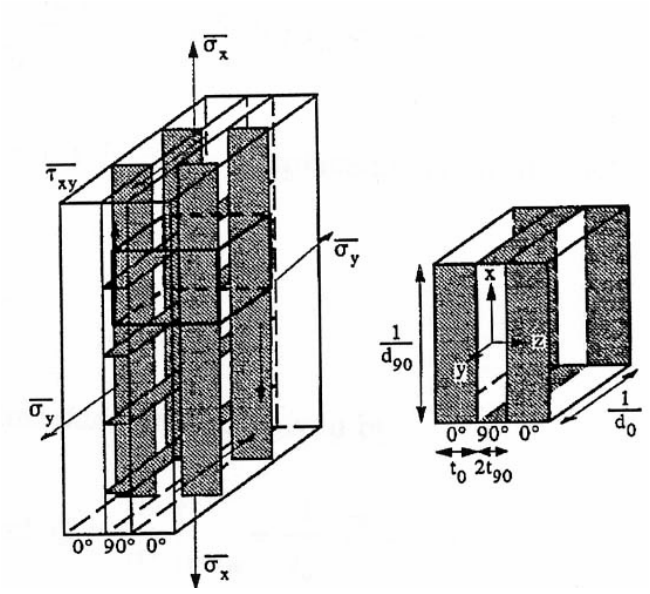

Figure 4.5: Unit cell for Henaff-Gardin model[1]

Equilibrium of the cracked layer and of the laminate and thermoelastic constitutive equations provide the governing equations which are solved by applying load appropriate boundary conditions and assumptions about the displacement fields. Schematics of the assumed displacement fields are given in Figure 4.6. Specifically, in the 90° layer, the displacement in the *y*-direction, *v*, is assumed to be constant along z and the displacement in the *x*-direction, *u*, is assumed to be parabolic along z, so that:

$$\begin{aligned} u &= u^{90} + \frac{z^2}{t^2_{90}}(u^0 - u^{90}) \\ v &= v^{90} \\ -t_{90} &\le z \le t_{90} \end{aligned} \tag{14}$$

Analogous assumptions are made for the 0° plies:

[1] Reprinted from *Composite Structures*, Vol. 36, Henaff-Gardin et al., "Doubly-periodic matrix cracking in composite laminates. Part I: general in-plane loading," p. 114, Copyright (1996), with permission from Elsevier.

$$u = u^0$$
$$v = v^0 - \frac{(z - t_0 - t_{90})^2}{t^2_0}(v^0 - v^{90}) \tag{15}$$
$$t_{90} \le |z| \le t_{90} + t_0$$

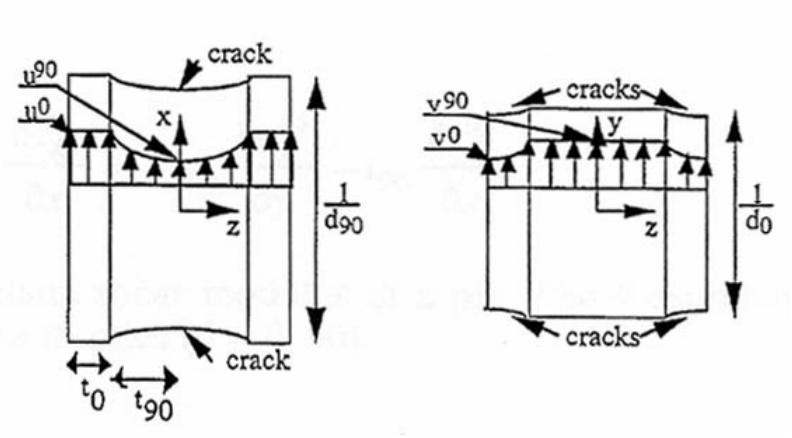

Figure 4.6: Assumed displacement fields for Henaff-Gardin model[2]

Evaluating derivatives $\frac{du}{dz}$ and $\frac{dv}{dz}$ from equations (14) and (15) at z = t_{90} and assuming relatively small out-of-plane displacements, one can find the interfacial shearing strains, γ^{90}_{xz} and γ^{0}_{yz}. To simplify the problem, mean displacements $\overline{u^{90}}$ and $\overline{v^{0}}$ are obtained by integrating eqns. (14) and (15) and substituted into the interfacial shear strain expressions, eliminating the z dependence from the problem. The resulting expressions for the interfacial shearing strains can be substituted into the general equilibrium equations. Averaging over the ply thickness gives:

[2] Reprinted from *Composite Structures*, Vol. 36, Henaff-Gardin et al., "Doubly-periodic matrix cracking in composite laminates. Part I: general in-plane loading," p. 115, Copyright (1996), with permission from Elsevier.

$$
\begin{aligned}
G_{23}\gamma^{90}{}_{xz} &= t_0\frac{\partial\sigma^0{}_x}{\partial x}+t_0\frac{\partial\tau^0{}_{xy}}{\partial y}=-t_{90}\frac{\partial\sigma^{90}{}_x}{\partial x}-t_{90}\frac{\partial\tau^{90}{}_{xy}}{\partial y}=\frac{3G_{23}}{t_{90}}(u^0-\overline{u^{90}})\\
G_{23}\gamma^0{}_{yz} &= t_0\frac{\partial\sigma^0{}_y}{\partial y}+t_0\frac{\partial\tau^0{}_{xy}}{\partial x}=-t_{90}\frac{\partial\sigma^{90}{}_y}{\partial y}-t_{90}\frac{\partial\tau^{90}{}_{xy}}{\partial x}=\frac{3G_{23}}{t_0}(\overline{v^0}-v^{90})
\end{aligned}
\tag{16}
$$

Taking the x-derivative of the first of equations (16) and the y-derivative of the second equation, and then adding the y-derivative of the first to the x-derivative of the second yields the following set of differential equations:

$$
\begin{aligned}
\frac{\partial\tau_{xz}}{\partial x} &= t_0\frac{\partial^2\sigma_x}{\partial x^2}+t_0\frac{\partial^2\tau^0{}_{xy}}{\partial x\partial y}=\frac{3G_{23}}{t_{90}}\left(\frac{\partial u_0}{\partial x}-\frac{\partial\overline{u_{90}}}{\partial x}\right)\\
\frac{\partial\tau_{yz}}{\partial y} &= t_0\frac{\partial^2\sigma_y}{\partial y^2}+t_0\frac{\partial^2\tau^0{}_{xy}}{\partial x\partial y}=\frac{3G_{23}}{t_0}\left(\frac{\partial\overline{v_0}}{\partial y}-\frac{\partial v_{90}}{\partial y}\right)\\
t_{90}\frac{\partial\tau_{xz}}{\partial y}+t_0\frac{\partial\tau_{yz}}{\partial x} &= t_{90}t_0\frac{\partial^2\sigma^0{}_x}{\partial x\partial y}+t_{90}t_0\frac{\partial^2\tau^0{}_{xy}}{\partial y^2}+t^2{}_0\frac{\partial^2\sigma^0{}_y}{\partial x\partial y}+t^2{}_0\frac{\partial^2\tau^0{}_{xy}}{\partial x^2}\\
&= 3G_{23}\left(\frac{\partial u_0}{\partial y}+\frac{\partial\overline{v_0}}{\partial x}-\frac{\partial\overline{u_{90}}}{\partial y}-\frac{\partial v_{90}}{\partial x}\right)
\end{aligned}
\tag{17}
$$

Note that the cross derivative terms ($\frac{\partial^2}{\partial x\partial y}$) are assumed to be zero.

Constitutive equations are used to express the displacement derivatives in terms of stresses:

$$
\begin{aligned}
\varepsilon^0{}_x &= \frac{\partial u^0}{\partial x}=\frac{\sigma^0{}_x}{E_1}-\frac{\nu_{12}}{E_1}\sigma^0{}_y\\
\varepsilon^0{}_y &= \frac{\partial\overline{v^0}}{\partial y}=\frac{\sigma^0{}_y}{E_2}-\frac{\nu_{12}}{E_1}\sigma^0{}_x\\
\gamma^0{}_{xy} &= \frac{\partial u^0}{\partial y}+\frac{\partial\overline{v^0}}{\partial x}=\frac{1}{G_{12}}\tau^0{}_{xy}
\end{aligned}
\tag{18}
$$

and

$$\varepsilon^{90}{}_{x} = \frac{\partial \overline{u^{90}}}{\partial x} = \frac{\sigma^{90}{}_{x}}{E_2} - \frac{\nu_{12}}{E_1}\sigma^{90}{}_{y}$$
$$\varepsilon^{90}{}_{y} = \frac{\partial v^{90}}{\partial y} = \frac{\sigma^{90}{}_{y}}{E_1} - \frac{\nu_{12}}{E_1}\sigma^{90}{}_{x} \tag{19}$$
$$\gamma^{90}{}_{xy} = \frac{\partial \overline{u^{90}}}{\partial y} + \frac{\partial v^{90}}{\partial x} = \frac{1}{G_{12}}\tau^{90}{}_{xy}$$

Considering laminate equilibrium, one can obtain expressions for the mean stresses (applied stresses) in terms of the individual ply stresses:

$$(t_0 + t_{90})\overline{\sigma_x} = t_0\sigma^0{}_x + t_{90}\sigma^{90}{}_x$$
$$(t_0 + t_{90})\overline{\sigma_y} = t_0\sigma^0{}_y + t_{90}\sigma^{90}{}_y \tag{20}$$
$$(t_0 + t_{90})\overline{\tau_{xy}} = t_0\tau^0{}_{xy} + t_{90}\tau^{90}{}_{xy}$$

Eqns. (20) can be used in Eqns. (17) to eliminate the 90° ply stresses and yield the governing equations in terms of the applied stresses and the 0° ply stresses:

$$\frac{\partial^2\sigma^0{}_x}{\partial x^2} - \lambda^2{}_x\sigma^0{}_x = -\mu^2{}_x\sigma^0{}_y - \mu^2{}_x\left(\frac{E_1}{\nu_{12}E_2}\overline{\sigma_x} - \overline{\sigma_y}\right)$$
$$\frac{\partial^2\sigma^0{}_y}{\partial y^2} - \lambda^2{}_y\sigma^0{}_y = -\mu^2{}_y\sigma^0{}_x - \mu^2{}_y\left(\frac{1}{\nu_{12}}\overline{\sigma_y} - \overline{\sigma_x}\right) \tag{21}$$
$$t^2{}_0 t_{90}\frac{\partial^2\tau^0{}_{xy}}{\partial x^2} + t_0 t^2{}_{90}\frac{\partial^2\tau^0{}_{xy}}{\partial y^2} = 3\frac{G_{23}}{G_{12}}(t_0 + t_{90})(\tau^0{}_{xy} - \overline{\tau_{xy}})$$

where $\lambda^2{}_x$, $\lambda^2{}_y$, $\mu^2{}_x$, and $\mu^2{}_y$ are material and geometry dependent parameters. Solving the governing differential equations then gives the 0° ply stress distributions. For biaxial mechanical loading, the following form of the solution was used by Henaff-Gardin [60]:

$$\sigma^0{}_x = A\cosh(R\lambda_x x) + B\cosh(R\lambda_y y) + K_x$$
$$\sigma^0{}_y = A\frac{\nu_{12}E_2(t_0 + t_{90})}{t_0E_2 + t_{90}E_1}\cosh(R\lambda_x x) + B\frac{t_{90}E_2 + t_0E_1}{\nu_{12}E_2(t_0 + t_{90})}\cosh(R\lambda_y y) + K_y \tag{22}$$

where R, A, B, K_x, and K_y are parameters which are dependent on geometry, crack densities, material properties, and applied stresses. The boundary conditions used were [60]:

1) In the 0° layer, zero average normal stress on the 0° ply crack surfaces

$$d_{90}\int_{x=-\frac{1}{2d_{90}}}^{x=\frac{1}{2d_{90}}}\sigma^0{}_y(x, y=\pm\frac{1}{2d_0})dx = 0 \tag{23}$$

2) In the 0° layer, equilibrium near a 90° ply crack

$$d_0\int_{y=-\frac{1}{2d_0}}^{y=\frac{1}{2d_0}}\sigma^0{}_x(x=\pm\frac{1}{2d_{90}}, y)dy = \frac{t_0+t_{90}}{t_0}\overline{\sigma_x} \tag{24}$$

Once the 0° ply stresses are established, eqns. (20) can be used to determine the 90° ply stresses.

Knowing the ply level stress distributions, the cracked ply elastic constants and the cracked laminate elastic constants can be found with the use of continuity of the mean cracked laminate strains ($\overline{\varepsilon^0{}_x} = \overline{\varepsilon^{90}{}_x}, \overline{\varepsilon^0{}_y} = \overline{\varepsilon^{90}{}_y}$) and of classical laminate theory. However, in determining the cracked ply elastic constants, one must ignore cracking in the 0° plies to determine the 90° cracked properties and vice versa.

In the current study, only uniaxial loading was considered, with cracking only occurring in the 90° plies. Thus, the problem is somewhat simplified from that described above. However, all the equations given above may still be used by setting the applied y-direction stress ($\overline{\sigma_y}$) equal to zero and by letting the 0° crack spacing be equal to the width of the specimen (in this case, 1 inch). Also in this case, the assumed y-displacement in the 0° layer also becomes constant.

Once the cracked elastic ply and laminate constants are known as a function of crack density, a strain energy release rate criterion is used to specify the onset and proliferation of matrix cracking. The strain energy release rate, G, is obtained by taking the derivative of the elastic

energy with respect to the cracked surface area in a unit volume of the cracked laminate. Cracking is said to only occur when G_c/G_{max} is less than one ($G_{max}>G_c$), where G_c is the critical strain energy release rate necessary for cracking to occur and G_{max} is the strain energy release rate associated with loading. In Henaff-Gardin and Lafarie-Frenot [57], the authors find the following relationship to hold:

$$\frac{G_c}{G_{\max}} = \tanh\left(\frac{1}{\eta}\right) - \frac{1}{\eta}\left(1 - \tanh^2\left(\frac{1}{\eta}\right)\right) \tag{25}$$

where η is a non-dimensional laminate and material parameter defined by:

$$\eta = \frac{2d_{90}}{R\lambda_x}$$

$$R = \sqrt{1 - \frac{\nu^2_{12}\left(\frac{t_0}{t_{90}} + 1\right)^2}{\left(\frac{t_0}{t_{90}}\frac{E_1}{E_2} + 1\right)\left(\frac{E_1}{E_2} + \frac{t_0}{t_{90}}\right)}}$$

$$\lambda_x = \frac{1}{t_{90}}\sqrt{\frac{3G_{23}\left(\frac{t_0}{t_{90}}\frac{E_1}{E_2} + 1\right)}{\frac{t_0}{t_{90}}E_1}}$$

Though G_c is strictly a material parameter, in this case, with the use of eqn. (25), it is found by first calculating G_{max} at first ply failure stress. The quantity G_{max}, as given in [57], is given to be a summation of mechanical loading and thermal expansion factors and is dependent on ply and laminate elastic properties as well as geometry. In the current study, moisture was assumed to affect strain energy in a similar manner as temperature, so an analogous expression was used for G^{moist}_{max} and added to the expression given in [57] to yield:

$$
\begin{aligned}
G_{\max} &= G^{mech}{}_{\max} + G^{th}{}_{\max} + G^{moist}{}_{\max} \\
G^{mech}{}_{\max} &= \left(\frac{t_0}{t_{90}}+1\right)\frac{\overline{\sigma}^2{}_x}{R\lambda_x}\frac{1}{E^{ini}{}_x}\frac{1}{\frac{t_0}{t_{90}}}\frac{\left[\nu^2{}_{12}\left(1+\frac{t_0}{t_{90}}\right)-\left(\frac{E_1}{E_2}+\frac{t_0}{t_{90}}\right)\right]^2}{\left(\frac{E_1}{E_2}-\nu^2{}_{12}\right)\left(\frac{E_1}{E_2}+\frac{t_0}{t_{90}}\right)^2} \\
G^{th}{}_{\max} &= \frac{1}{R\lambda_x}\frac{1}{E^{ini}{}_x}\frac{t_0}{t_{90}}\frac{\left(\alpha_2-\alpha_1\right)^2\Delta T^2}{\left(\frac{t_0}{t_{90}}+1\right)}\frac{E^2{}_1\left[\nu_{12}\left(1+\frac{t_0}{t_{90}}\right)-\left(\frac{E_1}{E_2}+\frac{t_0}{t_{90}}\right)\right]^2}{\left(-\frac{E_1}{E_2}+\nu^2{}_{12}\right)\left(\frac{E_1}{E_2}+\frac{t_0}{t_{90}}\right)^2} \\
G^{moist}{}_{\max} &= \frac{1}{R\lambda_x}\frac{1}{E^{ini}{}_x}\frac{t_0}{t_{90}}\frac{\left(\beta_2-\beta_1\right)^2\Delta M^2}{\left(\frac{t_0}{t_{90}}+1\right)}\frac{E^2{}_1\left[\nu_{12}\left(1+\frac{t_0}{t_{90}}\right)-\left(\frac{E_1}{E_2}+\frac{t_0}{t_{90}}\right)\right]^2}{\left(-\frac{E_1}{E_2}+\nu^2{}_{12}\right)\left(\frac{E_1}{E_2}+\frac{t_0}{t_{90}}\right)^2}
\end{aligned}
\tag{26}
$$

where

$$
\frac{1}{E^{ini}{}_x} = \frac{\left(-\frac{E_1}{E_2}+\nu^2{}_{12}\right)\left(\frac{t_0}{t_{90}}+1\right)\left(\frac{E_1}{E_2}+\frac{t_0}{t_{90}}\right)}{E_1\left[-\left(\frac{E_1}{E_2}\frac{t_0}{t_{90}}+1\right)\left(\frac{E_1}{E_2}+\frac{t_0}{t_{90}}\right)+\nu^2{}_{12}\left(\frac{t_0}{t_{90}}+1\right)^2\right]}
$$

According to Henaff-Gardin [57], if the criterion for matrix cracking is met with the first fatigue cycle, the initial crack density is equal to that found in quasi-static loading at the stress equal to the maximum fatigue stress. If the criterion for matrix cracking is not met from the first fatigue cycle, the number of cycles to matrix cracking must be found experimentally. In this study, for the purposes of finding G_c, it is assumed that the initial crack appears by itself at first ply failure so the initial crack density is taken to be $\frac{1}{\text{gage length}}$. The first ply failure stress was found by using classical lamination theory in conjunction with the maximum stress criterion (discussion on this ensues in Section 4.2.2.1). Thus, to find G_c, the calculated first ply failure stress and the

initial crack density of $\frac{1}{\text{gage length}}$ was input into eqns. (26) to find the initial G_{max}. With G_{max} known, the same crack density could be used to find η and the two values could be used in eqn. (25) to find G_c. With G_c known, the crack saturation density of the laminate may be easily obtained by calculating G_{max} for a range of crack densities. The largest value of d_{90} for which $\frac{G_c}{G_{max}}$ remains less than 1 is the crack saturation density.

A Mathematica code was written to carry out both the Henaff-Gardin analysis and is provided in Appendix B.

4.2.2 Damage Evolution Inputs

The inputs required for the Henaff-Gardin analysis include:

1) Unidirectional composite axial and transverse moduli, in-plane shear modulus, and Poisson's Ratio: E_1, E_2, ν_{12} – obtained experimentally
2) Unidirectional composite out-of-plane shear modulus: G_{23} – approximated using concentric cylinder model
3) Unidirectional composite coefficients of thermal expansion: α_1 and α_2 – obtained experimentally
4) Laminate (cross-ply) stress-free temperature: T_f – obtained experimentally
5) Unidirectional composite coefficients of moisture expansion: β_1 and β_2 – obtained experimentally
6) First ply failure stress: σ_{fpf} – approximated using classical lamination (see Sect. 4.2.2.1)
7) Applied temperature, T_{ref}
8) Applied maximum fatigue stress, $\overline{\sigma_x}$

The specific values used are given in Table 4.2.

Table 4.2: Damage evolution model inputs

Model Input	Value			Method of Determination
	27°C	125°C	Immersed	
E1 (msi)	17.3	17.3	17.3	Measured
E2 (msi)	1.27	0.97	1.06	Measured
G_{23} (msi)	0.4	0.3	0.4	Calculated - Concentric cylinder model
ν_{12}	0.43	0.43	0.43	Measured
α_1 (/°C)	-3.04E-7	-3.04E-7	-3.04E-7	Measured
α_2 (/°C)	4.08E-5	4.08E-5	4.08E-5	Measured
β_1 (/%M)	.00016	.00016	.00016	Measured
β_2 (/%M)	.00186	.00186	.00186	Measured
T_f (°C)	155	155	155	Measured
T_{ref} (°C)	27	125	27	Applied
ΔM	0	0	.014	Applied
$\overline{\sigma_x}$ (ksi)	102	102	102	Applied
σ_{fpf} (msi)	See Table 4.5 (Sect. 4.2.2.1)	See Table 4.5 (Sect. 4.2.2.1)	See Table 4.5 (Sect. 4.2.2.1)	Calculated – Classical Lamination Theory and Maximum Stress Criterion

For the CLT analysis, the elastic and thermal/moisture properties needed are also given in Table 4.2. Inputs and values necessary for the concentric cylinder model are given in Table 4.3.

Table 4.3: Concentric cylinder model inputs

Condition	E_1^{fiber} (msi)	E_2^{fiber} (msi)	G_{12}^{fiber} (msi)	ν_{12}^{fiber} $(=\nu_{23}^{fiber})$	E_1^{matrix} $(=E_2^{matrix})$ (msi)	G_{12}^{matrix} (msi)	ν_{12}^{matrix} $(=\nu_{23}^{matrix})$
Dry, 27°C	32.66	1.74	4.17	0.35	0.64	0.23	0.43
Dry, 125°C	32.66	1.74	4.17	0.35	0.36	0.14	0.43
27°C, Immersed	32.66	1.74	4.17	0.35	0.64	0.23	0.43

Experimental methods are described in Section 3.3 and results are presented in Section 3.3.5.1.

4.2.2.1 First ply failure stress calculations

The major choice to be made in making the first ply failure stress calculations is the choice of the failure criterion. Stresses in the 90° plies are calculated using classical lamination theory (CLT) and input into a failure criterion to establish first ply failure stress. In addition, one must decide what strength value to use in the failure criterion. For instance, experimental work done by Flaggs and Kural [63] shows that in cross-ply laminates with only one transverse ply, the first ply failure stress in the transverse plies can be as much as 2.48 times the value of the transverse tensile strength. This phenomenon was attributed to the constraint effect provided by the neighboring 0° plies. For increasing number of transverse plies relative to the number of 0° plies, the first ply failure stress in the transverse plies was found to approach the transverse tensile strength. In a recent, and very comprehensive, review of failure criteria by Hinton et al. [64], the issue of how to account for in-situ strength was found to be unresolved as yet. In the current study, the number of transverse plies (2) is equal to the number of 0° plies. However, since no experimental results are available as part of this study to determine the relationship between transverse tensile strength and laminate first ply failure stress, the transverse tensile strength will be used to determine first ply failure stress.

As far as failure criteria, a study by Kam and Sher [65] examined the maximum strain criterion, Hoffman's Criterion, the Tsai-Hill Criterion, and the Tsai-Wu Criterion and found them to be inconsistent, and there for insufficient. Kim and Hahn [66] found that the maximum stress criterion may underpredict first ply failure stress. Hinton et al. [64] also found most failure criteria to be generally unreliable to predict the onset of first failure. This was attributed mostly to lack of "good" experimental data and the variation in treatment of thermal residual stresses and effective ply strengths. Thus, since no theory has been found to be particularly accurate in predicting first ply failure, the maximum stress and maximum strain criteria are both considered in the current study for the sake of simplicity. The transverse tensile strengths (for maximum stress criterion) and strains-to-failure (for maximum strain criterion) used to determine the first ply failure stress are provided in Table 4.4.

Table 4.4: CLT transverse strength and strain inputs

Condition	X_t (ksi)	ε_{ult} (%)
Dry, 27°C	10.3	0.84
Dry, 125°C	8.6	1.3
27°C, Immersed	7.9	0.74

In calculating the first ply failure stress, one major issue is the inclusion of thermal residual stresses. While there is no question that thermal residual stresses are present upon initial curing of the laminates, physical aging of the laminates, particularly those that are post-cured at elevated temperature, may reduce the residual stresses. According to Kim and Hahn [66], post-curing for a "reasonable period of time" most likely does not result in any significant relaxation because curing stresses are lower at the postcuring temperatures since there is less thermal expansion mismatch. Moreover, the authors claim that the postcuring may induce more chemical shrinkage, making the net relaxation achieved during postcuring minimal. In their evaluation of various failure criteria, Hinton et al. [64] found the significance of thermal residual stresses to be a debated and "confusing" issue. In the current study, both cases (with and without thermal residual stresses) were evaluated.

Calculated values for first ply failure stress with/without included residual stresses and using both failure criteria are given in Table 4.5. One may conclude that the case in which the maximum stress criterion is used and the thermal residual stresses are considered is the best of these options based on the fact that the other cases result in first ply failure stresses that exceed the applied load of 102 ksi. According to experimental data (edge replication results) such as shown in Figure 4.7, multiple cracks do indeed appear at smaller stresses, so the first ply failure stress must be less than 102 ksi. Subsequent analysis results presented will reflect the inclusion of thermal residual stresses and the use of the maximum stress criterion to determine first ply failure stress.

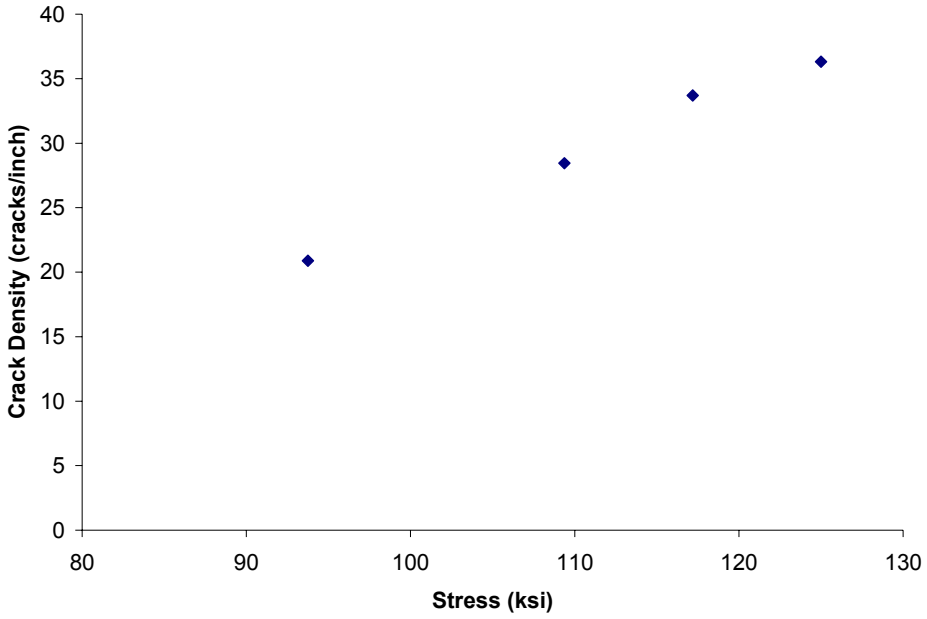

Figure 4.7: Crack density as a function of stress (single specimen)

Table 4.5: First ply failure stress calculations

Condition	First Ply Failure Stress (ksi)			
	Maximum Stress Criterion		Maximum Strain Criterion	
	With Thermal Residual Stress	Without Thermal Residual Stress	With Thermal Residual Stress	Without Thermal Residual Stress
Dry, 27°C	32.8	76.6	82.8	78.9
Dry, 125°C	71.8	81.3	125	121.9
27°C, Immersed	73.4	117.2	67.2	63.3

4.2.3 Damage Modeling Results

4.2.3.1 Crack Saturation Density

The conditions examined for the damage modeling were fatigue (80% UTS at 10 Hz) at: 1) room temperature, 2) 125°C, and 3) immersed fatigue at room temperature. The calculated values for G_c are given in Table 4.6 while Table 4.7 shows the results of the crack saturation density prediction under each of the conditions. In Table 4.7, the number in parentheses in the

experimental results column refers to the number of data points averaged to obtain the result given.

Table 4.6: Critical strain energy release rates

Test Condition	G_c (lb/in)
Dry, 27°C	0.36
Dry, 125°C	0.51
27°C, Immersed	0.55

Table 4.7: Crack density results

Test Condition	Experimental Crack Density (cracks/inch)	Predicted Crack Density (cracks/inch)
Dry, 27°C	30 ± 6 (4)	61
Dry, 125°C	14 ± 1 (2)	31
27°C, Immersed	43 ± 3 (4)	40

The analysis does generally predict the correct trend in going from room temperature to 125°C (crack density decreases), but the actual predicted crack densities in both cases are about twice as high as the experimental values. The predicted value for the saturation crack density for the immersed fatigue case is close to the experimental value, but the predicted decrease in crack density from the dry, room temperature value does not reflect the experimental result. Generally, one might expect that since elevated temperature and water immersion both result in an increase in the first ply failure stress, the crack densities in those cases should decrease. Experimentally, this only happens in the elevated temperature case and may indicate that matrix property degradation is overcome by other factors such as relief of thermal residual stresses, increased toughness, increased ductility, and creep/stress relaxation. In the case of immersed fatigue, experimental results showed very little matrix or transverse ply property degradation with moisture saturation, so the reason behind the increase in crack density in this case is not immediately obvious. The fact that the numbers do not generally agree with experimental results could well be a result of the inaccuracy of the model inputs. A discussion on this topic follows.

4.2.3.1.1 Input Sensitivity Analysis

As discussed in Section 4.2.2.1, the first ply failure values used in this study are most likely conservative. Higher first ply failure values would lead to lower crack densities. The other input to which the results may be particularly sensitive and for which no experimental values are available are the laminate G_{23} values under the various conditions. In the case of immersed fatigue, even more questions arise due to the evolution of properties with the continuously increasing moisture content.

The sensitivity of the analysis results to first ply failure stress are demonstrated in Figure 4.8. The x-axis of the plot refers to the increase in first ply failure stress over the values found by simply using the transverse tensile strength with the maximum stress criterion as given in Table 4.5. The y-axis is normalized by the crack densities given in Table 4.7. It is clear from the results that in considering first ply failure, not only must the effect of the constraints added by the 0° plies be determined, but they must be determined as a function of environment. In this case, it appears that the elevated temperature condition is the most sensitive to the first ply failure, while the dry, room temperature condition is the least sensitive. In addition, it was found that at room temperature, the experimental value could be obtained by doubling the first ply failure stress value based on the transverse tensile strength (32.8 ksi) while, for the elevated temperature case, the first ply failure stress only needs to be multiplied by a factor of 1.25. This result makes sense in that one would expect that at elevated temperatures when the resin is less stiff, the constraint imposed by the 0° plies is not as effective. Moreover, these results seem reasonable in regards to the study by Flaggs and Kural. [63]

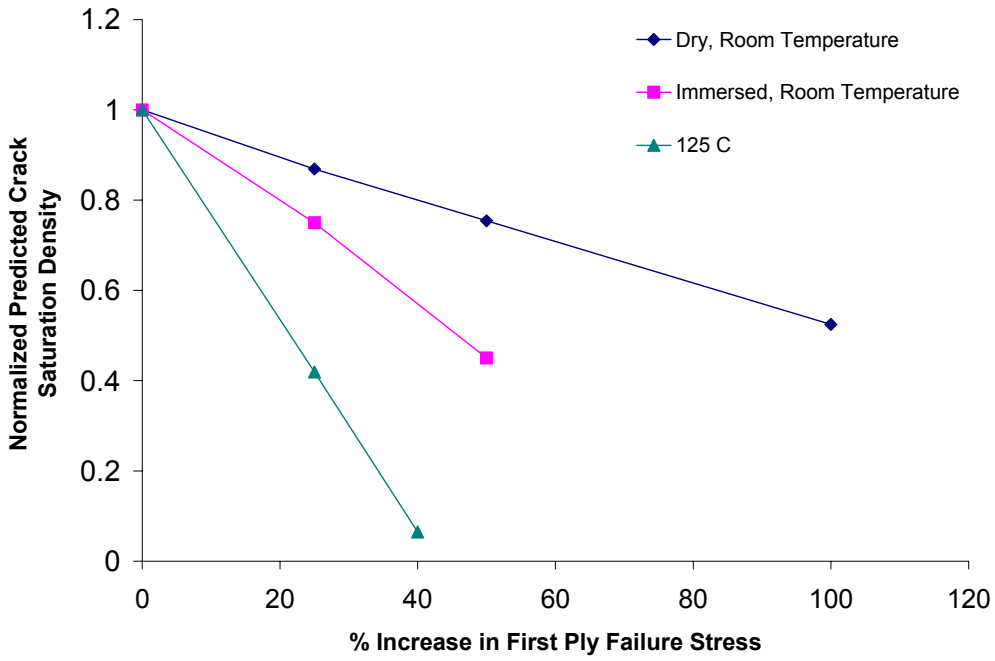

Figure 4.8: First ply failure sensitivity

Another input which can be difficult to measure and was therefore approximated in this study is the out-of-plane laminate shear stiffness, G_{23}. Figure 4.9 shows how the prediction results vary with this parameter. Again, the x-axis is normalized by the calculated G_{23} values given in Table 4.2, while the y-axis is normalized by the corresponding crack saturation density prediction given in Table 4.7. The figure implies that the crack saturation density is affected by G_{23} in much the same way no matter the environmental condition. Moreover, while the predictions are somewhat sensitive to the G_{23} value, inaccuracy in the input value used for this parameter, in and of itself, does not appear to be enough to explain the discrepancies between experimental and predictive results.

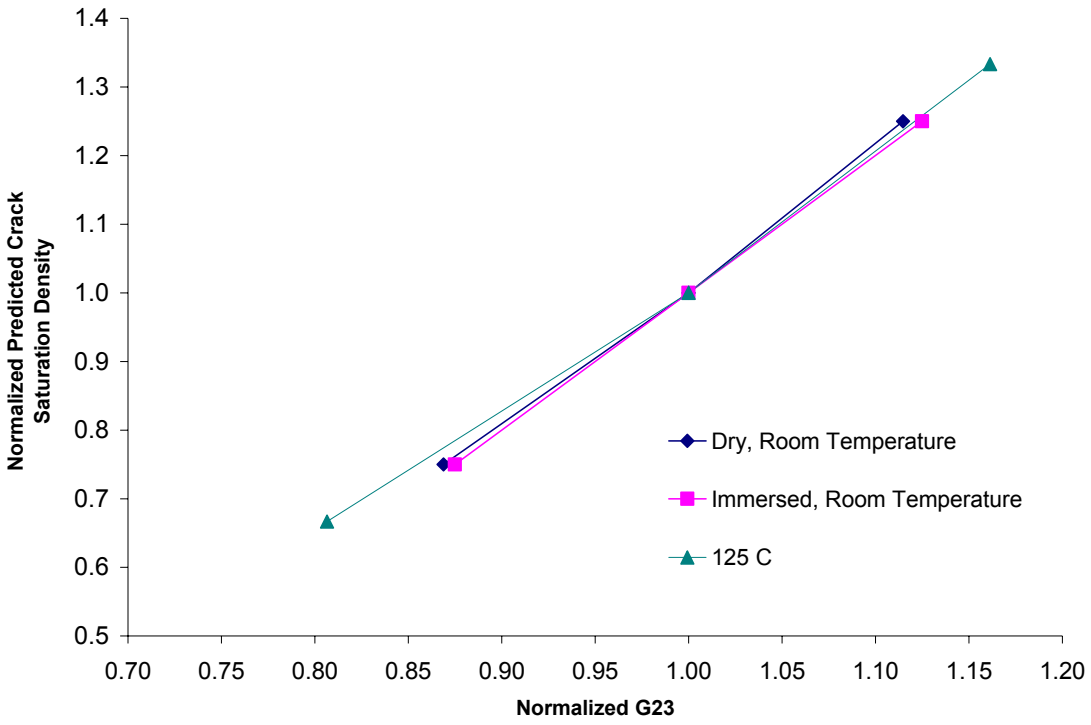

Figure 4.9: G_{23} sensitivity

As mentioned earlier, the consideration of the immersed fatigue case is more complicated in that evolving properties with moisture absorption must be accounted for. Experimental data suggests reduced laminate strength and stiffness at moisture saturation. The prediction results given above assume moisture saturation. While it is true that moisture diffusion during fatigue is enhanced as damage accumulates within the laminate, in this case, using the undamaged laminate moisture saturated properties should still provide a conservative prediction. This conclusion is based on several arguments. One is that the water temperature used in the immersed fatigue case is at room temperature, which means that the diffusion rate will be slow in general (for $[0]_6$ laminate, diffusion coefficient at room temperature was found to be 2.6×10^{-10} cm^2/sec versus 1.73×10^{-9} cm^2/sec at 65°C). In addition, the timeframe involved in the immersed fatigue tests is relatively short (anywhere from 20 minutes to 28 hrs) compared to the moisture absorption time scale. As can be seen in Figure 4.10, at 28 hours, even at 65°C, absorption for the damaged laminates is far less than the undamaged saturation content. Note that the specimen fatigue cycling in this case was done prior to immersion in the water bath (as opposed to immersed fatigue). The third issue is that the majority of the surface area exposed to

the water is actually that of the 0° plies, so even less moisture is reaching interior to the 90° plies. However, if using the properties of the undamaged pre-saturated specimens provides a conservative prediction, than a smaller crack saturation density prediction can be expected if more accurate inputs are used. Thus, it appears that the mechanism by which the crack saturation density of a specimen fatigued in an immersed condition increases remains unaccounted for.

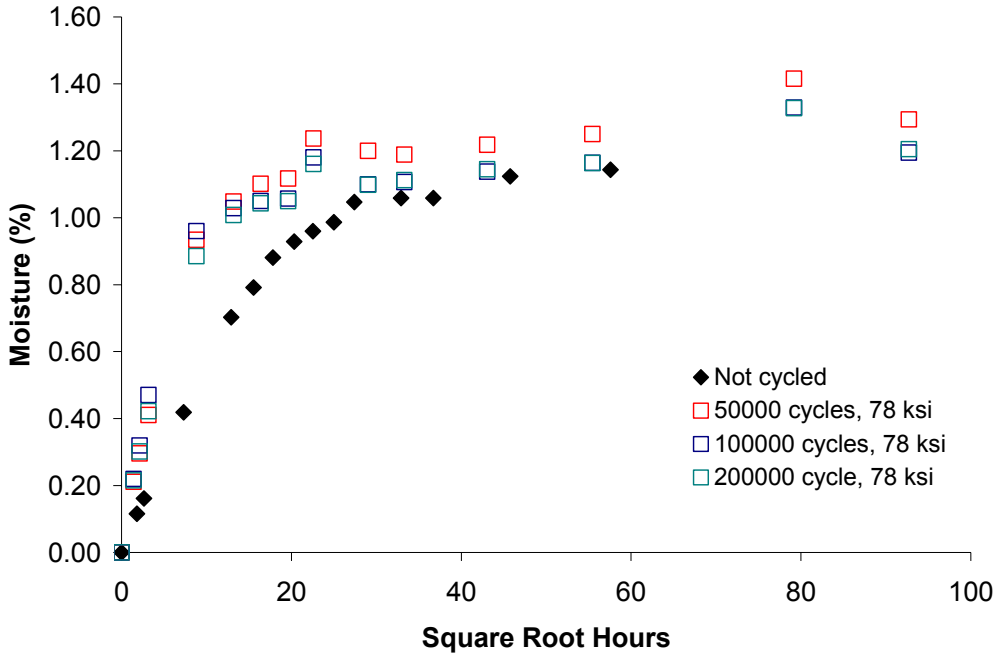

Figure 4.10: Undamaged versus damaged moisture diffusion at 65°C

4.2.3.2 Stiffness Loss

Stiffness loss versus crack density predictions are given in Figure 4.11. Two sets of dry, room temperature experimental data and one set of immersed fatigue (room temperature) data are also shown in the plot. In the case of the room temperature data one specimen (per data set) underwent an interrupted fatigue process in which the specimen was fatigued for a pre-determined number of cycles, tested for stiffness and crack density, and then fatigued to the next pre-determined evaluation point. In the case of immersed fatigue, the process needed to be modified since the specimens were fitted with fluid cells that needed to be removed to test for

stiffness and crack density. Since a "damage-free" fluid cell mounting and removal process could not be guaranteed, separate specimens were used for each number of fatigue cycles evaluated. Such a process generally results in quite a bit of scatter in data. In addition, because it is logistically impossible to get a stiffness measurement with the fluid cell attached, the stiffness measurement must be taken after the fluid cell is removed. As it is likely that the specimen has dried somewhat by the time the post-fatigue stiffness test is done, effectively, a dry stiffness measurement was taken. In this case, unless an increased level of damage (other than cracking) over that incurred in dry fatigue has taken place, one would expect the data to follow along with the results from the dry, room temperature testing. In Figure 4.11, one can see that the immersed fatigue data falls within the range of the dry, room temperature data. In addition to the radiographs, this result provides evidence that the immersed fatigue specimens do not undergo a greater degree of delamination than dry fatigue specimens.

Elevated temperature data is also not available for evaluation due to equipment difficulties. An attempt to use single specimens as was done for room temperature was met with complications in that it was necessary to remove specimens from the test chamber to perform the edge replica in a room temperature environment. This intermittent cooling and heating appeared to have an adverse affect on fatigue lives and rendered the data unobtainable and/or unreliable. An attempt to use multiple specimens as was done for the immersed fatigue data was also unsuccessful as the data obtained was scattered and did not follow any reasonable trend. This behavior was attributed to the material issues described in Section 3.2 and equipment issues described in Section 3.3.5.1.

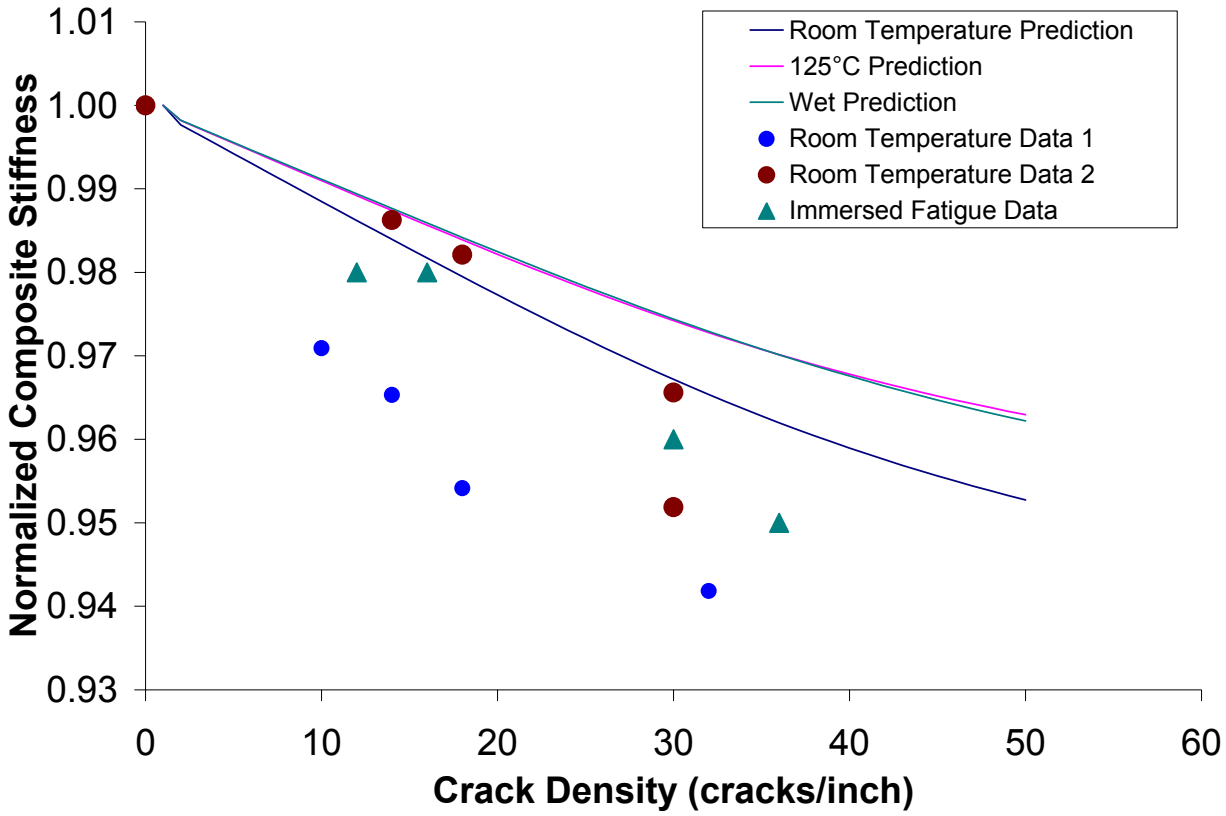

Figure 4.11: Stiffness loss versus crack density

Since it was difficult to examine the accuracy of the stiffness loss aspect of the model with the data, other methods were used for comparison. Specifically, the two other methods used for comparison were FEM modeling and the Hashin model [67]. The FEM results refer to a 2-D model (quarter unit cell) evaluated in ANSYS. While the three methods do not agree completely, they are reasonably close, suggesting that any shortcomings in the Henaff-Gardin method of determining stiffness loss is not unique but is also present in other traditionally accepted methods. However, all three methods generally overpredict the experimental room temperature values, especially at the higher crack density values. This increasing discrepancy may suggest that delamination does indeed play a role in the fatigue process, but this result was not apparent in the radiographs done previously.

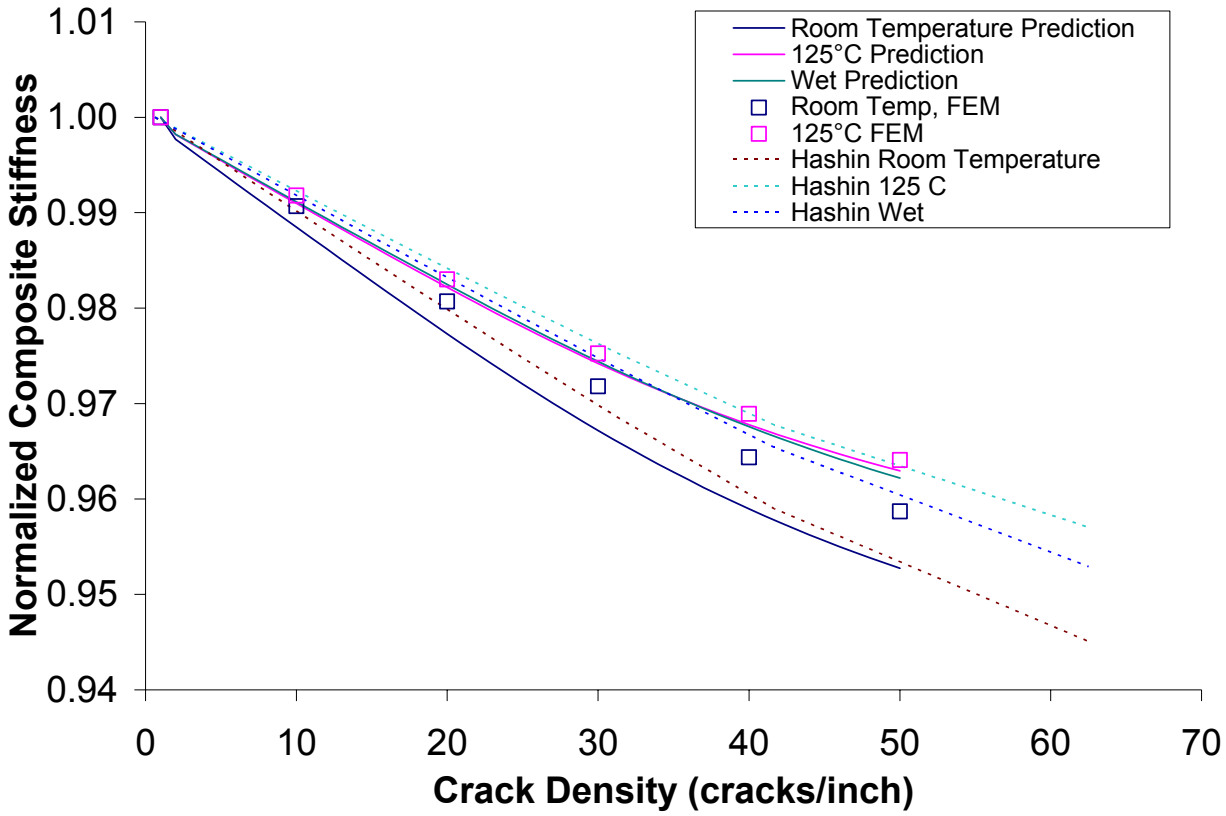

Figure 4.12: Comparison of stiffness loss prediction models

4.3 Summary of Analytical Results

In the analytical phase of this study, two micromechanical based models were selected for evaluation. The models were selected based upon the perceived ease of obtaining the inputs necessary to run the models, the extent to which empirical parameters are incorporated into the models, and the robustness of the models in terms of the ability to evaluate varying environments. To that end, the Gao and Reifsnider [51] composite strength model and the Henaff-Gardin [57-60] damage model were chosen for detailed evaluation.

The composite strength modeling effort was successful in predicting dry, room temperature unidirectional composite strength. Experimental evidence suggests that the unidirectional strengths can be used to directly to predict cross-ply laminate strength. Moreover, it was shown that the increase in pre-saturated laminate strength could be predicted with the use of a CLT

analysis that includes thermal and residual stresses. Thus, ultimately, one could use the unidirectional strength prediction to also predict cross-ply strength as a function of moisture content. The strength predictions at elevated temperatures were not as accurate and tended to be quite conservative. No definitive reason behind this result was found, but further evaluation showed that conservative predictions may be a consequence of inaccurate matrix shear stiffness and matrix shear strength. Inaccuracy in the matrix shear strength values used is quite possible as was only estimated from the matrix tensile strength. The matrix shear stiffness was calculated from matrix tensile stiffness by assuming that the resin was isotropic. Thus, inputs may be inaccurate if the resin is actually anisotropic.

The damage model proved difficult to evaluate due to the complications in obtaining model inputs. The complications encountered included material and equipment abnormalities and difficulty in determining input values such as first ply failure stress and out-of-plane shear stiffness. The analysis was particularly sensitive to first ply failure stress. In this study, it was determined by including full thermal and hygral residual stresses in a CLT analysis along with the use of transverse tensile strength in the maximum stress criterion. Generally, the analysis correctly predicted the decrease in crack saturation density found in going from dry, room temperature fatigue to dry, elevated temperature fatigue but incorrectly predicted a decrease in crack saturation density in going from the dry, room temperature condition to the immersed fatigue condition. On a quantitative basis, the crack saturation densities predicted for the dry, room temperature condition and the dry, elevated temperature conditions were 50% higher than experimental values. This result was attributed in large part to the uncertainty in the first ply failure stress. A more reliable method of determining the exact value of the first ply failure stress or its relationship to the transverse tensile strength has yet to be developed. A more accurate value is likely to correct the quantitative discrepancies in the model predictions for the dry room temperature and elevated temperature conditions, but the prediction for the immersed fatigue case is likely to remain significantly conservative. As yet, the mechanism behind the increased crack saturation density in immersed fatigue specimens (over that of dry fatigue specimens) has not been identified.

Stiffness loss versus crack density results were also ambiguous due to lack of consistent experimental data. The available data shows that the prediction works reasonably well for dry, room temperature stiffness loss except at higher crack densities. A comparison with other generally recognized stiffness loss prediction schemes such as FEM analysis and the Hashin model reveals a good agreement between them and the Henaff-Gardin analysis. The fact that the agreement of the model does over-predict stiffness at higher crack densities suggests that delamination may indeed be an issue though such a phenomenon was not substantiated by the radiography results. However, more accurate data is clearly needed to assess the stiffness loss results, particularly at elevated temperature and for immersed fatigue.

5 SUMMARY AND CONCLUSIONS

The goal of this work was to create a better understanding of how temperature and moisture may affect strength and fatigue behavior of carbon/epoxy composite materials. This included not only generating and examining experimental evidence, but also considering the accuracy of existing models in predicting such behavior.

Experimentally, difficulties were encountered in acquiring necessary data in that both the material and the testing equipment exhibited problems. The conclusions formed from the experimental phase of this work include:

1) Most thermal properties for the resin and composite could be obtained in a straightforward manner, except the stress-free temperature. In this case, a somewhat subjective approach was used to estimate the value.
2) Resin and transverse laminate properties do not necessarily follow the same trends with temperature and moisture. This result suggests significant processing differences as well as possible interfacial degradation in the transverse laminates.
3) Coefficients of moisture expansion may be obtained with a combined experimental and analytical approach. A method described by Tsai et al. [42] proved useful for this purpose though the calculated stress-free temperature that came from the analysis did not appear to be accurate.
4) Tensile tests on unidirectional and composite laminates reveal that the strengths of the two degrade in a very similar manner with temperature. Such a result implies that cross-ply strength predictions can be obtained directly from unidirectional strength predictions and that reasonable estimates of unidirectional strength can be obtained based on cross-ply results. This is significant since $[0/90]_{ns}$ laminates are much easier to test than $[0]_n$ laminates.
5) The tensile strength of cross-ply laminates does increase with moisture content. This phenomenon is attributed to moisture induced relief of thermal residual stresses.
6) Fatigue testing results indicate that both temperature and moisture may shorten fatigue lives of specimens as compared to that of dry, room temperature conditions. However,

moisture only appears to affect fatigue lives in the actual immersed condition (as opposed to the condition in which the specimen is pre-saturated, but fatigued dry). This result indicates that the shortened fatigued lives in the immersed fatigue case may be a consequence of more than just material property degradation.

7) Radiography results indicate that the crack saturation density of fatigued specimens decreases with temperature (dry or in an immersed condition), but increases for the immersed fatigue condition. Again, results from pre-saturated specimens fatigued dry show no difference from that of dry specimens fatigue dry at room temperature. The decrease in crack density at elevated temperatures may be attributed to factors such as increased toughness, stress relaxation, etc., overcoming material property degradation. The mechanism behind the increase in crack density for the immersed fatigue case, however, is not obvious since it is unlikely that significant material property degradation took place within the time frame associated with the fatigue testing. Thus, this result may be yet another indication that other factors besides bulk material property variation plays a role in immersed fatigue behavior.
8) Crack density results as determined from edge replication and X-radiography do not agree. The discrepancy is most likely due to some combination of the fact that the edge replication process results in an opening of the cracks which makes them more visible and also of the possibility of being able to see smaller cracks with edge replication. As both methods are widely used and relied upon, it is of interest to further pursue the accuracy of each.

The following conclusions were drawn from the analytical phase of this study:

1) A micromechanics based composite strength model can be successfully used to predict room temperature strength of $[0]_n$ composites. These predictions can be directly extended to determine cross-ply strengths. In addition, cross-ply strengths can be predicted as a function of moisture with the application of a CLT analysis which include thermal and hygral residual stresses. The strength model may also be used to conservatively predict strength as a function of temperature. Because the predictions are conservative, they may be of use in design applications. To obtain more accurate

predictions, one would need more accurate assessments of matrix shear yield strength and matrix shear stiffness at elevated temperatures.

2) Evaluation of a damage model to predict crack density and its affect on composite stiffness proved inconclusive. While experimental issues are partly to blame for the ambiguity in the results, several model inputs were also found to be difficult to obtain. The most important of these inputs was the first ply failure stress, to which the results of the analysis are quite sensitive. Unless a reliable experimental method for determining the first ply failure stress is developed, one must resolve the issues of the how to include residual hygro-thermal stresses and find a suitable failure criterion to incorporate. As yet, these issues are generally unresolved in the literature. An alternative solution to the above described problem would be to directly determine the critical strain energy release rate. The experimental implications of such an endeavor have not been investigated as part of this study.
3) The damage model did predict the decrease in crack density observed between dry, room temperature fatigue testing and dry, elevated temperature fatigue testing. The increase in crack density observed for the immersed fatigue case was not predicted and it is unlikely that more accurate inputs would result in an accurate prediction for this case.
4) Composite stiffness loss results from the analysis agree reasonably well with other well established stiffness loss determination methods, indicating that the theory falls in step with traditional ideas. The predictions were found to be somewhat conservative compared to the available data, indicating that other damage mechanisms (most likely, delamination) may be an issue. However, delamination was not apparent in the radiographs.

While the results of the overall study were largely inconclusive, a contribution was made to the overall understanding of thermal and hygral effects on strength and fatigue behavior of carbon/epoxy composites. Moreover, the study highlighted complications involved in incorporating models which claim to be adaptable to varying environments. Much work is still needed in improving experimental and/or analytical methods for determining basic material properties before models can be truly validated and relied upon to accurately account for environmental factors without the use of empirical parameters.

6 FUTURE WORK

Since the results of this study were somewhat inconclusive, the need for additional work is clearly indicated. These efforts should include the following:

1) Obtain reliable experimental results to more clearly identify the accuracy of modeling results. Aside from obtaining material which is more consistent and testing on reliable testing apparatus, this will include the following:
    a. Devising a way in which elevated temperature and immersed interrupted fatigue tests may be conducted using single specimens throughout a range of fatigue cycles. This will eliminate some degree of scatter in fatigue data. For immersed fatigue testing, the use of a laser extensometer may be of use in this effort.
    b. Develop an experimental method to determine in-situ first ply failure stress for transverse plies in cross-ply laminates. For the dry, room temperature case, one may investigate the use of acoustic emission techniques; however, the immersed fatigue case and the elevated temperature case, the solution may be more complicated.
    c. As an alternative to the above, one may try to experimentally determine critical strain energy release rates for direct input into the Henaff-Gardin analysis. Again, while this may be practical for the dry, room temperature conditions, experimental techniques for the elevated temperature and immersed fatigue conditions may become complicated.
2) Further investigate the discrepancy between crack density results as determined by radiography and edge replications. This may require a careful effort in which images from each method are matched up such that one can directly compare them and establish whether cracks are too small to show up on radiographs or not opened up enough to show up on radiographs.
3) Further investigation of the relationship between the tensile and shear yield stress of polymers, particularly as a function of temperature would prove useful in obtaining more accurate composite strength predictions as a function of temperature. Alternatively,

development of experimental methods to directly determine shear yield strength would serve the same purpose.

4) A detailed experimental investigation into the effects of temperature and moisture on fiber fracture and interfacial properties would help to explain the differences observed in fatigue lives among the different test conditions.
5) The mechanism which drives the crack saturation density of immersed fatigue specimens to be higher than that of specimens tested dry is as yet unknown. Material property degradation does not appear to be an issue for the time frame and water temperature involved and the phenomenon is unlikely to be accurately predicted by models such as that given by Henaff-Gardin. The exact nature of this behavior should be explored and incorporated into modeling efforts.
6) Once the experimental results are better defined, the models may be re-examined in more detail.

7 REFERENCES

1. Ellyin, Fernand. Rohrbacher, Christof. "The influence of aqueous environment, temperature and cyclic loading on glass-fibre/epoxy composite laminates," *Journal of Reinforced Plastics & Composites*, Vol. 22 (2003) pp. 615-636.

2. Choqueuse, D. Davies, P. Mazeas, F. Baizeau, R. "Aging of composites in water: Comparison of five materials in terms of absorption kinetics and evolution of mechanical properties," *Proceedings of the 1995 Symposium on High Temperature and Environmental Effects on Polymeric Composites*, ASTM STP 1302, Conshohocken, PA: 1997, pp. 73-96.

3. Effect of moisture on the tensile and interlaminar shear strengths of glass or carbon fiber reinforced PEI, *Journal of Materials Science Letters*, Vol. 19 (2000), pp. 579-581.

4. Weitsman, Y. J. and Elahi, M. "Effects of Fluids on the Deformation, Strength and Durability of Polymeric Composites – An Overview," *Mechanics of Time Dependent Materials*, Vol. 3 (2000), pp. 107-126.

5. Suh D., Ku, M., Nam, J., Kin, B., and Yoon, S. "Equilibrium of Water Uptake of Epoxy/Carbon Fiber Composites in Hygrothermal Environmental Conditions," *Journal of Composite Materials*, Vol. 35 (3), pp. 264-278.

6. Zhou, J. and Lucas, J. P. "Hygrothermal effects of epoxy resin. Part I: the nature of water in epoxy," *Polymer*, Vol. 40 (1999), pp. 5505-5512.

7. Blikstad, M., Sjoblom, P. O. W., and Johannesson, T. R. "Long-Term Moisture Absorption in Graphite/Epoxy Angle-Ply Laminates," *Journal of Composite Materials*, Vol. 18 (1), pp. 32-46.

8. Gillat, O. and Broutman, I. J. "Effect of an External Stress on Moisture Diffusion and Degradation in a Graphite-Reinforced Epoxy Laminate," *ASTM STP 658*, Philadelphia, PA: ASTM (1976), pp. 61-83.

9. Roy, S and Xu, W. "Modeling of diffusion in the presence of damage in polymer matrix composites", *International Journal of Solids and Structures*, Vol. 38 (1), pp. 115-125.

10. Obst, A. W., VanLandingham, M. R., Eduljee, R. F., Gillespie, J. W., Griesheim, G. E., and Tosi, K. F. "The effect of hygrothermal cycling on the microcracking behavior of fabric laminates," *Technology Transfer in a Global Community International SAMPE Technical Conference*, Vol. 28 (1996), pp. 994-1002.

11. Patel, S. and Case, S. "Durability of hygrothermally aged graphite/epoxy woven composite under combined hygrothermal conditions," *International Journal of Fatigue*, Vol. 24 (2002), pp. 1295-1301.

12. Roy. S., Xu, W., Patel, S., and Case, S. "Modeling of moisture diffusion in the presence of bi-axial damage in polymer matrix composite laminates," *International Journal of Solids and Structures*, Vol. 38 (2001), pp. 7627-7641.

13. Hahn, H. T. "Residual Stresses in Polymer Matrix Composite Laminates," *Journal of Composite Materials*, Vol. 10 (1976), pp. 266-278.

14. Demonet, C. M. "Interaction of moisture with resin matrix composites," *21st International SAMPE Technical Conference*, 1989, pp. 231-238.

15. Shen, C. and Springer, G. S. "Effects of moisture and temperature on the tensile strength of composite materials," *Environmental Effects on Composite Materials*, Westport, CT: Technomic Publishing Company, Inc. (1981), pp. 79-93.

16. Bradley, W. L. and Grant, T. S. "The effect of moisture absorption on the interfacial strength of polymeric matrix composites," *Journal of Materials Science*, Vol. 30 (21), pp. 5537-5542.

17. Zhang, M. and Mason, S. E. "The effects of contamination on the mechanical properties of carbon fiber reinforced epoxy composite materials," *Journal of Composite Materials*, Vol. 33 (14), pp. 1363-1374.

18. Zhuang, H. and Wightman, J. P. "The Influence of Surface Properties on Carbon Fiber/Epoxy Matrix Interfacial Adhesion," *Journal of Adhesion*, Vol. 62 (1996), pp. 213-245.

19. Mear, S. T, Wheat, H. G., and Marcus, H. L. "Corrosion Fatigue Behavior of a Graphite/Epoxy Composite for Marine Applications," Proceedings of the 8th International Offshore and Polar Engineering Conference, May 24-29, 1998.

20. Sloan, F. E. and Seymour, R. J. "Effect of seawater exposure on Mode I interlaminar fracture and crack growth in graphite/epoxy," *Journal of Composite Materials*, Vol. 26(18), pp. 2655-2673.

21. Kosuri, R. and Weitsman, Y. "Sorption processes and immersed fatigue response of gr/ep composites in sea water," Proceedings of the ICCM-10, Whistler, British Columbia, Canada, 4: pp. 177-184.

22. Smith, L.V. and Weitsman, Y.I. "The immersed fatigue response of polymer composites," *International Journal of Fatigue*, Vol. 82 (1996), pp. 31-42.

23. Komai, K., Minoshima, K., Shibutani, T., and Nomura, T. "The influence of water on the mechanical properties and fatigue strength of angle-ply carbon/epoxy composites," *JSME*

International Journal, Series 1: Solid Mechanics, Strength of Materials, Vol. 32 (4), pp. 588-595.

24. Nakanishi, Y. and Shindo, A. "Deterioration of CFRP and GFRP in salt water," *Progress in Science and Engineering of Composites*, ICCM – IV (1982), pp. 1009-1016.

25. McLaughlin, P. V. D. Jr., McShane, H. A., Cochran, R., and Armstrong-Carroll, E. "Effects of High Heat on the Strength and Fatigue Life of Unidirectional Polymer-Matrix Composites," Proceedings of the ASME Aerospace and Materials Divisions, AD Vol. 51/MD Vol. 73 (1996), pp. 427-441.

26. Takeda, N. and Ogihara, S. "In situ observation and probabilistic prediction of microscopic failure processes in CFRP cross-ply laminates," *Composites Science and Technology*, Vol. 52 (1994), pp. 183-195.

27. Detassis, M., Pegoretti, A., and Migliaresi, C. "Effect of temperature and strain rate on interfacial shear stress transfer in carbon/epoxy model composites," *Composites Science and Technology*, Vol. 53 (1995), pp. 39-46.

28. Wimolkiatisak, A. S. and Bell, J. P. "Interfacial Shear Strength and Failure Modes of Interphase-Modified Graphite-Epoxy Composites," *Polymer Composites*, Vol. 10 (3), pp. 162-172.

29. Reifsnider, K. L. and Case, S. W. "Mechanics of Temperature-Driven Long-Term Environmental Degradation of Polymer-Based Composite Systems," ASME Materials Division American Society of Mechanical Engineers, MD-Vol. 69-1 (1995), pp. 225-230.

30. Case, S. W. "Mechanics of Fiber-Controlled Behavior in Polymeric Composite Materials," Ph.D. Dissertation, Virginia Polytechnic Institute and State University, 1996.

31. Loverich, J. S., Russell, B. E., Case, S. W., and Reifsnider, K. L. "Life prediction of PPS composites subjected to cyclic loading at elevated temperatures," *Time Dependent and Nonlinear Effects in Polymers and Composites*, ASTM STP 1357, Philadelphia: ASTM (2000), pp. 310-317.

32. Sjogren, A. and Asp, L. E. "Effects of temperature on delamination growth in a carbon/epoxy composite under fatigue loading," *International Journal of Fatigue*, Vol. 24 (2002), pp. 179-184.

33. Almen, G. R., Byrens, R. M., MacKenzie, P. D., Maskell, R. K., McGrail, P. T., and Sefton, M. S. "977 – A family of new toughened epoxy matrices," *34th International SAMPE symposium*, Covina, CA: SAMPE, 1989, pp. 259-270.

34. Almen, G., MacKenzie, P., Malhotra, V., and Maskell, R. "977: Characterization of a family of new toughened epoxy resins," *35th International SAMPE Symposium*, 1990, pp. 419-431.

35. Browning, C. E., Husman, G. E., and Whitney, J. M. "Moisture absorption and desorption of composite materials," *Journal of Composite Materials*, Vol. 10, pp.2.

36. Karasek, M. L., Strait, L. H., Amateau, M. F., and Runt, J. P. "Effect of temperature and moisture on the impact behavior of graphite/epoxy composites: Part I-Impact energy absorption," *Journal of Composites Technology and Research*, Vol. 17 (1), pp. 3-10.

37. Karasek, M. L., Strait, L. H., Amateau, M. F., and Runt, J. P. "Effect of temperature and moisture on the impact behavior of graphite/epoxy composites: Part II-Impact damage," *Journal of Composites Technology and Research*, Vol. 17 (1), pp. 11-16.

38. Asp, L. E. "The effects of moisture and temperature on the interlaminar delamination toughness of a carbon/epoxy composite," *Composites Science and Technology*, Vol. 58 (1998), pp. 967-977.

39. Shen, C. and Springer, G. S. "Moisture Absorption and Desorption of Composite Materials," *Journal of Composite Materials*, Vol. 10 (1976), p. 18.

40. Loos, A. C. and Springer, G. S. *Environmental Effects on Composite Materials*, Lancaster, PA: Technomic Publishing Company, Inc., 1981.

41. Zhou, J. and Lucas, J. P. "The effects of a water environment on anomalous absorption behavior in graphite/epoxy composites," *Composites Science and Technology*, Vol. 53 (1995), pp. 57-64.

42. Tsai, C L, Wooh, S C, Hwang, S F, and Du, Y. "Hygric Characterization of Composites Using an Antisymmetric Cross-ply Specimen," *Experimental Mechanics*, Vol. 41 (3), pp. 270-276.

43. Odegard, G. and Kumosa, M. "Elastic-plastic and failure properties of a unidirectional carbon/PMR-15 composite at room and elevated temperatures," *Composites Science and Technology*, Vol. 60 (2000), pp. 2979-2988.

44. The composite materials handbook – MIL 17, Lancaster, PA: Technomic Publishing Company, 1990.

45. Tsai, S.W. and Hahn, H.T., *Introduction to Composite Materials*, Technomic Publishing Company, Inc., 1980.

46. Rosen, B.W. "Tensile Failure of Fibrous Composites," *AIAA Journal*, Vol. 2 (1964), pp. 1985-1991.

47. Smith, R. L., Phoenix, S. L., Greenfield, M. R., Henstenburg, R. B., Pitt, R. E. "Lower-Tail Approximations for the Probability of Failure of Three-Dimensional Fibrous Composites

with Hexagonal Geometry," *Proceedings of the Royal Society of London A*, Vol. 388, 1983, pp. 353-391.

48. Zhou, S. J., Curtin, W. A. "Failure of Fiber Composites: A Lattice Green Function Model," *Acta Metallurgica et Materialia*, Vol. 43, No. 8, 1995, pp. 3093-3104.

49. Hedgepeth, J. M., Van Dyke, P. "Local Stress Concentrations in Imperfect Filamentary Composite Materials," *Journal of Composite Materials*, Vol. 1, 1967, p. 294-309.

50. Bandorawalla, T., "Micromechanics-Based Strength and Lifetime Prediction of Polymer Composites," Ph.D. dissertation, Virginia Polytechnic Institute and State University, 2002.

51. Gao, Z. and Reifsnider, K. L. "Micromechanics of Tensile Strength in Composite Systems," *Composite Materials: Fatigue and Fracture, Fourth Volume*, ASTM STP 1156, Philadelphia, PA: ASTM (1993), pp. 453-470.

52. Reifsnider, K. L. and Case, S. W. *Damage Tolerance and Durability of Composite Materials*, John Wiley &Sons, Inc., New York (2002), p. 241.

53. Batdorf, S. B. "Tensile strength of unidirectional reinforced composites—I," *Journal of Reinforced Plastics and Composites*, Vol. 1 (1982), pp. 153-176.

54. DiBeneditto, A. T. "Measurement of thermomechanical stability of interphases by the embedded single fiber test," *Composites Science and Technology*, Vol. 42 (1992), pp. 103-123.

55. Case, S. W. and Reifsnider, K, L. *MRLife 12* Manual, 1999.

56. Curtin, W. A. and Takeda, N. "Tensile strength of fiber-reinforced composites: II. Application to polymer matrix composites," *Journal of Composite Materials*, Vol. 32 (1998) pp. 2060-2081.

57. Henaff-Gardin, C., Lafarie-Frenot, M. C. "The use of a characteristic damage variable in the study of transverse cracking development under fatigue loading in cross-ply laminates," *International Journal of Fatigue*, Vol. 24 (2002), pp. 389-395.

58. Henaff-Gardin, C. and Lafarie-Frenot, M. C. "Fatigue behavior of thermoset and thermoplastic cross-ply laminates," *Composites*, Vol. 23 (1992), pp. 109-116.

59. Henaff-Gardin, C. and Lafarie-Frenot, M.C. "Specificity of matrix cracking development in CFRP laminates under mechanical or thermal loadings," *International Journal of Fatigue*, Vol.24 (2002), pp. 171–177.

60. Henaff-Gardin, C., Lafarie-Frenot, M.C., and Gramby, D. "Doubly-periodic matrix cracking in composite laminates. Part I: general in-plane loading," *Composite Structures*, Vol. 36 (1-2), pp. 113-130.

61. Akshantala, N. V. and Talreja, R. "A mechanistic model for fatigue damage evolution in composite laminates," *Mechanics of Materials*, Vol. 29 (1998), pp. 123-140.

62. Akshantala, N. V. and Talreja, R. "A micromechanics based model for predicting fatigue life of composite laminates," *Materials Science and Engineering A*, Vol. 285 (2000), pp. 303-313.

63. Flaggs, D. L. and Kural, M. H. "Experimental Determination of the In Situ Transverse Lamina Strength in Graphite/Epoxy Laminates," *Journal of Composite Materials*, Vol. 16 (1982), pp. 103-116.

64. Hinton, M. J., Kaddour, A. S., and Soden, P. D. "A Comparison of the Predictive Capabilities of Current Failure Theories for Composite Laminates, Judged Against Experimental Evidence," *Composites Science and Technology*, Vol. 62 (2002), pp. 1725-1797.

65. Kam, T. Y. and Sher, H. F. "Nonlinear and First-Ply Failure Analyses of Laminated Composite Cross-Ply Plates," *Journal of Composite Materials*, Vol. 29 (1995), pp. 463-482.

66. Kim, R. Y. and Hahn, H. T. "Effect of Curing Stresses on the First Ply Failure in Composite Laminates," *Journal of Composite Materials*, Vol. 13 (1979), pp. 2-16.

67. Hashin, Z. "Analysis of Stiffness Reduction of Cracked Cross-Ply Laminates," *Engineering Fracture Mechanics*, Vol. 25 (1986), pp. 771-778.

APPENDIX A – GAO AND REIFSNIDER MODELING MATHEMATICA CODE

Inputs and Calculated Parameters

Note: Required manual inputs are in italics

Fiber, matrix properties

```
Em = 4.4 * 10^9; (*matrix modulus in Pa*)
Ef = 232. * 10^9; (*fiber modulus in Pa*)
ν12m = .43;      (*matrix Poisson's Ratio*)
Gm = Em / (2 * (1 + ν12m)); (*matrix shear modulus*)
τ0 = 25.88 * 10^6; (*shear yield stress in Pa*)
```

Fiber statistical parameters

```
σo=3.17*10^9; (*fiber reference strength*)
m=5.1; (*fiber Weibull modulus*)
Lo=25.*10^-3; (*fiber reference length*)
```

Composite Parameters

```
vf = .53; (*fiber volume fraction*)
Num = Area * vf / Af; (*total number of fibers*)
Ec = vf * Ef + (1 - vf) * Em; (*bulk composite modulus*)
E1 = (Ef * Af + Em * Am) / (Af + Am); (*effective broken core modulus*)
η = 1;(*shear parameter*)
ni = {6 , 8, 9, 10, 11, 11 , 12 , 13, 13 , 14 , 15, 15, 16 , 16 , 16 , 17 , 17, 18, 18, 18, 19, 19, 20, 20, 20, 21, 21,
  21, 22, 22, 22, 23, 23, 23, 23, 24, 24, 24, 24, 25, 25, 25, 25};
(*number of neighboring fibers for the corresponding number of adjacent broken fibers
  (i.e. 6 adjacent fibers of 1 broken fiber, 8 intact fibers neighboring 2 adjacent broken fibers, etc.)*)
```

Geometrical Parameters

```
rf = .0000035; (*fiber radius in m*)
d1 = rf/Sqrt[vf] - rf; (*diameter of matrix ring around fiber*)
Af = π * rf^2; (*fiber area*)
Am = π * (rf + d1)^2 - π * rf^2; (*matrix area*)
Area = w * t; (*specimen area*)
L = .1524; (*specimen length*)
w = .0127; (*specimen width*)
t = .001016; (*specimen thickness*)
```

Model Parameters

```
elem=Dimensions[ni][[1]]; (*highest number of adjacent fiber breaks considered*)
```

Determine model parameters as a function of the number of adjacent fiber breaks (i)

```
Do[r0[i_] = Sqrt[i * (rf + d1)^2];
 R2[i_] = r0[i] + 2 * rf + d1;
 E2[i] = (ni[[i]] * Af * Ef + (π * ((r0[i] + 2 * rf + d1)^2 - r0[i]^2) - ni[[i]] * Af) * Em)/(π * ((r0[i] + 2 * rf + d1)^2 - r0[i]^2));
 λ[i] = Sqrt[(2 * R2[i])/(R2[i]^2 - r0[i]^2) * Gm/E2[i] * 1/(2 d1)];
 α[i] = 1/r0[i] * Gm/E1 * 1/d1;
 β[i] = r0[i]/(R2[i]^2 - r0[i]^2) * Gm/E2[i] * 1/d1;
 ϕ[i] = R2[i]/(R2[i]^2 - r0[i]^2) * Gm/E2[i] * 1/d1;
 γ1[i] = 1/2 * (α[i] + β[i] + ϕ[i] - Sqrt[(-α[i] - β[i] - ϕ[i])^2 - 4 * α[i] * ϕ[i]]);
 γ2[i] = 1/2 * (α[i] + β[i] + ϕ[i] + Sqrt[(-α[i] - β[i] - ϕ[i])^2 - 4 * α[i] * ϕ[i]]);

 , {i, 1, elem}]
```

Model Calculations

Calculate displacements as a function of number of adjacent fiber breaks (i) and load step (j)

```
Do[Do[σf[j] = σo * j / 10;
  U0a[x_, i, j] = η * τ0 / (r0[i] * E1) * x^2 + C1[i, j];
  U1a[x_, i, j] = C2[i, j] * (Exp[λ[i] * x] - Exp[-λ[i] * x]) + 2 * r0[i] * η * τ0 / ((R2[i]^2 - r0[i]^2) * E2[i] * λ[i]^2) * (1 - Exp[-λ[i] * x]) + σf[j] / Ef x;
  U0b[x_, i, j] = C3[i, j] * Exp[-Sqrt[γ1[i]] * x] + C4[i, j] * Exp[-Sqrt[γ2[i]] * x] + σf[j] / Ef x;
  U1b[x_, i, j] = -(γ1[i] - α[i]) / α[i] * C3[i, j] * Exp[-Sqrt[γ1[i]] * x] - (γ2[i] - α[i]) / α[i] * C4[i, j] * Exp[-Sqrt[γ2[i]] * x] + σf[j] / Ef x,
  {i, 1, elem}], {j, 1, 10}]
```

Apply boundary conditions and solve for constants of integration

```
Do[Do[eqn1[i, j] = U1b[a, i, j] - U1a[a, i, j] == 0;
eqn2[i, j] = U0b[a, i, j] - U0a[a, i, j] == 0;
eqn3[i, j] = ((∂x U1b[x, i, j] - ∂x U1a[x, i, j]) /. x → a) == 0;
eqn4[i, j] = ((∂x U0b[x, i, j] - ∂x U0a[x, i, j]) /. x → a) == 0;
constants[i, j] = Solve[{eqn1[i, j], eqn2[i, j], eqn3[i, j], eqn4[i, j]}, {C1[i, j], C2[i, j], C3[i, j], C4[i, j]}];
  t1[i, j] = Table[constants[i, j][[1, k, 1]], {k, 1, 4}];
  pC1[i, j] = Position[t1[i, j], C1[i, j]][[1, 1]];
pC2[i, j] = Position[t1[i, j], C2[i, j]][[1, 1]];
pC3[i, j] = Position[t1[i, j], C3[i, j]][[1, 1]];
pC4[i, j] = Position[t1[i, j], C4[i, j]][[1, 1]];
C1[i, j] = constants[i, j][[1, pC1[i, j], 2]];
C2[i, j] = constants[i, j][[1, pC2[i, j], 2]];
C3[i, j] = constants[i, j][[1, pC3[i, j], 2]];
  C4[i, j] = constants[i, j][[1, pC4[i, j], 2]];
  , {i, 1, elem}], {j, 1, 10}]
```

Solve for distance a (region of matrix yielding and plastic deformation) as a function number of adjacent fiber breaks and load step

```
  Do[Do[a1[i, j] = FindRoot[(U0a[a, i, j] - U1a[a, i, j]) * Gm / (2 * d1) - τ0 == 0, {a, 1}][[1, 2]];,
    {i, 1, elem}], {j, 1, 10}]
Do[Do[a[i,j]=a1[i,j],{i,1,elem}],{j,1,10}]
```

Substitute values of a into displacement expressions

```
Do[Do[U0a[x_,i,j]=U0a[x,i,j]/.a→a[i,j];
   U1a[x_,i,j]=U1a[x,i,j]/.a→a[i,j];
   U0b[x_,i,j]=U0b[x,i,j]/.a→a[i,j];
   U1b[x_,i,j]=U1b[x,i,j]/.a→a[i,j];,{i,1,elem}],{j,1,10}]
```

Calculate stress concentrations

```
Do[Do[sc[i, j] = (∂x U1a[x, i, j] / (σf[j] / Ef)) /. x → 0, {i, 1, elem}], {j, 1, 10}]
```

Calculate ineffective lengths

```
Do[d2[x_, i, j] = ∂x U1b[x, i, j] / (σf[j] / Ef), {i, 1, elem}, {j, 1, 10}];
```

Batdorf Analysis

Calculate probabilities of finding i number of adjacent fiber breaks for each load step

```
Do[

    Q[1, j] = Num * L/Lo * (σf[j]/σo)^m;

        lam[i, j] = δ[i, j] * (sc[i, j]^(m+1) - 1) / (sc[i, j]^m * (sc[i, j] - 1) * (m + 1));

    Q[i + 1, j] = Q[i, j] * ni[[i]] * lam[i, j]/Lo * (sc[i, j] * σf[j]/σo)^m;,

    {i, 1, elem}, {j, 1, 10}];
```

```
Do[Do[
Qtable[i]=Table[{Log[σf[j]],Log[Q[i,j]]},{j,2,10}],{i,1,elem}]];
```

Solve for and Xt

```
Do[qfit[j]=Fit[Qtable[j],{1,x},x],{j,1,elem}];
Do[lnσ[i]=Solve[qfit[i]==0,x],{i,1,elem}]
Table[{i,lnσ[i][[1,1,2]]},{i,1,elem}]
```

```
σfr = Exp[lnσ[37][[1, 1, 2]]]; (*stress at catastrophic failure*)
ϵc = σfr/Ef; (*bulk composite strain*)
Xt = Ec * ϵc / 6900000 (*strength calculation*)
```

APPENDIX B – HENAFF-GARDIN MODELING MATHEMATICA CODE

Model Inputs

```
E1 = 17.3; (*0 degree modulus, msi*)
E2 = 1.27; (*90 degree modulus, msi*)
G23 = .4; (*out of plane shear modulus,msi*)
ν12 = .43; (*composite Poisson's Ratio*)
α1 = -3.04 * 10^-7; (*0 degree CTE*)
α2 = 4.08 * 10^-5; (*90 degree CTE*)
Tf = 155; (*Stress free temperature, C*)
Tref = 27; (*Applied temperature*)
ΔT = Tref - Tf;
MC = 0; (*moisture concentration*)
ΔM = 1.52 * MC; (*change in moisture concentration assuming 0 initial moisture content*)
β1 = .016; (*0 degree coefficient of moisture expansion*)
β2 = .186; (*90 degree coefficient of moisture expansion*)
t0 = .008; (*0 degree ply thickness*)
t90 = .008; (*90 degree ply thickness*)
d0 = 1; (*axial crack spacing*)
```

Stress Calculations

```
σxo[x_, y_, d90_] = A[d90] * Cosh[R * λx * x] + B[d90] * Cosh[R * λy * y] + Kx;
σx90[x_, y_, d90_] = ((t0 + t90) * σxbar - t0 * σxo[x, y, d90]) / t90;

σyo[x_, y_, d90_] = A[d90] * ((ν12 * E2 * (t0 + t90)) / (t0 * E2 + t90 * E1)) * Cosh[R * λx * x] + B[d90] * ((t90 * E2 + t0 * E1) / (ν12 * E2 * (t0 + t90))) * Cosh[R * λy * y] + Ky;
σy90[x_, y_, d90_] = ((t0 + t90) * σybar - t0 * σyo[x, y, d90]) / t90;
```

$$\lambda x = \sqrt{\frac{3*G23}{t0*t90^2} * \frac{(t0*E1 + t90*E2)}{E1*E2}};$$

$$\lambda y = \sqrt{\frac{3*G23}{t0^2*t90} * \frac{(t90*E1 + t0*E2)}{E1*E2}};$$

$$\mu x = \sqrt{\frac{3*G23}{t0*t90^2} * (t0 + t90) * \frac{\nu 12}{E1}};$$

$$\mu y = \sqrt{\frac{3*G23}{t0^2*t90} * (t0 + t90) * \frac{\nu 12}{E1}};$$

$$R = \sqrt{1 - \frac{\mu x^2 * \mu y^2}{\lambda x^2 * \lambda y^2}};$$

$$A[d90\_] = \left(-\left(\frac{(t0 + t90)}{t0}\ \sigma xbar - Kx\right) * \frac{(t0*E1 + t90*E2)}{(t0 + t90)*\nu 12*E2} * Cosh\left[\frac{R*\lambda y}{2*d0}\right] - Ky * \frac{2*d0}{R*\lambda y} * Sinh\left[\frac{R*\lambda y}{2*d0}\right]\right) \Big/$$
$$\left(\frac{4*\nu 12*E2*d0*d90*(t0 + t90)}{(t90*E1 + t0*E2)*R^2*\lambda x*\lambda y} * Sinh\left[\frac{R*\lambda x}{2*d90}\right] * Sinh\left[\frac{R*\lambda y}{2*d0}\right] - \frac{(t0*E1 + t90*E2)}{(t0 + t90)*\nu 12*E2} * Cosh\left[\frac{R*\lambda x}{2*d90}\right] * Cosh\left[\frac{R*\lambda y}{2*d0}\right]\right);$$

$$B[d90\_] = \left(\left(\frac{(t0 + t90)}{t0}\ \sigma xbar - Kx\right) * \frac{(t0 + t90)*\nu 12*E2}{(t90*E1 + t0*E2)} * \frac{2*d90}{R*\lambda x} * Sinh\left[\frac{R*\lambda x}{2*d90}\right] + Ky * Cosh\left[\frac{R*\lambda x}{2*d90}\right]\right) \Big/$$
$$\left(\frac{4*\nu 12*E2*d0*d90*(t0 + t90)}{(t90*E1 + t0*E2)*R^2*\lambda x*\lambda y} * Sinh\left[\frac{R*\lambda x}{2*d90}\right] * Sinh\left[\frac{R*\lambda y}{2*d0}\right] - \frac{(t0*E1 + t90*E2)}{(t0 + t90)*\nu 12*E2} * Cosh\left[\frac{R*\lambda x}{2*d90}\right] * Cosh\left[\frac{R*\lambda y}{2*d0}\right]\right);$$

$$Kx = \frac{\mu x^2*\mu y^2}{\mu x^2*\mu y^2 - \lambda x^2*\lambda y^2} * \left(\left(1 - \frac{\lambda y^2}{\mu y^2} * \frac{E1}{\nu 12*E2}\right) * \sigma xbar + \left(\frac{\lambda y^2}{\mu y^2} - \frac{1}{\nu 12}\right) * \sigma ybar\right);$$

$$Ky = \frac{\mu x^2*\mu y^2}{\mu x^2*\mu y^2 - \lambda x^2*\lambda y^2} * \left(\left(\frac{\lambda x^2}{\mu x^2} - \frac{E1}{\nu 12*E2}\right) * \sigma xbar + \left(1 - \frac{\lambda x^2}{\mu x^2} * \frac{1}{\nu 12}\right) * \sigma ybar\right);$$

Applied Stress

```
σxbar=.102; (*axial stress*)
σybar=0; (*transverse stress*)
```

Cracked Elastic Constants Calculations

```
Clear[σxbar,σybar]
E10 = E1;
E20 = E2;
ν120 = ν12;
ν210 = E20/E10 * ν120;
E190[1] = E1;
E290[1] = E2;
ν1290[1] = ν12;
ν2190[1] = ν210;
cdsat = 100; (*arbitrary maximum crack density value for iteration purposes*)
```

$$\text{Do}\left[\text{A11}[\text{d90}] = \frac{2*\text{t0}*\text{E10}}{(1-\nu 120*\nu 210)} + \frac{2*\text{t90}*\text{E290}[\text{d90}]}{(1-\nu 1290[\text{d90}]*\nu 2190[\text{d90}])};\right.$$

$$\text{A22}[\text{d90}] = \frac{2*\text{t0}*\text{E20}}{(1-\nu 120*\nu 210)} + \frac{2*\text{t90}*\text{E190}[\text{d90}]}{(1-\nu 1290[\text{d90}]*\nu 2190[\text{d90}])};$$

$$\text{A12}[\text{d90}] = \frac{2*\text{t0}*\nu 210*\text{E10}}{(1-\nu 120*\nu 210)} + \frac{2*\text{t90}*\nu 2190[\text{d90}]*\text{E190}[\text{d90}]}{(1-\nu 1290[\text{d90}]*\nu 2190[\text{d90}])};$$

$$\text{Ex}[\text{d90}] = \frac{\text{A11}[\text{d90}]*\text{A22}[\text{d90}] - \text{A12}[\text{d90}]^2}{2*(\text{t0}+\text{t90})*\text{A22}[\text{d90}]};$$

$$\text{Ey}[\text{d90}] = \frac{\text{A11}[\text{d90}]*\text{A22}[\text{d90}] - \text{A12}[\text{d90}]^2}{2*(\text{t0}+\text{t90})*\text{A11}[\text{d90}]};$$

$$\nu\text{xy}[\text{d90}] = \frac{\text{A12}[\text{d90}]}{\text{A22}[\text{d90}]};$$

$$\left.\nu\text{yx}[\text{d90}] = \frac{\text{A12}[\text{d90}]}{\text{A11}[\text{d90}]};,\ \{\text{d90},\ 1,\ \text{cdsat},\ 1\}\right]$$

Strain Calculations

Ply level axial and transverse strains

$$\epsilon\text{xbar0}[\text{d90\_}] = \frac{1}{\text{E10}}*\text{d0}*\text{d90}*\int_{\frac{-1}{2*\text{d0}}}^{\frac{1}{2*\text{d0}}}\int_{\frac{-1}{2*\text{d90}}}^{\frac{1}{2*\text{d90}}}\sigma\text{xo}[\text{x},\ \text{y},\ \text{d90}]\,\text{dx}\,\text{dy} - \frac{\nu 120}{\text{E10}}*\text{d0}*\text{d90}*\int_{\frac{-1}{2*\text{d0}}}^{\frac{1}{2*\text{d0}}}\int_{\frac{-1}{2*\text{d90}}}^{\frac{1}{2*\text{d90}}}\sigma\text{yo}[\text{x},\ \text{y},\ \text{d90}]\,\text{dx}\,\text{dy};$$

$$\epsilon\text{xbar90}[\text{d90\_}] = \frac{1}{\text{E290}[\text{d90}]}*\text{d0}*\text{d90}*\int_{\frac{-1}{2*\text{d0}}}^{\frac{1}{2*\text{d0}}}\int_{\frac{-1}{2*\text{d90}}}^{\frac{1}{2*\text{d90}}}\sigma\text{x90}[\text{x},\ \text{y},\ \text{d90}]\,\text{dx}\,\text{dy} - \frac{\nu 1290[\text{d90}]}{\text{E190}[\text{d90}]}*\text{d0}*\text{d90}*\int_{\frac{-1}{2*\text{d0}}}^{\frac{1}{2*\text{d0}}}\int_{\frac{-1}{2*\text{d90}}}^{\frac{1}{2*\text{d90}}}\sigma\text{y90}[\text{x},\ \text{y},\ \text{d90}]\,\text{dx}\,\text{dy};$$

$$\epsilon\text{ybar0}[\text{d90\_}] = \frac{1}{\text{E20}}*\text{d0}*\text{d90}*\int_{\frac{-1}{2*\text{d0}}}^{\frac{1}{2*\text{d0}}}\int_{\frac{-1}{2*\text{d90}}}^{\frac{1}{2*\text{d90}}}\sigma\text{yo}[\text{x},\ \text{y},\ \text{d90}]\,\text{dx}\,\text{dy} - \frac{\nu 210}{\text{E20}}*\text{d0}*\text{d90}*\int_{\frac{-1}{2*\text{d0}}}^{\frac{1}{2*\text{d0}}}\int_{\frac{-1}{2*\text{d90}}}^{\frac{1}{2*\text{d90}}}\sigma\text{xo}[\text{x},\ \text{y},\ \text{d90}]\,\text{dx}\,\text{dy};$$

$$\epsilon\text{ybar90}[\text{d90\_}] = \frac{1}{\text{E190}[\text{d90}]}*\text{d0}*\text{d90}*\int_{\frac{-1}{2*\text{d0}}}^{\frac{1}{2*\text{d0}}}\int_{\frac{-1}{2*\text{d90}}}^{\frac{1}{2*\text{d90}}}\sigma\text{y90}[\text{x},\ \text{y},\ \text{d90}]\,\text{dx}\,\text{dy} - \frac{\nu 2190[\text{d90}]}{\text{E290}[\text{d90}]}*\text{d0}*\text{d90}*\int_{\frac{-1}{2*\text{d0}}}^{\frac{1}{2*\text{d0}}}\int_{\frac{-1}{2*\text{d90}}}^{\frac{1}{2*\text{d90}}}\sigma\text{x90}[\text{x},\ \text{y},\ \text{d90}]\,\text{dx}\,\text{dy};$$

Application of continuity of strain in each direction

```
Do[eqn1[d90]=Coefficient[∈xbar0[d90],σxbar]-Coefficient[∈xbar90[d90],σxbar]==0;
eqn2[d90]=Coefficient[∈xbar0[d90],σybar]-Coefficient[∈xbar90[d90],σybar]==0;
eqn3[d90]=Coefficient[∈ybar0[d90],σxbar]-Coefficient[∈ybar90[d90],σxbar]==0;
eqn4[d90]=Coefficient[∈ybar0[d90],σybar]-
Coefficient[∈ybar90[d90],σybar]==0;,{d90,2,cdsat,1}]

Do[soln[d90]=Solve[{eqn1[d90],eqn2[d90],eqn3[d90],eqn4[d90]},{E190[d90],E290[d90],ν129
0[d90],ν2190[d90]}];
nu1290[d90]=soln[d90][[1,1,2]];
nu2190[d90]=soln[d90][[1,2,2]];
Em190[d90]=soln[d90][[1,3,2]];
Em290[d90]=soln[d90][[1,4,2]];
E190[d90]=Em190[d90];
E290[d90]=Em290[d90];
ν1290[d90]=nu1290[d90];
ν2190[d90]=nu2190[d90];,{d90,2,cdsat,1}]
```

Calculation of cracked axial laminate modulus

$$\text{Do}\left[\text{Ex}[\text{d90}] = \frac{\text{E10}+\text{E290}[\text{d90}]}{2},\ \{\text{d90},\ 1,\ \text{cdsat}\}\right]$$

Strain Energy Release Rate

$$Exi = \left(\frac{\left(\frac{-E1}{E2} + \nu 12^2\right) * \left(\frac{t0}{t90} + 1\right) * \left(\frac{E1}{E2} + \frac{t0}{t90}\right)}{E1 * \left(-\left(\frac{E1}{E2} * \frac{t0}{t90} + 1\right) * \left(\frac{E1}{E2} + \frac{t0}{t90}\right) + \nu 12^2 * \left(\frac{t0}{t90} + 1\right)^2\right)} \right)^{-1};$$

Maximum strain energy release rate calculation, Gmaxm = mechanical contribution, Gmaxt = thermal contribution, Gmaxw = moisture contribution

$$Do\left[Gmaxm[d90] = \left(\frac{t0}{t90} + 1\right) * \frac{\sigma xbar^2}{R * \lambda x} * \frac{1}{Exi} * \frac{1}{t0 / t90} * \frac{\left(\nu 1290[d90]^2 * \left(1 + \frac{t0}{t90}\right) - \left(\frac{E190[d90]}{E290[d90]} + \frac{t0}{t90}\right)\right)^2}{\left(\frac{E190[d90]}{E290[d90]} - \nu 1290[d90]^2\right) * \left(\frac{E190[d90]}{E290[d90]} + \frac{t0}{t90}\right)^2};\right.$$

$$Gmaxt[d90] = -\frac{1}{R * \lambda x} * \frac{t0}{t90} * \left((\alpha 1 - \alpha 2)^2 \Delta T^2 E190[d90]^2 * \left(-\left(\frac{E190[d90]}{E290[d90]} + \frac{t0}{t90}\right) + \nu 1290[d90] * \left(\frac{t0}{t90} + 1\right)\right)^2\right) /$$
$$\left(Exi * \left(\frac{t0}{t90} + 1\right) * \left(\frac{-E190[d90]}{E290[d90]} + \nu 12^2\right) * \left(\frac{E190[d90]}{E290[d90]} + \frac{t0}{t90}\right)^2\right);$$

$$Gmaxw[d90] = -\frac{1}{R * \lambda x} * \frac{t0}{t90} * \left((\beta 1 - \beta 2)^2 \Delta M^2 E190[d90]^2 * \left(-\left(\frac{E190[d90]}{E290[d90]} + \frac{t0}{t90}\right) + \nu 1290[d90] * \left(\frac{t0}{t90} + 1\right)\right)^2\right) /$$
$$\left(Exi * \left(\frac{t0}{t90} + 1\right) * \left(\frac{-E190[d90]}{E290[d90]} + \nu 12^2\right) * \left(\frac{E190[d90]}{E290[d90]} + \frac{t0}{t90}\right)^2\right);$$

$$Gmax[d90] = Gmaxm[d90] + Gmaxt[d90] + Gmaxw[d90];, \{d90, 1, cdsat, 1\}\Big]$$

$\sigma fpf = .0328;$ (*first ply failure stress, msi*)

$d90i = 1;$ (*initial crack density in 90 degree ply*)

$$\eta i = \frac{2 * d90i}{R * \lambda x};$$ (*characteristic parameter*)

$$Gc = Gmax[1] * Tanh\left[\frac{1}{\eta i}\right] - \frac{1}{\eta i} * \left(1 - \left(Tanh\left[\frac{1}{\eta i}\right]\right)^2\right);$$ (*critical strain energy release rate calculation*)

```
Gcrit=Gc/.σxbar→σfpf;
σxbar=.102; (*applied stress, msi*)
Gcrit/Gmax[61](*approximately 61 cracks/inch crack saturation density*)
1.00417
```

VITA

Sneha Patel Davison

Sneha Patel Davison was born on April 6, 1974 to Ramesh and Hemlatta Patel in Danbury, Connecticut. She was raised in Danbury until the age of eight at which time the family moved to Ridgeway, Virginia. She graduated from Magna Vista High School in 1992 and obtained her B.S. degree in Engineering Science and Mechanics from Virginia Tech in 1996. She then continued on with graduate school at Virginia Tech and accepted a position as a graduate research assistant working for Dr. Scott Case in the Materials Response Group in the summer of 1997. In June of 1999, she earned her Masters of Science degree in Engineering Mechanics with a thesis entitled "Durability of Advanced Woven Polymer Matrix Composites for Aerospace Applications." Her doctoral work, also completed at Virginia Tech, has focused on the enviro-mechanical durability of advanced polymer composite materials.